HIGH POWER DYE LASERS

W. W. Morey, et al

United Technologies Research Center

Prepared for:

Office of Naval Research
Advanced Research Projects Agency

30 September 1975

HIGH POWER DYE LASERS

REPORT R75-921617-13
FINAL TECHNICAL REPORT

PERIOD COVERED: 1 JANUARY 1973 TO 30 SEPTEMBER 1975

W.W. Morey
W.H. Glenn
C.M. Ferrar

Prepared under
CONTRACT N00014-73-C0284
for
Advanced Research Project Agency
ARPA ORDER#1806

UNITED TECHNOLOGIES RESEARCH CENTER
EAST HARTFORD, CONNECTICUT 06108

UNITED TECHNOLOGIES

156

SECURITY CLASSIFICATION OF THIS PAGE (When Data Entered)

REPORT DOCUMENTATION PAGE

READ INSTRUCTIONS BEFORE COMPLETING FORM

1. REPORT NUMBER: R75-921617-13	2. GOVT ACCESSION NO.
3. RECIPIENT'S CATALOG NUMBER	
4. TITLE (and Subtitle): HIGH POWER DYE LASERS	5. TYPE OF REPORT & PERIOD COVERED: Final Technical 1/1/73-9/30/75
	6. PERFORMING ORG. REPORT NUMBER: R75-921617-13
7. AUTHOR(s): Morey, W. W., Glenn, W. H. and Ferrar, C. M.	8. CONTRACT OR GRANT NUMBER(s): N00014-73-C-0284
9. PERFORMING ORGANIZATION NAME AND ADDRESS: United Technologies Research Center, 400 Main Street, East Hartford, CT 06108	10. PROGRAM ELEMENT, PROJECT, TASK AREA & WORK UNIT NUMBERS
11. CONTROLLING OFFICE NAME AND ADDRESS: Office of Naval Research, Department of Navy, Arlington, CA 22217	12. REPORT DATE: 9/30/75
	13. NUMBER OF PAGES: 156
14. MONITORING AGENCY NAME & ADDRESS (if different from Controlling Office): Director, Physics Programs, Physical Sciences Division, Office of Naval Research, 800 N. Quincy Street, Arlington, VA 22217	15. SECURITY CLASS. (of this report): Unclassified
	15a. DECLASSIFICATION/DOWNGRADING SCHEDULE

16. DISTRIBUTION STATEMENT (of this Report)

Approved for public release, distribution unlimited.

17. DISTRIBUTION STATEMENT (of the abstract entered in Block 20, if different from Report)

18. SUPPLEMENTARY NOTES

19. KEY WORDS (Continue on reverse side if necessary and identify by block number)

High Power Dye Lasers
Vortex Stabilized Flashlamps

20. ABSTRACT (Continue on reverse side if necessary and identify by block number)

This report discusses the development of a high average power, flashlamp pumped dye laser. This program has resulted in the development of a dye laser with a power output of 102 watts at a repetition rate of 250 Hz. This was made possible by the development of a vortex stabilized flashlamp that can be operated at high average power and high repetition rate. The report discusses the properties of the flashlamp in detail and describes two laser configurations that were tested, a longitudinal dye flow laser and a transverse dye flow laser. A pulse compression scheme to obtain a high time resolution with a long laser pulse is presented and some preliminary experiments are described.

D FORM 1 JAN 73 1473 EDITION OF 1 NOV 65 IS OBSOLETE

SECURITY CLASSIFICATION OF THIS PAGE (When Data Entered)

UNITED TECHNOLOGIES
RESEARCH CENTER

Report Number: R75-921617-13
Final Technical Report for the period
1 January 1973 to 30 September 1975

HIGH POWER DYE LASERS

ARPA Order No.:	1806 AMEND No. 16
Program Code:	5E20
Contractor:	United Technologies Research Center
Effective Date of Contract:	1 January 1973
Contract Expiration Date:	30 September 1975
Amount of Contract:	$373,984
Contract Number:	N00014-73-C-0284
Principal Investigator:	Dr. William H. Glenn (203) 565-5411
Scientific Officer:	Director, Physics Programs ONR
Short Title:	High Power Dye Lasers
Reported by:	W. W. Morey, W. H. Glenn and C. M. Ferrar

Sponsored By
Advanced Research Projects Agency
ARPA Order No. 1806

TABLE OF CONTENTS

	Page
I. TECHNICAL REPORT SUMMARY	I-1
REFERENCES FOR SECTION I	I-4
FIGURES	
II. VORTEX STABILIZED FLASHLAMP	II-1
Introduction	II-1
Electrical Characteristics	II-2
Flashlamp Gasdynamics	II-6
Power Distribution in Flashlamp	II-11
Flashlamp Cooling and Thermal Limits	II-14
Optical Characteristics	II-16
REFERENCES FOR SECTION II	II-22
FIGURES	
III. AXIAL FLOW DYE LASER	III-1
Introduction	III-1
Ray Tracing Program	III-2
Dye Pumping System	III-5
Laser Tests	III-6
Laser Output Fall Off	III-8
Single Shot Optical Distortion	III-11
REFERENCES FOR SECTION III	III-13
FIGURES	
IV. TRANSVERSE FLOW DYE LASER	IV-1

Table of Contents (Cont'd)

	Page
Introduction	IV-1
Ray Tracing Program	IV-2
Flow System	IV-3
Laser Tests	IV-4
REFERENCES FOR SECTION IV	IV-7
FIGURES	
V. HIGH RESOLUTION DYE LASER RANGING	V-1
Modulation Techniques	V-1
Frequency Sweeping the Dye Laser	V-4
A Fast Scanning Interferometer for Frequency Sweeping	V-10
Conclusions and Recommendations	V-13
REFERENCES FOR SECTION V	V-15
FIGURES	
VI. CONCLUSIONS	VI-1
REFERENCES FOR SECTION VI	VI-4

I. TECHNICAL REPORT SUMMARY

The object of this program has been the development of high average power, flashlamp pumped dye laser technology. The program has resulted in the development of a dye laser with an average power output in excess of 100 watts at a repetition rate of 250 Hz, and it appears feasible to scale up the device to a power of the order of 1 kilowatt. Applications for such dye lasers include underwater communication and ranging, target illumination and designation, underwater and atmospheric propagation studies, remote sensing and monitoring and photochemical processing including isotope separation. Application involving ranging generally require a short duration pulse, typically 10-20 nanoseconds. This is difficult to achieve with reasonable efficiency using a flashlamp pump. For this reason, consideration was also given in this program to means of obtaining a high effective time resolution using a long duration pulse and some preliminary experiments directed toward this and were carried out.

Dye lasers can be pumped either by flashlamps or by visible ion lasers. The laser pumping is very efficient in the conversion of pump radiation to dye laser radiation however the overall efficiency of such a system is quite low due to the inefficiency of the pumping laser. Laser pumping with present or projected ion lasers does not constitute a viable approach to obtaining power in excess of about 10 watts.

Flashlamp pumped dye lasers were first demonstrated by Sorokin (Ref. I-1) using coaxial flashlamps. In these lamps the discharge takes place in an annular region between the dye cell which forms the inner wall of the lamp and a cylindrical outer jacket. The wall thickness of the outer jacket can be made as thick as necessary to withstand the shock of the discharge. The inner wall is reinforced by the liquid within the dye cell. Using these lamps, high efficiency and high energy per pulse can be obtained. These lamps are not suitable for high average power operation, however, because of their limited life and limited repetition rate. Linear flashlamps are also widely used for pumping dye lasers. These lamps are simpler to construct than the coaxial lamps and are easier to replace. Their lifetime is somewhat better than the coaxial lamps; when fired at about 1/3 of their explosion limit the lifetime is typically 10,000 shots. These are not well suited for high power operation. Operating at a repetition rate of 10 pps, this lifetime corresponds to only 15 minutes of operation.

The United Technologies Research Center has developed a fast risetime flashlamp that is particularly well suited for long term, high power and high repetition rate pumping of a dye laser. The lamp is operated with a vortex flow of gas at a pressure of one to several atmospheres. The walls of the discharge chamber are well removed from the arc to allow for shock wave dissipation and to eliminate wall vaporization.

The fast gas flow provides cooling for the lamp to allow high average power operation and carries away any material that is eroded from the electrodes. The vortex flow is established by injecting the gas tangentially near the walls of the lamp. It swirls inward and exits through holes in the electrodes. This flow pattern also serves to stabilize the position of the discharge. In the normal mode of operation a low current glow type discharge of a few milliamperes is maintained in the lamp. The flow pattern stabilizes this discharge on the axis of the lamp. The main discharge is then produced by discharging a capacitor through the lamp with an external switch. This pulsed discharge follows the path of the stabilized glow discharge and is thus stabilized itself along the lamp axis. The lamp may be operated without the glow "sustainer" discharge and the vortex flow will tend to stabilize the capacitor discharge along the axis because of the pressure distribution, however this mode of operation is less reliable.

During the course of this program, two laser configurations were investigated, an axial dye flow system and a transverse dye flow system. The first to be investigated was the axial flow system. In this configuration the flashlamp is coupled to the dye medium by an exfocal spherical pumping cavity. In this cavity the flashlamp and the dye cell are aligned along the diameter of a reflecting sphere. This type of cavity was originally chosen because it provides a symmetrical electrical environment for the flashlamp. This symmetrical environment assists in the stabilization of the arc. In the early versions of the flashlamp the sustainer discharge was not used. The lamp was triggered by means of a third electrode and it was found that the symmetrical environment was necessary to prevent the arc from stretching along the envelope and destroying it. When the sustainer discharge is used, the symmetrical environment is not necessary.

The spherical cavity has a number of advantages. It provides for an azimuthally uniform distribution of the pumping light. The collection efficiency compares quite favorably to that of an elliptical cavity. It does have some disadvantages in that there is some blockage of the light by the structures needed to support the dye cell and the flashlamp. It also allows convenient access to only one end of the dye cell.

The spherical cavity laser used a longitudinal dye flow, the dye entered and left the cell through four tubes located at each end of the cell. This laser was operated at a power level of slightly over 40 watts and a repetition rate of up to 100 Hz. The power output from this laser was limited by the dye change-over rate. The maximum flow velocity of the dye was determined by the onset of cavitation at the sharp corners in the flow where the dye entered and left the cell. The maximum change-over rate was limited to about 166 changes per second. Even at this change-over rate, the power output reached a maximum at about 100 Hz and decreased at higher rates. There was evidence to indicate that the acoustic or thermal disturbance produced in the dye by the sudden deposition of the pumping energy was propagating upstream in the flow and was degrading the optical quality of the dye

solution prior to the time it entered the dye cell. This could be the result of release of dissolved gases or to the initiation of cavitation in the flow which was just below the threshold for cavitation. A number of modifications to the flow system such as the smoothing of the transition sections were made but the longitudinal flow system was fundamentally limited by the dye change-over rate. The longitudinal flow laser is shown in Fig. I-1.

In order to overcome this difficulty, a transverse flow system was designed and fabricated. This system is shown in Fig. I-2. In this system, a redesigned flashlamp was located along one focus of a cylindrical elliptical cavity. The cavity was cut in the plane of the other latus rectum. A transverse dye flow channel was located in this plane. A high capacity dye pumping system capable of supplying a flow of 40 gallons/minute was also fabricated. This allowed for a dye exchange rate of 500-1000 times per second, depending on the thickness of the dye flow channel. This laser produced an output power of 102 watts at a repetition rate of 250 Hz. The poweroutput from this laser was limited by the power supply and switching circuitry used to drive the flashlamp. Through optimization of the coupling efficiency of the lamp and dye, the flow geometry, lamp cooling, switching circuits, and laser resonator optics, substantially high efficiencies and power should be obtainable from this type of laser.

Section II of this report discusses in detail the characteristics of the flashlamps that were used in this program. Topics covered include the electrical characteristics, switching requirements, gas dynamics, energy balance, cooling requirements, effects of different fill gases and the power output and spectral characteristics. Section III covers the axial flow laser and discusses the factors that limited the average power output of this laser. Section IV describes the transverse flow laser that was built to overcome the limitations of the axial flow laser.

Section V presents a pulse compression scheme that can be used to obtain a high time resolution with a long duration laser pulse. This scheme involves sweeping the wavelength of the laser during the pulse. Suitable signal processing at the detector can then provide a time resolution that is much shorter than the actual duration of the pulse. Some preliminary experiments to sweep the wavelength are reported and recommendations are made for further work. Section VI summarizes the work and indicates directions for further increase in average power and efficiency.

The personnel who contributed to the work reported here included, in addition to the authors, A. R. Clobes, A. J. DeMaria, G. L. Ladd, and M. E. Mack.

REFERENCES FOR SECTION I

I-1 Sorokin, P. P., J. R. Lankard, E. C. Hammond and V. T. Moruzzi: IBM J. Res. Development 11, 130 (1967).

FIG. I–1

UTRC HIGH POWER DYE LASER

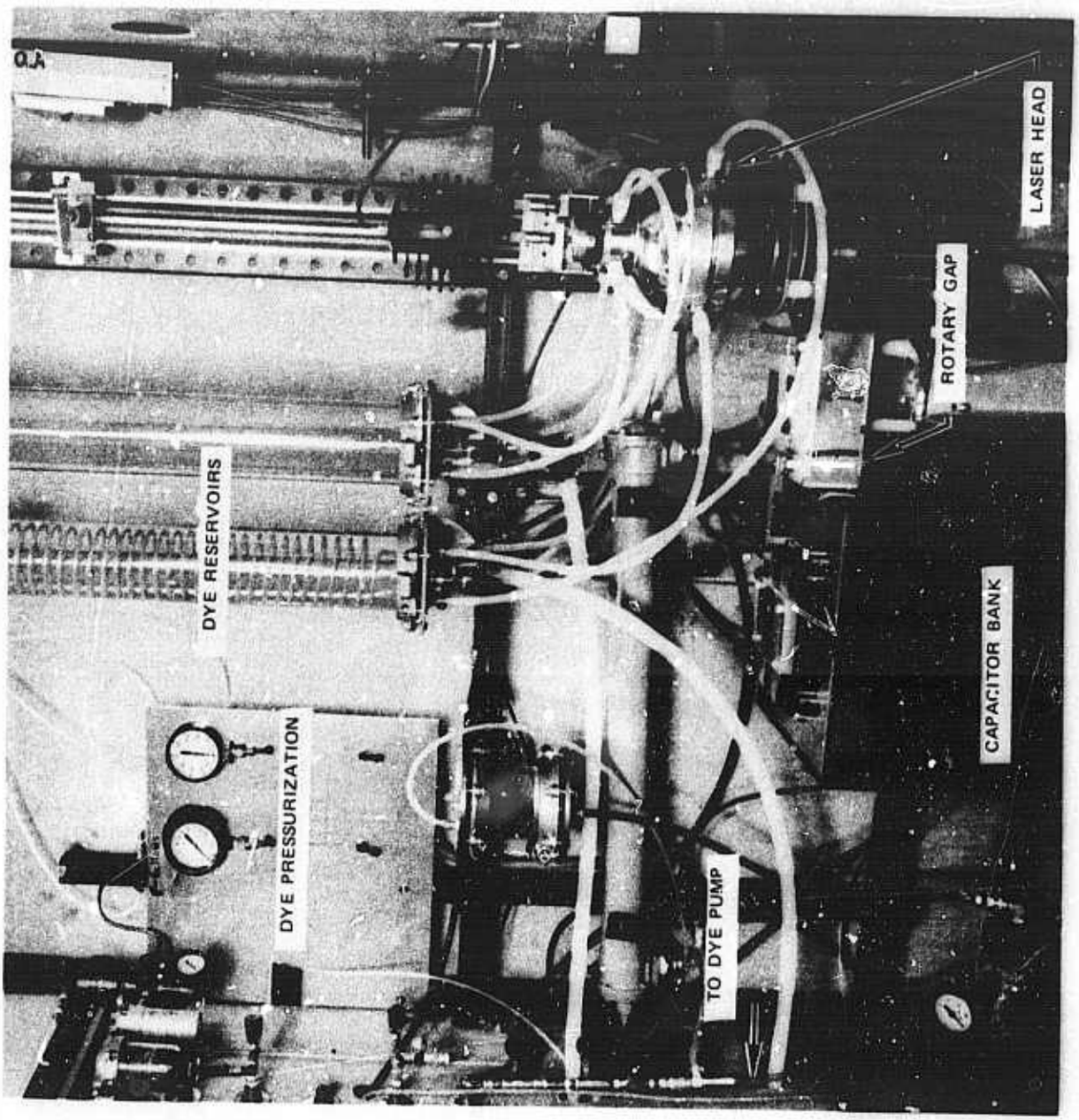

FIG. I–2

TRANSVERSE FLOW HIGH POWER DYE LASER

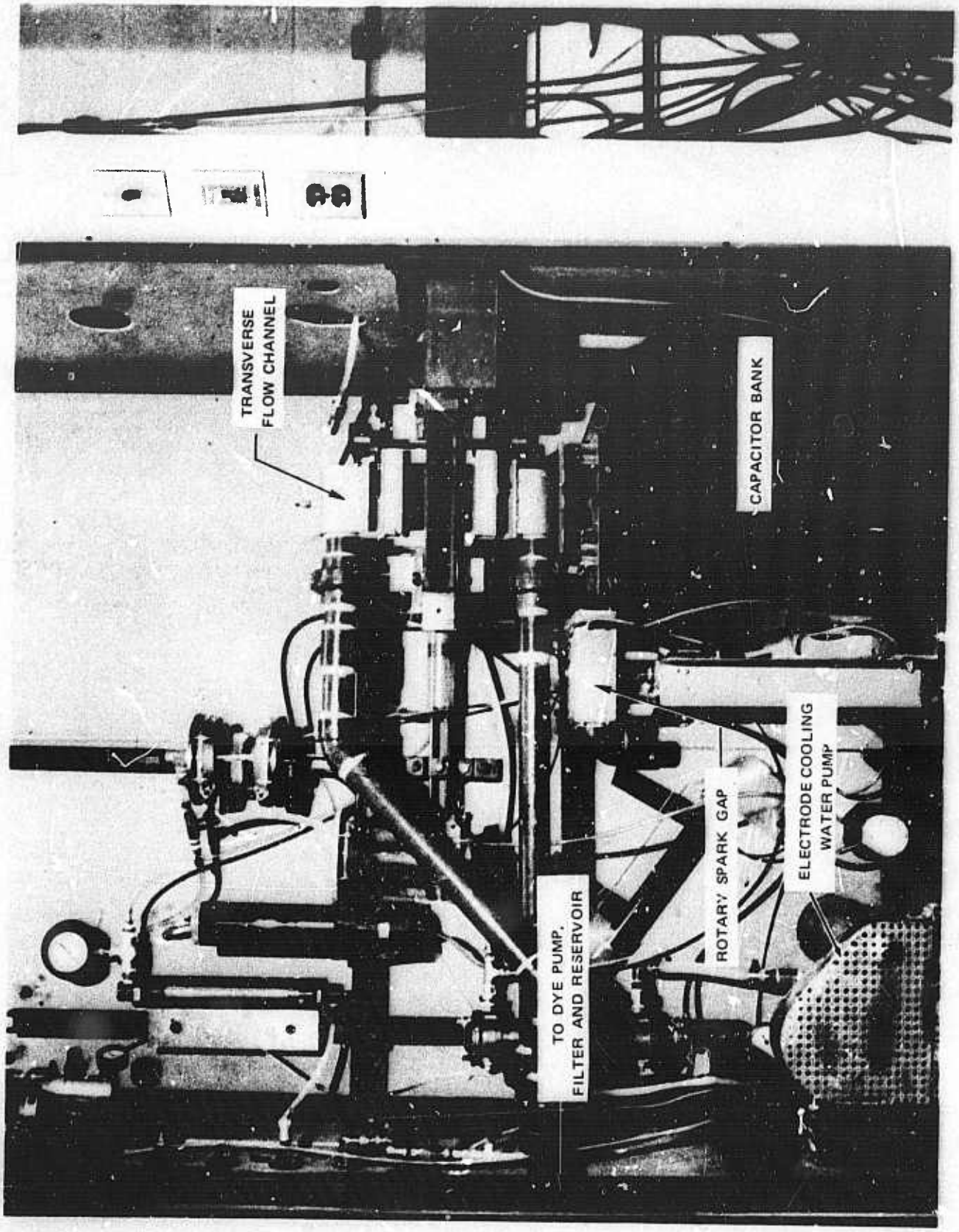

II. VORTEX STABILIZED FLASHLAMP

Introduction

To optically pump a dye laser a flashlamp must have peak radiant emittances greater than 50 kW/cm^2 (preferably several MW/cm^2), and for best efficiencies the pulse width should be on the order of a microsecond or less. Commercially available wall stabilized flashlamps of the linear or coaxial design are adequate for the dye laser pump on a single shot or low repetition rate (< 30 Hz) basis. The wall stabilized flashlamps are severely restricted, however, in three ways. In the first place an acoustic shock is produced in the flashlamp that can easily explode the tube if the discharge energy is too large or the pulse width too small. Secondly, due to plasma erosion of the confining wall, the flashlamps are limited in lifetime to typically 2 x 10^5 discharges provided the energy loadings are reduced to 25 percent of the single shot explosion energy (Ref. II-1). Calculations show that the wall of most quartz tubes will not withstand a temperature difference over 1000°C (650°C is a safe limit). As a consequence, the commercial flashlamps are also limited to a maximum average power loading since practically all the heat generated must be transferred through the confining wall.

The UTRC vortex stabilized flashlamp allows a considerable extension in the pulse energy loading per unit length, the lifetime, and average power handling capability of the flashlamp. This is accomplished by tangentially injecting argon into the flashlamp at the base of one of the electrodes to create a vortex flow. The argon is exhausted out the center of the two electrodes. The vortex flow produces a low pressure region along the interelectrode axis. This action stabilizes the electrical discharges on the axis, keeping it away from the flashlamp wall. Therefore, by separating the plasma from the confining wall and exhausting the gas from the flashlamp, we eliminate wall erosion and greatly reduce the amount of heat that must be transferred through the wall. In addition, the larger wall diameter required for the vortex flashlamp allows a higher single shot energy loading per unit length of discharge.

Two different vortex flashlamps were designed and built for the high power dye laser program. The first flashlamp had a 6 cm long arc and was designed to fit in a hemispherical reflector. Figure II-1 is a photograph of the 6 cm flashlamp and dye cell mounted in their respective hemispheres. The flashlamp shown in Fig. II-1 was modified to allow for water cooling of the electrode tips and quartz envelope. A schematic of the modified 6 cm flashlamp assembly is shown in Fig. II-2. Argon enters the plenum as shown and is injected tangentially to the envelope at the base of the lower electrode. The swirling argon moves upward and then inward, exiting out the center of each electrode. The top electrode has four struts that run to the sides of the hemisphere. Two of the struts are for argon exhaust and two for cooling water. Figure II-3 shows the flashlamp disassembled. The flashlamp was designed so that it could be easily assembled and disassembled for maintenance and replacement of parts.

For the transverse dye flow system we designed a 10 cm long flashlamp that mounts in an elliptical reflector. The design is similar to the 6 cm flashlamp except that both electrodes are recessed so that the envelopes seals on both ends of the tube are removed from the hot arc region. The argon gas can be injected at either end of the flashlamp, but it still exhausts out the center of both electrodes. Figure II-4 shows a photograph of the 10 cm flashlamp mounted in the elliptical reflector. Figure II-5 shows two views of the flashlamp operating with 52 kW average input power. At these power levels the discharge is so bright that it dazzles the eyes even with 2 welder's goggle filters.

Since the flashlamp gas is exhausted to the atmosphere we are currently limited to the use of argon. With a closed cycle gas handling system, consisting of a heat exchanger, compressor, reservoir tank, and filter, the flashlamp could use the heavier, expensive gases xenon and krypton. At the present time we felt that little would be gained in using these gases. This topic will be discussed further in the section II-6.

A principal disadvantage of the vortex flashlamp over the wall stabilized flashlamp is its inherently smaller length to diameter ratio (L/D). In general, this reduces the collection efficiency for focusing the available flashlamp light into a dye cell due to light loss out the ends of the flashlamp.

The following sections will go into greater detail in discussing the operation and performance of the vortex flashlamp. We will first discuss the switching requirements and electrical characteristics of the flashlamp. Then we will discuss the gas flow and dynamics of the discharge expansion with its associated acoustic shock. The discharge energy balance will be analyzed next and then thermal loading and cooling requirements will be presented. Finally, the optical and spectral characteristics of the flashlamp will be described.

Electrical Characteristics

Switching

Figure II-6 shows the basic electrical circuit used with the flashlamp. A switching element is needed to discharge the electrical energy stored in the capacitor into the flashlamp. The first vortex flashlamp was triggered by a sparking third electrode that was inserted through the gas exit hole in the high voltage electrode (see Fig. II-1). The main discharge was arranged to hold off the desired firing voltage by the addition of a small mixture of CO_2. In essence, the flashlamp acted as a triggered spark gap to discharge the capacitor. This scheme worked, not always reliably, up to repetition rates of about 30 Hz. Beyond this point the residual ionization products build up and lower the breakdown voltage of the main arc so that it is no longer possible to discharge the desired energy

per pulse. This problem has been eliminated by the introduction of an external switch and a sustainer discharge. The sustainer consists of a dc discharge of a few milliamperes which is continuously run between the lamp electrodes so that in effect the arc is always broken down. When the lamp is to be fired, the switch to the capacitor is closed and main discharge proceeds along the path of the sustainer. This allows the discharge of any desired energy into the arc, independent of the static breakdown voltage.

The requirements on the switch are rather stringent. It must be able to hold off 30 kV, switch 15 kA peak currents, 335 A rms, and operate at several hundred Hz. In addition, it must have low inductance and low loss. These requirements are currently state-of-the-art capabilities for developmental models of hydrogen thyratrons and solid state thyristors. Table II-1 is a list of switches that have been considered for the flashlamp. The ignitron can easily handle the peak currents, but has only a low repetition rate capability. The EG&G developmental thyratron

Table II-1

High Power Switches

Switch	Peak Cur. (kA)	RMS Cm. (A)	Max. Rep Rate for 2 μsec Pulse (H_z)
Ignitron			
GE, GL - 37207	300	120	8
Hydrogen Thyratron			
1. EG&G HY-5	5	125	300
2. EVV, GHT9	7.5	335	1000
3. EG&G Developmental model	15	350	300
Thyristors			
RCA developmental model	6	380	200
Spark Gap			
1. Air blast, RADC	1.24 mw avg. Power	-	300
2. Rotary Gap	15	300	200

would work for our application, but is expensive, has no guarantee, and requires a long delivery time. The English Electric Valve Co. recently developed a thyratron that could be used in our system with some modifications at reduced power levels. RCA also makes a developmental thyristor bank by connecting large numbers of smaller thyristors each rated at 600 V, 35 A rms in series-parallel combinations. Thyristor banks could be scaled up to meet our requirements. This again is expensive and requires a long delivery time. R. Gray at RADC has developed an air blast spark gap that runs at 300 Hz with average power levels up to 1.25 MW (Ref. II-2). To obtain these high powers, however, a 75 hp turbine blower was required to generate the air blast. The lifetime and reliability of such a device is also uncertain.

Rotary Spark Gap

For practical reasons we chose to build a rotary spark gap similar in design to ones used in early radar sets (Ref. II-3, II-4). A gap between two tungsten electrodes is repetitively bridged by a third tungsten electrode carried on a rapidly rotating disc. Such a structure can be incorporated into a low inductance stripline and does not significantly contribute to the overall inductance. The rotary gap has been operated in conjunction with the flashlamp at repetition rates up to 500 Hz, and there appears to be no reason why such a gap cannot be operated at rates up to a few kHz. Figure II-7 illustrates how the rotary spark gap works, and Fig. II-8 shows a cross sectional schematic of the rotary spark gap and the manner in which it connects to the discharging capacitor and laser assembly. The two fixed electrodes were weighed before assembly of the spark gap. A record was kept of the running time of the flashlamp in succeeding test runs. After an accumulated running time of 14.6 min with power inputs ranging from 3.2 kw to 16 kw (8.8 kw average), the fixed spark gap electrodes were removed and reweighed. It was found that the anode lost .342 grams or .8 percent of its mass while the cathode lost .446 grams or 1 percent of its mass. This corresponds to 1.4 and 1.8 grams lost per hour of running time. Reports of electrode wear from rotary spark gaps used in early radars indicated a much smaller rate of wear (Ref. II-3). The rate of electrode erosion expressed in grams per amp-hour is 0.75 g/amp-hour for the anode and .98 g/amp hour for the cathode which is more than two orders of magnitude greater than in the radar sets. The pulse currents that we used, however were two orders of magnitude greater than those used for the radar gap measurements.

The electrode wear in the flashlamp, on the other hand, has been rather small even after accumulated running times of about 30 minutes. Only a small amount of wear appears around the exhaust holes in the center of the electrodes. The considerably smaller rate of erosion from the flashlamp electrodes is probably due to more effective water cooling. In the flashlamp, water is brought to within a centimeter of the outside surface of the tungsten tip on the end of the electrodes. This greatly reduces the average surface temperature and extends the life of the electrodes.

In addition to rapid electrode wear, the rotary spark gap is also limited in power handling capability. We found that for power inputs near that listed in Table II-1 the rotary spark gap could draw a continuous arc and fail to open the flashlamp circuit to allow a recharging of the capacitor. This problem could be solved, as in the case of a fixed spark gap, by using a high speed blower.

Circuit Parameters

The transformer inductance in the high voltage power supply gives reactance limited charging of the capacitor. Without any charging resistance the capacitor voltage can overshoot the dc voltage level by as much as 51 percent with the 2 μF capacitor and the powerstat at is maximum setting. Other capacities and powerstat positions change the amount of overshoot. When a two hundred ohm ballast resistor is placed in the charging line, however, the overshoot is eliminated. The charging time is 2 msec.

The sustainer discharge is ignited by running the sustainer supply up to about 25 to 30 kV. Upon ignition an orange glow discharge is stabilized in position on the electrode axis. The glow discharge carries about 4 mA. This type of discharge has been observed only when a small amount (2-10 percent) of nitrogen is added to the argon in the flashlamp. With pure argon or with small amounts of CO_2 added to the argon we observed a thin filamentary arc that discharged the line and electrode capacitance at a several hundred Hz repetition rate. In this instance the sustainer power supply could not provide enough current to drive the sustainer arc continuously.

Typical voltage and current waveforms are shown in Fig. II-9. The current was measured with a Rogowski coil and the voltage with a properly matched Tektronix high voltage probe. The flashlamp discharge is highly underdamped with as much as a 64 percent current reversal. The current also appears to damp faster in one direction than in the other. This is not fully understood at the present time. Due to the expansion of the discharge column the flashlamp circuit is nonlinear with respect to a time varying discharge resistance and inductance. Markiewicz and Emmett have derived the response of a wall stabilized flashlamp (Ref. II-5) by considering that the plasma voltage and current relationship is given by

$$V = \pm K_o \, i^{1/2}$$

where V and i are the lamp voltage and current and K_o is a constant. Their analysis, however, does not allow for a time varying inductance that would be a significant factor in the analysis of our flashlamp. Their α parameter for our flashlamp would be between 0.2 and 0.3.

The inductance of the flashlamp circuit was measured with a grid dip meter. To do this the spark gap was shortened with a copper strip, a 1/4 inch copper tube was placed between the electrodes, and the 2 μF discharge capacitor was replaced

with a smaller one. The net inductance of the circuit was 150 nH. This inductance gives an effective damp resistance to the first two current loops of 0.06 Ω. The capacitor and inductance circuit impedance, $\sqrt{L/C}$, is 0.19 Ω. To obtain a critically damped waveform for our flashlamp with matched impedances would require a reduction in the inductance by about a factor of 10. This would be impossible to achieve with the physical dimensions of the present flashlamp.

Flashlamp Gasdynamics

Flashlamp Pressure

Figure II-10 shows the results of measurements and calculations of the gas pressure in the 6 cm flashlamp at different radii from the center of the flashlamp axis. The pressure at the center of the vortex drops to 63 percent of its value at the wall. This pressure distribution probably changes drastically as the flashlamp is run at repetition rate. An effect of pressure changes is noted on the laser output and will be discussed later. At an argon flow rate of 5 liters/sec (STP) the pressure at the wall of the flashlamp was 11 psig (1.78 atm). At this flow rate the gas in the flashlamp changes over at a rate of 24 times per sec. The arc volume, however, changes over at a much faster rate of 913 times per second.

For the 10 cm flashlamp the gas change-over rates are about 12 times per sec for the lamp volume and 513 times per sec for the arc volume. These change-over rates are for a flow of 5 ℓ/sec. The maximum flow rate that could be obtained from the argon supply lines for the flashlamp is about 8 ℓ/sec. Using higher flow rates than 5 ℓ/sec increases the pressure in the flashlamp. This has distinct advantages as we will discuss later, but brings the quartz envelope closer to its damage threshold.

Shock Wave Generation

The electrical breakdown process in gases has been described by many authors (Ref. II-6). Initially, the flashlamp is broken down by an avalanche process that forms a filamentary streamer between electrodes. A large current of electrons rushes into the streamer, ionizing and rapidly heating the gas. As the gas temperature rises so does the pressure, and the filamentary channel starts to expand. The electrical resistance of the channel also falls to a low value. With a low inductance circuit the electrical energy discharges so rapidly that the hot channel expands faster than the speed of sound in the gas. The rapid expansion, then, produces a large density of gas molecules at the edge of the hot channel creating a shock front. After the electrical energy has dissipated, the shock front continues to travel outward and eventually impacts the wall of the flashlamp.

The dynamics of a shock wave produced by the sudden release of energy was first treated by G. I. Taylor (Ref. II-7) for the case of a spherical explosion and then later by Shao-Chi Lin (Ref. II-8) for the cylindrical case, which is more applicable to our problem.

Using a more detailed analysis, Drabkina (Ref. II-9) has included the effects of the release of energy over a period of time rather than instantaneously. She obtained for the shock front radius

$$R = (\alpha/\rho_o)^{1/4} \left[\int_o^t E(t)^{1/2} dt\right]^{1/2}$$

where α is a dimensionless constant which depends only on the ratio of specific heats and can be calculated from the energy integral; ρ_o is the undisturbed gas density, and E is the discharge energy per unit length. These results are also discussed in a review article by Marshak (Ref. II-10). Drabkina also demonstrated that the outwardly progressing shock front travels at a faster rate than the luminous boundary and, of course, the two boundaries separate after a certain period of time. By defining the luminous channel radius, R_c as the radius at which the gas temperature falls to 10,000°K Drabkina shows that R_c is insensitive to the actual temperature chosen to define the boundary and that

$$R_c = L\{E(t)\}^M \left[\int_o^t E(t)^{1/2} dt\right]^N$$

where for argon at 1 atm L = 1.1, M = 0.43 and N = .460. The units used in these formulas are CGS. If the energy is supplied at a steady state rate the luminous radius becomes

$$R_c = .91 \{E(t)\}^{.273} t^{.46}$$

For a comparison with our flashlamp, consider a 200 J discharge in 3 μsec. If we allow for optical, spark gap, and electrical circuit losses totaling 25 percent, then the luminous radius from the above formula is 5.1 mm. This agrees with our observed result shown in Fig. II-11. The arc diameters measured for Fig. II-11 were taken from Polaroid photos of about similar exposures. The 1000 J data point however, was taken for a flashlamp pulse whose duration was about 13 times longer than the pulse duration used to obtain the other data points. We found that the luminous arc radius is given approximately by

$$R_c = AE^x$$

where A is a constant, E the energy of the discharge, and x is 0.44. The radius was only slightly affected by sizeable changes in the pulse duration, gas pressure, and length. Data collected by Marshak (Ref. II-10) from several different experiments and with different gases indicates that a value of x beteen 0.4 and 0.5 describes the radii of most systems. The theory, of course, is only approximate and does not include important factors of how the energy is deposited in the dynamically changing arc column. In addition, it does not take into account the pressure distribution.

Figure II-12 shows the results of measurements made on the expansion of the arc in time. To obtain this data we used a high speed framing camera. The values for the arc diameter were taken from the photographs. It is interesting to note that the arc continues to expand for times out to 8 μsec, and we observed no irregularities in the expansion due to the first and second current reversals.

Energy in Acoustic Shock

To estimate the energy used to produce the acoustic shock we assume that the initial filamentary arc expands, and, like a cylindrical piston, adiabatically compresses an annular cylinder of gas. No heat is assumed transferred from the hot luminous region to the region where the gas is piling up to form the shock front. This is so because the discharge time is short in comparison to the heat diffusion rate. The radius of the compressed gas cylinder is given by the shock front radius (R_2) just after the discharge. The radius of the "expanding piston" (R_1) is probably just slightly greater than the luminous arc diameter. These two radii are shown in Fig. II-13 where a schematic of the ratio of the density to the unperturbed density is plotted for three different times after the discharge.

Assuming the initiating breakdown starts with a zero radius, we can estimate the energy used to compress the gas into the shock front as

$$W = 2\pi L \int_0^{R_1} P \, r\,dr$$

where L is the length of the discharge and P is the pressure in the front. For an adiabatic compression

$$PV^\gamma = P_o(\pi R_2^2 L)^\gamma$$

where γ is the ratio of specific heats and P_o the initial (or undisturbed) pressure. Substituting for the pressure in the integral we get

$$W = \pi L P_o R_2^2 \left[\left\{1 - (R_1/R_2)^2\right\}^{1-\gamma} - 1\right]/(\gamma-1)$$

Using Drabkina's analysis (Ref. II-9) and considering a uniform release of energy, the pressure just behind the shock front is given by

$$P_F = .209\ (\rho_o E)^{1/2}/\tau$$

where τ is the pulse duration. For a 200 J discharge (150 J after losses), 3 μsec pulse, and 6 cm arc, P_F = 45.9 atm. The initial and final states for the adiabatic compression are related by

$$P_o(R_2^2)^\gamma = P_F(R_2^2 - R_1^2)^\gamma$$

We can then find $(R_2/R_1)^2$ in terms of the pressures.

$$1 - (R_1/R_2)^2 = (P_o/P_F)^{1/\gamma}$$

thus

$$W = \pi L P_o R_2^2 \left[(P_F/P_o)^{(\gamma-1)/\gamma} - 1\right]/(\gamma-1)$$

For a linear deposition of energy, R_2 would be given by (using results in Ref. II-10)

$$R_2 = 3.018 E^{1/4}\ \tau^{1/2} = 6.57 \text{ mm}$$

Therefore, with a 200 J, 6 cm long, 3 μsec discharge, W = 4.6 J. This represents only 2.3 percent of the total input energy. This result supercedes a calculation presented in an earlier report that we feel overestimated the energy used to generate the shock wave.

Flashlamp Explosion Limit

Figure II-13 shows the position of the shock front at 3 different times after the discharge. The pressure just behind the shock front is also given next to the time indication. The pressure just prior to the shock front impacting the wall is a little over 7 atm. The values for Fig. II-13 were based on the formulation and data from Ref. II-10. These results are only approximate but do give a reasonable estimate of the size of the shock front.

The difference between the wall pressure at the time of the shock wave impact and the pressure outside the wall must be less than the bursting pressure of the quartz envelope. Considering the hoop stress placed on the quartz envelope by a pressure differential across the tube, the maximum pressure applied across the wall would be

$$P_x = \omega \sigma_x / R$$

where ω is the tube thickness, R the tube radius, and σ_x the maximum allowable tensil stress for fused quartz. We would not want the shock front pressure at the wall (P_s) plus the static wall pressure (P_w) minus the pressure outside the wall (P_o) to exceed P_x. That is,

$$P_s + P_w - P_o \lesssim P_x$$

From Ref. II-10 we can estimate the pressure of the shock front at the wall by

$$P_s = \frac{8.02 \times 10^{-2} E}{R^2 L}$$

where L is the flashlamp discharge length, E the discharge energy, and R the radius of the wall (all in CGS units). The energy that we can safely discharge is then

$$E_x = 12.5 LR^2 (\omega \sigma_x / R - P_w - P_o)$$

Tests on the allowable tensile stress for fused quartz tubing will be given in the next section. 2000 psig is usually considered a safe stress limit for fused quartz; however, a properly annealed tube may withstand up to 7000 psi. Many tubes break, however, at 4000 psi due to small scratches and imperfections in the tube material. If we allow a 4000 psig stress limit, the maximum allowable energy loading for our 6 cm flashlamp with a 1.65 cm radius, 0.2 cm thick wall, and 11 psig wall pressure would be E_x = 666 J, and allowing for the 25 percent losses, the total discharge energy allowed is 832 J. Actually, we have discharged up to 1000 J in the 6 cm flashlamp, but with a 30 to 40 μsec pulse. The explosion energy result above is not valid for a 30 to 40 μsec pulse because the shock wave impacts the wall before the entire energy has been discharged. In addition, end effects have not been considered and this could increase the damage threshold by 20 to 30 percent.

It is interesting to note that in the above formulation the explosion energy is independent of the pulse length of the discharge. The shorter the discharge time, the further the shock front has to travel to impact the wall, and consequently the pressure just behind the front decays to the same value at the wall. For pulses lasting longer than the time for wall impact the above calculation is no longer

true. This case would occur in wall stabilized flashlamps where the shock wave can reverberate several times before the capacitor energy is dissipated. The damage energy for wall stabilized flashlamps has been shown to have a square root dependence on the pulse length (Ref. II-11).

The flashlamp can be damaged quite readily if the arc forms along the inside wall of the envelope. In this case the full force of the discharge is brought to bear on the quartz. It is important therefore to make sure that the arc remains stabilized on the axis of the electrodes.

Vibration of Lamp Envelope

During the course of one operation when the flashlamp had been operating at a 5 kW power level, the PRF was slowly decreased from a value above 100 Hz to a value a little below 100 Hz. At this point the lamp envelope exploded. Since the input power level was moderate, this led us to suspect that a resonant vibration frequency of the envelope had been reached. Therefore, a test was made to determine the vibration frequency of the envelope and how it vibrated under the impulse from an actual discharge. A light, short piece of thin wall stainless steel tubing was compressed between the lamp envelope surface and the center of a small audio speaker. The voltage developed across an 1.1 kΩ resistor by the speaker movements was then monitored with an oscilloscope. When the lamp envelope was tapped sharply with a hard object a definite ringing frequency of 833 Hz could sometimes be observed. This is shown in Fig. II-14a. Figure II-14b shows the envelope vibration with an 80 J flashlamp discharge. In order to produce a large build up in the vibration amplitude near 100 Hz PRF, the vibrations would have to be re-enforced in a coherent manner every 10 msec. This seems unlikely from the vibration waveform shown in Fig. II-14b. The envelope breakage in this case might have been due to an improperly annealed envelope that had scratches or prestressed areas, or possibility to the arc forming on the wall for one shot.

The measurement shows that envelope vibration may be a problem at PRF's around 400 and 800 Hz. We have operated the flashlamp at 500 Hz, however, with no difficulty.

Power Distribution in Flashlamp

The electrical energy stored in the capacitor is distributed into different parts of the flashlamp circuit when the flashlamp is discharged. It is important to know how the stored energy is distributed so we can determine the heat loading in repetition rate operation on the various elements of the circuit. The maximum heat loading allowed by any particular element determines the maximum power input to the flashlamp.

The energy lost in the rotary spark gap was calculated from measurements made of the circuit current and voltage waveforms. Knowing the instantaneous voltage drop across the spark gap and the current, we calculated a 6 percent loss in the spark gap. A certain amount of energy is lost to the circuit resistance. This loss was not measured, but should amount to no more than a fraction of a percent if the circuit resistance is kept well below the minimum arc resistance (.06Ω). The discharging arc heats the electrodes at the terminating points of the arc. This loss is not easy to measure in our system and is inferred from the difference between the total energy and the sum of all the other losses.

The electrical energy deposited in the arc goes into three separate places; the acoustic shock, optical radiation, and heat. The energy used to produce the acoustic shock was estimated in the section entitled Energy in Acoustic Shock as 2.6 percent. The optical energy for $\lambda > 190$ nm was measured both calorimetrically and radiometrically. A calorimeter was made from two concentric copper cylinders. The cylinders were insulated from each other with spacers and the inside of the inner cylinder was painted black to absorb all the flashlamp light. A heater wire was placed on the outside surface of the inner cylinder to calibrate the instrument with a known heat input. The calorimeter was then placed over the 6 cm flashlamp to measure the total light energy transmitted. Figure II-15 shows the results of the calorimetric measurement; 14 percent of the input energy is transmitted as light from the flashlamp. This result also agrees with a measurement made on the flashlamp spectra with a calibrated spectroradiometer. The radiometer measurements will be discussed in the section entitled Optical Characteristics. The optical energy measurements are only good for $\lambda > 190$ nm where the fused quartz envelope is transparent; radiation emitted for $\lambda < 190$ nm would be absorbed by the envelope. There is an additional amount of light blocked by the ends of the flashlamp; this amounts to about 20 percent of the total light emitted. Therefore, since the calorimeter measured 14 percent transmitted out the side of the flashlamp, a total of about 17 percent of the energy discharged is emitted as optical radiation ($\lambda > 190$ nm) by the discharge.

The average temperature of the argon gas exiting the flashlamp was measured with a 15 mil thermocouple placed inside the hollow bore of the grounded electrode and near the tip of the electrode. Figure II-16 is a stripchart recording of the gas temperature taken during a run at 5750 watts input. The exhaust gas temperature reaches equilibrium in about 10 seconds at a value of 740°C above room temperature. The rate of heat removal by the ejected gas is given by

$$\dot{Q} = \dot{m}\, C_p\, \Delta T$$

where $\dot{m}$ is the mass flow of the gas, C_p the specific heat, and ΔT the temperature rise. The mass flow of the argon was 8.92 g/sec. This gives 3430 watts or 60 percent of the input power.

The flashlamp had a double walled, fused quartz envelope. This construction allowed cooling of the surface of the inner flashlamp envelope by flowing nitrogen gas or water between the two quartz cylinders. We measured the temperature rise of nitrogen gas flowing between the double walled envelope. In a manner described above we could then calculate the heat carried away by the nitrogen from the outside surface of the inner quartz tube. With the 5 kW average power into the flashlamp the temperature of the nitrogen cooling gas stabilized at 100-105°C after one minute of operation. Knowing the mass flow and heat capacity of the gas, we computed that 180 watts or 3.6 percent of the total input power was being carried away from the surface of the lamp envelope. The argon flowing around the inside surface probably removes about another 3.6 percent of heat from the quartz wall.

The flashlamp wall is heated from three sources: absorption of radiation, damping of the acoustic shock, and heat diffusion from the hot arc region. The diffusion of heat from the arc region can be calculated by solving the steady state heat conduction equation, using the azimuthal symmetry of the flashlamp geometry. The heat flow per unit length from the hot arc to the outside of the quartz wall by diffusion is given by

$$\dot{q} = 2\pi(T_1-T_3)k_A k_Q/[k_Q \ln(r_2/r_1) + k_A \ln(r_3/r_2)]$$

where T_1 is the average temperature in the arc zone; T_3 the temperature of the outside wall; k_A and k_Q the thermal conductivities of argon and quartz; r_1, r_2 and r_3 the radii of the arc, inner surface, and outer surface of the quartz wall. At 20 kW input power $T_1 \approx 2620°C$, $T_3 \approx$ room temperature. Using the dimensions of the flashlamp, we obtain 80 watts transferred to the outside wall. This represents only .4 percent of the input power. The convection of heat to the wall is avoided by the vortex flow which continually flows inward and carries the majority of the heat out the center of the electrodes.

The heat deposited in the wall from vibration damping of the shock front impact would also represent a smallfraction of the wall heat loading since the fraction of power into the acoustic wave is itself only about 2.6 percent. The actual fraction of the 2.6 percent that heats the quartz wall by vibration dampening was not determined.

Data published by the synthetic quartz manufacturers shows that less than 1/2 percent of the radiation between 190 nm $< \lambda <$ 3000 nm is absorbed. The majority of the wall heating, then, must come from radiation absorption for $\lambda <$ 190 nm and $\lambda >$ 3000 nm.

Figure II-17 summarizes the approximate power distribution for the flashlamp. The electrode heating of about 10 percent makes up the difference to give 100 percent. The temperature rise of the electrode cooling water was measured with a 5 kw input. This indicated that 55 percent of the power input was being carried away by the

cooling water from both electrodes. The majority of this heat, however, comes from cooling the hot gas exhausted through the long narrow opening in the center of the electrodes.

Flashlamp Cooling and Thermal Limits

Cooling the Flashlamp

When operating the flashlamp for periods of 5 to 10 minutes at 15 kW average power we found that the quartz envelope would heat to a reddish glow (probably about 700-900°C). The flashlamp was modified to include a double walled tube to allow cooling the envelope. Initially, we attempted to cool the envelope by flowing water between the two quartz tubes. With water cooling the flashlamp would run for only a few seconds before the quartz tubes would burst into thousands of pieces. This result was observed with both the 6 cm and 10 cm flashlamps and when using cooling water that was run through a deionizer before entering the lamp housing.

We found that the flashlamp was breaking because the arc would suddenly form along the envelope wall after a few seconds of running. Shortly after jumping to the wall the arc would thermally stress the quartz tube to its breaking strength. We suspect that impurities or dissolved gases in the water were being ionized by the uv light. This action produced a conducting cylinder around the flashlamp and destabilized the arc so that it had a high probability of forming along the surface of the envelope.

It is also interesting to note that a large number of bubbles were formed in the water jacket immediately after starting the flashlamp at repetition rate and long before the water could have a chance to boil. The acoustic impact produces an intense ultrasonic wave in the liquid that may have caused the release of dissolved gases from the solution. Because of these problems water cooling of the flashlamp envelope was abandoned in favor of nitrogen gas cooling. In the section entitled Power Distribution in Flashlamp, we showed that the amount of heat that must be removed from the flashlamp envelope is only about 4 percent of the input power. To cool the flashlamp envelope at 25 kW input, for example, would require a nitrogen flow of about 2.5 ℓ/sec (STP) with a temperature rise of 300°C. With water cooling, on the other hand, we would need only a flow of 1 ℓ/min with a 15° temperature rise to handle the heat flow.

Figure II-18 shows the arrangement used for water cooling the flashlamp electrodes. A closed loop of deionized water is circulated for cooling the high voltage electrode. Tap water, that also passes through the heat exchanger for the deionized water, cools the grounded electrode. The demineralizer can be connected in or out of the circuit loop as shown and is removed from the loop to reduce pump resistance and allow a higher flow rate. The pump flow rate of 8 liters/min can carry away up to 40 kW for a 70°C rise in temperature and is more than adequate for cooling one electrode. The electrodes are designed to allow the cooling water to

flow to the tungsten electrode tips. This removes heat from the tungsten tips and the center bore of the electrodes where the hot gases are being exhausted.

Thermal Stress Limits

The quartz flashlamp envelope is heated mainly by the absorption of far uv and infrared light emitted from the arc discharge. The amount of heat absorbed is about 8 percent of the input power to the flashlamp. The heat must be removed, otherwise the quartz tube would rise in temperature to the strain point (1140°C) and deform. In removing the heat, temperature gradients are set up across the quartz wall. Since the quartz expands, internal stresses are developed which are compressive at the hot boundaries and tensile at the cooler boundaries.

The thermal stress for different temperature differentials across a quartz tube wall is plotted in Fig. II-19. Figure II-20 shows the normal hoop stress at the bursting pressure of several different quartz tubes. These two figures are taken from earlier work completed at UTRC under a NASA contract (Ref. II-11). Figure II-20 shows that a hoop stress of 2000 psi is a safe limit for most quartz tubes. Exceptional quartz tubes, however, if properly annealed and free of high stress point microscratches can withstand hoop stresses up to 7000 psi.

For a 2000 psi stress limit, Fig. II-19 gives a temperature differential of 650°C across the tube wall. Using the thermal conductivity of fused quartz (k), the tube area (A), and the wall thickness (t), we can compute the heat flow across the wall of the tube that can safely be handled as

$$Q = \frac{kA\Delta T}{t} = 7910 \text{ watts.}$$

If water cooling were used then practically all the heat would be removed from the outer surface. With 8% of the input power as the heat to be transferred we obtain 100 kW as a safe limit on the input power to the flashlamp with water cooling.

With nitrogen gas cooling the situation is more complicated. The heat would be removed from both sides of the tube wall. A solution of the steady state heat conduction equation for a uniform deposit of heat gives a parabolic temperature profile in the wall. Since the cooling gases have a low heat capacity in comparison with water, the cooling gas temperature must rise several hundred degrees to accommodate the amount of heat being transferred from the wall. The quartz tube, then, must rise in temperature to an even higher value to transfer the heat to the gas. The maximum temperature allowed in the tube wall would be about 1000°C. At temperatures near 1000°C the quartz can devitrify and develop a haze of very fine cracks (Ref. II-12), and at 1140°C we reach the strain limit of quartz.

We have run the flashlamp safely at input power levels of 15 kW with only convection cooling on the outside surface. In this case the envelope became a dull red. When the envelope cooled back to room temperature no damage was observed. With the forced nitrogen cooling we estimate that we could safely run at long periods with 25 to 50 kW input power. Long term operation of the flashlamp at these power levels has not been tested yet, however.

Optical Characteristics

Use of Different Gases

Flashlamps for most laser applications are filled with the heavy rare gas xenon. Xenon generally gives a higher output/input efficiency for generating light than other gases (Ref. II-1, 10). For very short pulse, high current discharge there exists a limiting radiance (watts/cm^2/ster) for each gas. Generally, the lower atomic weight gases have a higher saturation radiance. The radiance of the lower atomic weight gases, however, is reached more slowly as the power density increases, making them much less efficient radiators at lower power densities (Ref. II-13). For our flashlamp conditions (1 atm pressure, 15 kA peak current, and nonconfinement) it was not clear whether the heavier gases would give a significant advantage in optical output. That is, it is not certain at what point of the radiance saturation the lamp is operating. Furumoto and Ceccon have shown, for example, that for wall stabilized, coaxial flashlamps a low pressure xenon fill is about twice as efficient as an argon fill for pumping a dye laser (Ref. II-14).

Our present vortex stabilized flashlamp exhausts the gas flowing through the lamp to the atmosphere. This makes the use of the heavier and more expensive gases such as xenon and krypton impractical. A well sealed, impurity free, closed cycle pump could be built, however, that would allow use to use the heavier gases.

In order to evaluate the effectiveness of different gases for our vortex flashlamp we constructed a sealed-off, noncirculating flashlamp with a 6 cm electrode spacing. The flashlamp was connected to a gas filling station. Optical power or energy from the sealed off flashlamp was measured with different gas fills. Figure II-21 shows a comparison of the light intensity from 3 different gas fills and an ablating wall flashlamp (Ref. II-15). We found that the rare gas gave more light output when a small amount of an impurity gas like nitrogen or CO_2 was present. The reason for this is not presently understood. The gas fill pressures for Fig. II-21 are 1 atm except for the ablating wall lamp which is discussed by Ferrar (Ref. II-15). From Fig. II-21 we see that xenon has about 13 percent more peak light power and over 50 percent more light energy output than argon. Most of the increase in light energy, however, comes at times after the laser pulse has terminated.

We placed a small cell filled with rhodamine 6G in ethanol near the sealed off flashlamp. By monitoring the fluorescence output we could determine the effectiveness of the different gas fills in exciting the dye. Figure II-22 shows the fluorescence intensity for 200 J discharges in pure xenon, pure argon, xenon with N_2 impurity and argon with N_2 impurity. First of all the fluorescence results show a large effect of adding the impurity gas N_2, especially on the peak output with an argon fill where the intensity was increased by 250 percent. Figure II-22 also shows practically no difference in the peak fluorescence output between an argon-N_2 fill and a xenon-N_2 fill. The xenon again gives more total light output with a longer pulse. The longer pulse may not be useful, though, in the laser pumping due to an early termination of the laser pulse by acousto-optic distortion which occurs after the first 2 μsec of the pumping pulse. With 12 J discharge energies, we found that the fluorescence intensity from the xenon-N_2 discharge was 80 percent greater than from the argon-N_2 discharges. This implies we have nearly reached the saturation power in xenon, with the 200 J discharges.

Since xenon is 3.3 times as dense as argon we can expect that the arc column will not expand as much with xenon as with argon. In fact, from the section entitled Flashlamp Gasdynamics, we know that the column radius is inversely proportional to the 1/4 power of the gas density. This implies that the discharge diameter in xenon would be about 75 percent of that in argon. Therefore, the radiance of the arc would be about 25 percent greater for xenon. The effective optical power for generating fluorescence, however, is the same. If the dye laser were operating near the threshold pumping level than the xenon could produce an improvement in laser output with a focused reflector to take advantage of the increased flux available from the smaller arc. The laser, however, operates many times over threshold, and consequently, the small increased radiance from the use of xenon would not be of any great significance in the laser output.

A small amount of CO_2 was originally added to the argon to increase the breakdown voltage of the flashlamps. It was found that the CO_2 also gives an increase in the light output from the flashlamp. Figure II-23 shows the results of optical energy measurements from the sealed off flashlamp with a one atmosphere fill of argon and the listed partial pressure of N_2 and CO_2. After about 50 torr of N_2 the flashlamp light output begins to decrease. This is not shown in Fig. II-23. We currently use N_2 in the vortex flashlamp to produce the sustained glow discharge as discussed in the section entitled Flashlamp Gasdynamics.

Energy, Power, and Spectrum

The spectral irradiance from the flashlamp was measured with a 1/4 meter monochromator and photomultiplier. A quartz diffuser plate was placed just ahead of the entrance slit on the monochromator to allow a uniform illustration of the grating and photocathode. This system was carefully calibrated using two quartz iodine standard lamps (Ref. II-16). The monochromator was placed so that the diffuser plate was 1 meter from the axis of the flashlamp. The flashlamp arc was

then completely blocked except for a 1.0 mm section at about the middle of the arc. By measuring the voltage produced across a resistor by the photodetector current, we could determine the peak spectral irradiance in watts/cm^2 from the flashlamp at chosen wavelengths from the ultraviolet to the red. For light attenuation and spectral blocking that was required at certain wavelengths, 4 neutral density filters and 6 color filters were calibrated throughout the spectrum. The calibration accuracy was estimated to be 12 percent at the visible wavelengths and about 20 percent at the uv wavelengths.

Figure II-24 shows the results of the optical power and energy measurements from the flashlamp for 1 mm of exposed arc at $\lambda < 500$ nm. To include the entire 60 mm arc we must multiply the scales in Fig. II-24 by 60. From these results we see that the peak power of the flashlamp is starting to saturate for energy inputs greater than 200 J. The optical energy, however, continues to increase about linearly; that is, the light pulse duration is increasing but not the peak power as we continue to discharge more energy. In fact, if we also consider the increasing arc diameter we find that the radiance of the arc (watts/cm^2/ster) saturates at a lower input level of 100 J. Two possible explanations for this effect were given by Marshak (Ref. II-10). One explanation proposed the locking in of radiation at the higher input energies by an outside layer on the arc that has a high optical density. The other explanation which seemed more plausible was that the effective specific heat of the arc plasma increases at such a steep rate that further appreciable increase in T would call for an increase in energy concentration in the discharge, something difficult to attain the practice. The specific heat of the plasma increases because more energy is going into producing higher order ionization at the expense of a temperature rise.

The peak irradiance measurements taken from the oscilloscope traces, were made at the monochromator calibration points from 250 nm to 700 nm. These measurements are shown by the circles in Fig. II-25. The spectral measurement indicates a continuous radiation at the visible wavelengths and probably some line emission in the uv. To compare these results with a blackbody radiation that has the same dimensions as the flashlamp arc we must calculate the radiance (N_λ) in terms of the irradiance (H_λ). This is given by

$$H_\lambda = \int_{\text{arc surface}} N_\lambda \Omega \cos\theta \, dA \approx N_\lambda \ell d/R^2$$

where Ω is the solid angle to 1 cm^2 at the detector, ℓ the arc length, d the arc diameter, and R the distance from the arc to the detector. The approximations use the fact that R$\gg$d and ℓ. For an equivalent blackbody source

$$N_\lambda = 1.19 \times 10^{-19}/\lambda^5\{\exp(1.438/_\lambda T) - 1\}$$

in units of watts/ster-cm^2-nm.

Then,

$$H_\lambda = 8.34 \times 10^{-25}/\lambda^5 \{\exp(1.438/\lambda T)-1\}$$

in units of watts/cm^2-nm for the blackbody. The solid line curve in Fig. II-25 gives the results of the above formula for H_λ with T = 24,540°K. This temperature, then, approximates the radiating plasma temperature in the arc channel for a 150 J discharge.

To estimate the total output power from the lamp at its peak irradiance we take the area under the spectral irradiance curve (Fig. II-25) and multiply by 60 mm to allow for the entire arc length. The peak light power generated by the lamp is then found by multiplying the later figure by the ratio of the solid angle from a cylindrical radiating surface (π^2) to the solid angle of 1 cm^2 at a 1 meter distance. Thus

$$P_{FL} = \pi^2 10^4 \int H_\lambda d_\lambda \approx 6.2 \text{ MW}$$

The peak power discharged by the capacitor into the flashlamp circuit is estimated from the light pulse or current duration as 43 MW. The electrical to optical efficiency for the flashlamp is then η_{FL} = 6.2 MW/43 MW = .14 or 14 percent. It is interesting to compare the flashlamp total power with the total power that would be emitted by a 24, 540°K blackbody.

$$P_{BB} = \pi A \sigma T^4 = 84.7 \text{ MW}$$

where σ is the Stefan-Boltzmann constant and A the area of the lamp surface. This result shows that the discharge cannot possible radiate as a blackbody over the entire spectrum.

Figure II-26 shows a more detailed spectrum of the flashlamp from λ 450 nm to λ 300 nm. The spectrum was taken with a 1.5 m spectrograph in several sections. Three sections are overlayed in the figure. The spectral lines from a mercury calibration lamp are shown just below the flashlamp spectrum to identify the wavelengths. The spectrographic data shows that the flashlamp spectrum is not a continuum for $\lambda < 500$ nm, and indeed, consists of a broad diffuse line spectra. There is a particularly strong band system around 357 nm. This emission is thought to be created by the argon metastable atoms transferring energy to the nitrogen molecules as in the case of an argon-nitrogen transfer laser (Ref. II-17). The transfer process could explain the increase in optical power we observed when we add N_2 or CO_2 to the argon discharge. The N_2 or CO_2 molecules in this case could be deactivating the excited metastable argon atoms making them available for excitation and reemission.

Effect of Repetition Rate

When the flashlamp is run at 100 Hz repetition rate and 200 J per pulse we found that the peak intensity would fall off about 5 to 10 percent after the first few shots and then reach a steady state value. Further investigation showed that the fall off was even greater at higher repetition rates. In addition, we found that the fall off in peak intensity was very sensitive to the flashlamp pressure if the pressure was below a critical value. The flashlamp pressure was monitored with a gauge on the grounded electrode housing. Since the mass flow of gas through the flashlamp is proportional to the square root of the pressure, the lamp pressure also gives a measure of the gas flow. If the gas flow was reduced too low, the flashlamp would explode at high power inputs. This occurred at 5 psig and 250 Hz in one instance.

Figure II-27a and b show overlaying traces of the steady state flashlamp intensity for two different pressures and repetition rates. Both "a" and "b" are for 200 J discharges, but a 4 F capacitor was used for the traces in "a" and a 2 F capacitor was used for the traces in "b". This is the reason for the difference in pulse shape. The vertical scales of "a" and "b" are not related.

The flashlamp light was monitored with an SD-100 solid state photodiode that has maximum sensitivity in the red and near infrared part of the spectrum and no sensitivity for $\lambda < 360$ nm. As a consequence, the pulses in Fig. II-27 shows a biased part of the spectrum. The actual drop in intensity in the uv could be much larger than indicated in Fig. II-27, although this was not measured.

The most likely cause of the flashlamp intensity falling down to a much lower, steady state value is the reduction in gas density due to heating the incoming gas prior to succeeding shots. Previous measurements we have made show that a reduction in gas density below 1 atm effects the light output from an argon discharge. The very hot gas in the luminous arc region is well removed between shots; however, the incoming gas could be heated in several ways: 1) by diffusion of heat from the hot arc region, 2) direct heating of the gas from the arc plasma extending around the electrodes, 3) heat removal by the argon from the flashlamp wall. We are uncertain as to which of the three heating mechanisms is predominant. The second effect, however, seems most likely since at lower pressures we have observed the plasma to extend significantly around the electrode tips. The hotter gas decreases the gas density in the flashlamp. In fact, from our measurements of light output vs argon gas density, we can conclude that a 10 percent drop in light intensity requires only a 90°C rise in gas temperature. A 50 percent drop in light intensity requires a 1700°C temperature rise.

Second Light Pulse

When we monitored the flashlamp light pulse with a longer oscilloscope trace we found a second light pulse occuring 28 μsec after the main light pulse. Figure

II-28 shows traces of the flashlamp intensity taken with a red filter and a blue filter in front of the photodiode. The simultaneous discharge current is shown by the bottom trace. It is interesting to note that no current flows through the flashlamp at the time of the second light burst.

The first explanation for the light burst was that the shock wave, after reflecting from the flashlamp wall, returned to recompress the gas and raise its temperature back to a high enough level for reemission. The time for a sound wave to go out to the wall and back would be about 100 μsec. If we use the results of the shock wave analysis in the section entitled Flashlamp Gasdynamics we get 67 μsec. This result does not agree with the observed 28 μsec delay.

What could be happening is that, as the low density arc volume rapidly cools, the higher pressure in the shock front forces gas back toward the arc region and compresses the lower density, core raising its temperature back to the observed reemission level. This process could occur long before the shock front travels out and back from the wall.

The second light pulse becomes more intense with larger discharge energies and occurs at earlier times when the flashlamp pressure is reduced. In fact, in Fig. II-27 a one can just barely see the start of the second light pulse at about 9.2 μsec in the trace with the lower pressure. The initiating time of the second light pulse also decreases with increasing repetition rate of the flashlamp. This is seen in Fig. II-27b where the second light pulse starts at 6.5 μsec for the 250 Hz repetition rate. This is a further indication that the initial gas temperature has increased, and hence the gas density decreased, at higher input powers.

REFERENCES FOR SECTION II

II-1. EG&G Data Sheet 1002-D; ILC Technical Bulletin No. One, An Introduction to Flashlamps.

II-2. Gray, R.: Proceedings of the 9th Hydrogen Thyratron Symposium (1966).

II-3. Glascoe, G. N. and J. V. Lebacqz: Pulse Generators: Radiation Laboratory Series, (McGraw-Hill, New York, 1948), Vol. 5, p. 278.

II-4. Ferrar, C. M: Rotary Spark Gap Switching for High Power Dye Lasers, Appl. Opt. 13, 1998 (1974).

II-5. Markiewicz, J. P. and J. L. Emmett: Design of Flashlamp Driving Circuits, IEEE JQE QE-2, 707 (1966).

II-6. Somerville, J. M.: The Electric Arc, Methuen's Monographs on Physical Subjects, John Wiley and Sons, Inc., New York, 1959.

II-7. Taylor, G. I.: Proc. Ray Soc. (London) A201, 159 (1950).

II-8. Lin, Shao-Chi: Cylindrical Shock Waves Produced by Instantaneous Energy Release, J. Appl. Phys. 25, 54 (1954).

II-9. Drabkina, S. I.: Theory of the Development of the Channel of the Gas Discharge, JETP 21, 473 (1951).

II-10. Marshak, I. W.: Strong Current Pulsed (Spark) Discharges in Gas, used in Pulsed Light Sources, Sov. Phys. Usp. 5, 478 (1962).

II-11. United Technologies Research Center Report No. J-910900-3, Development and Tests of Small Fused Silica Models of Transparent Walls for the Nuclear Light Bulb Engine, NASA Contract No. SNPC-70 (1970).

II-12. General Electric Company: Fused Quartz Catalog, Form Q16, July 1970.

II-13. Vanyukov, M. P. and A. A. Mak: High-Intensity Pulsed Light Sources, Sov. Phys. Usp. 66, 137 (1958).

II-14. Furumoto, H. W. and H. L. Ceccon: Optical Pumps for Organic Dye Lasers, Appl. Opt. 8, 1613 (1969).

II-15. Ferrar, C. M.: Simple High Intensity Short Pulse Flashlamps, Rev. Sci. Inst. 40, 1436 (1969).

II-16. Stair, R., W. E. Schneider, and J. K. Jackson: A New Standard of Spectral Irradiance, Appl. Opt. 2, 1151 (1963).

II-17. Searles, S. K. and G. A. Hart: Laser Emission at 3577 and 3805 Å in Electron-Beam-Pumped Ar-N_2 Mixtures, Appl. Phys. Lett. 25, 79 (1974).

FIG. II-1

AXIAL FLOW DYE LASER

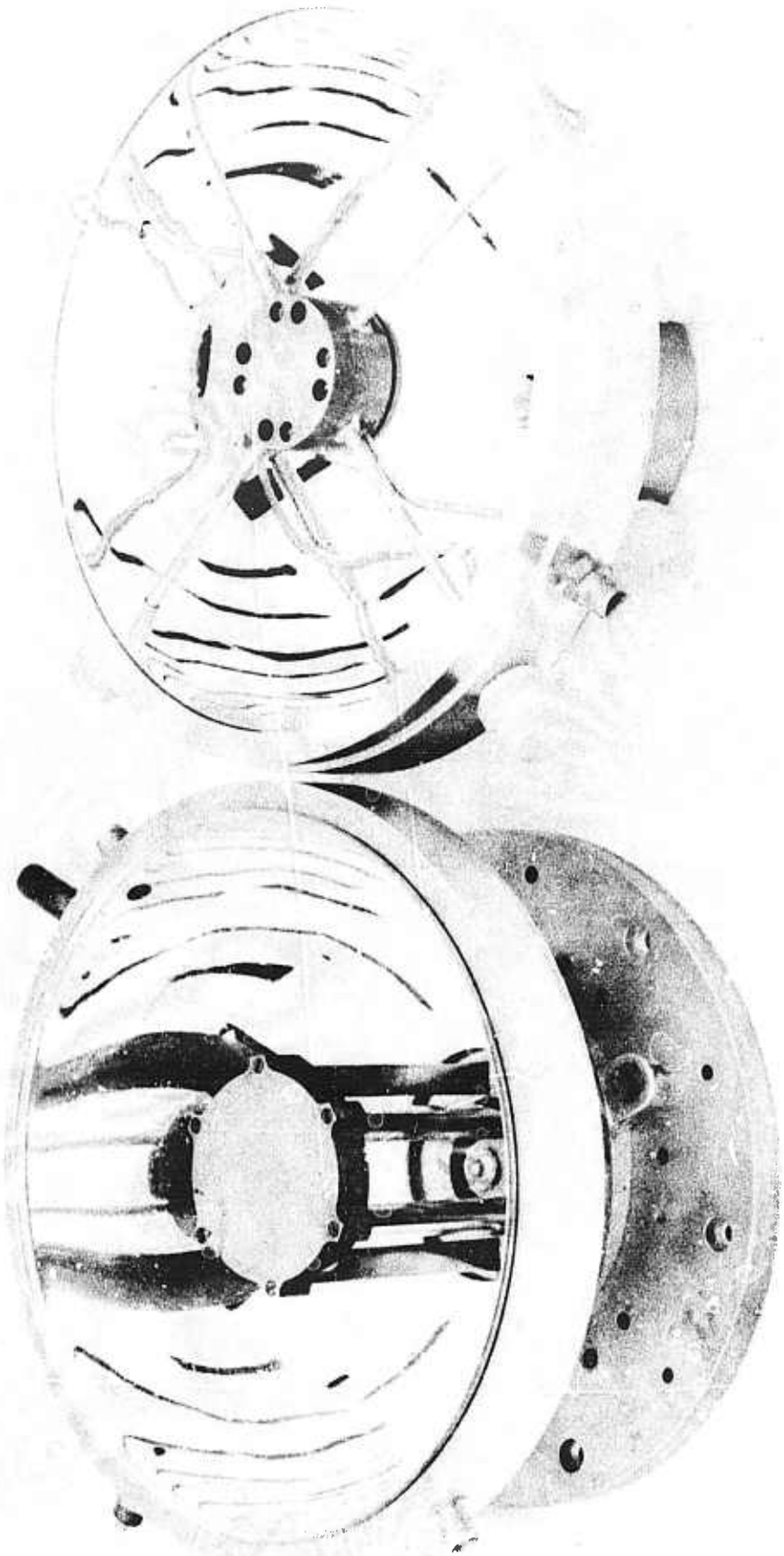

R10-74-37

CONSTRUCTION OF ARC LAMP

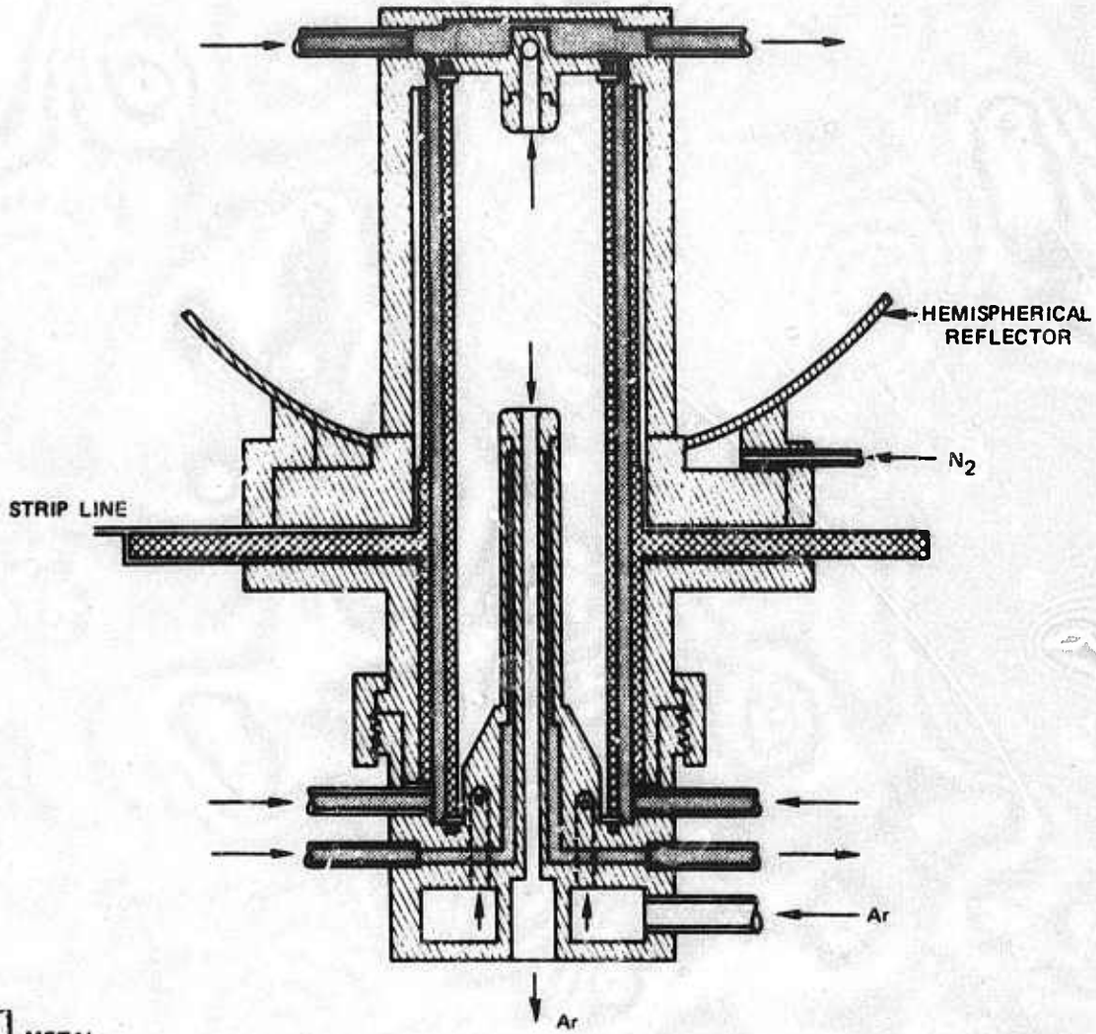

FIG. II–3

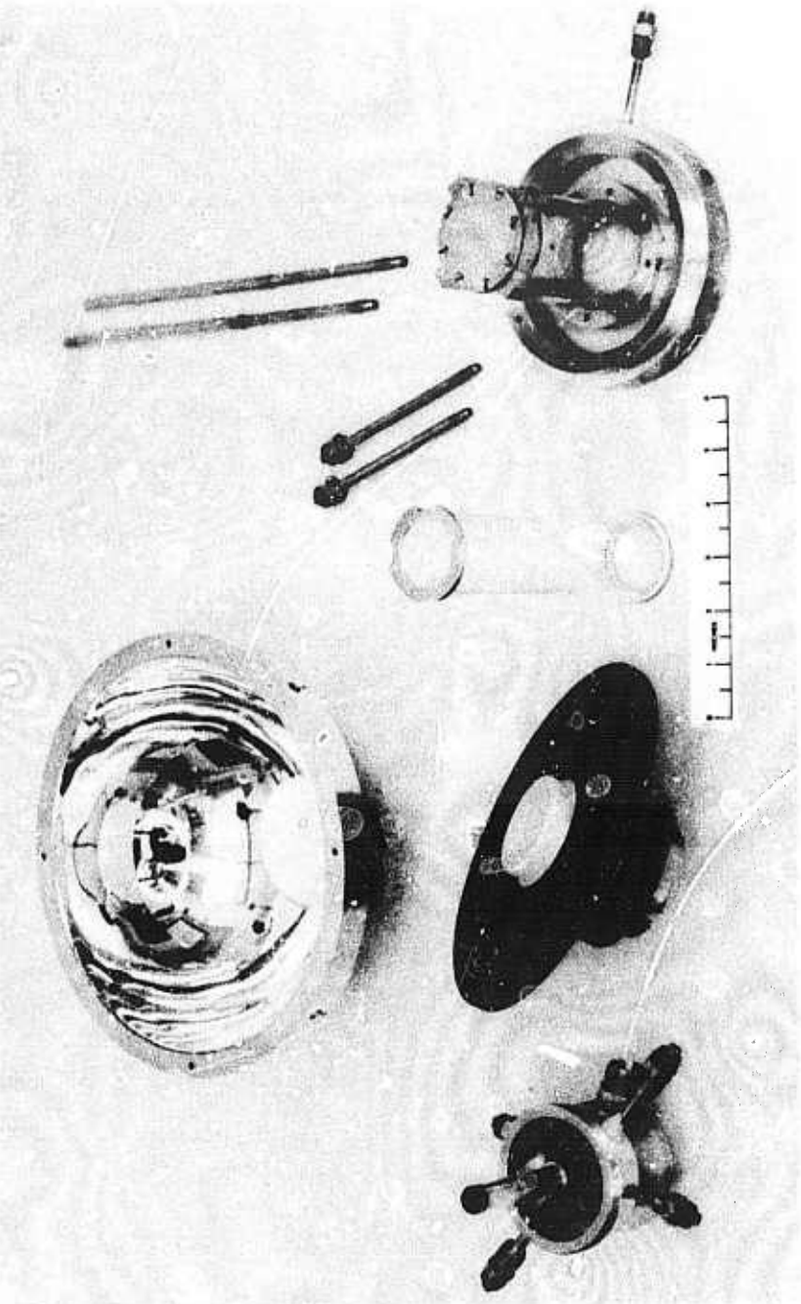

VORTEX STABILIZED FLASHLAMP ASSEMBLY

R10–74–33

FIG. II–4

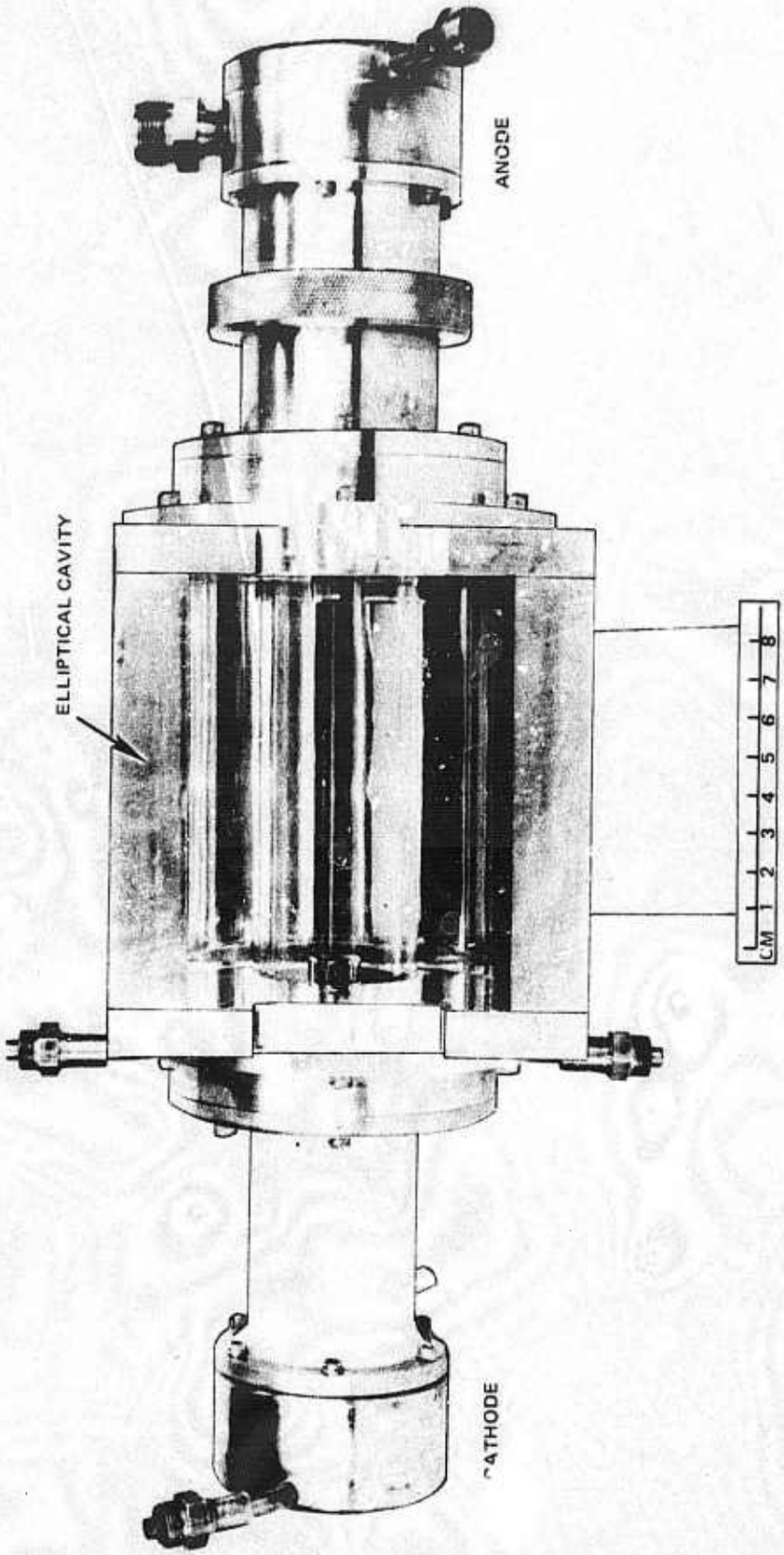

10 CM VORTEX LAMP

FIG. II–5

TWO VIEWS OF 10 CM VORTEX STABILIZED FLASHLAMP OPERATING AT 257 Hz WITH 204J DISCHARGES (52 kW AVERAGE POWER)

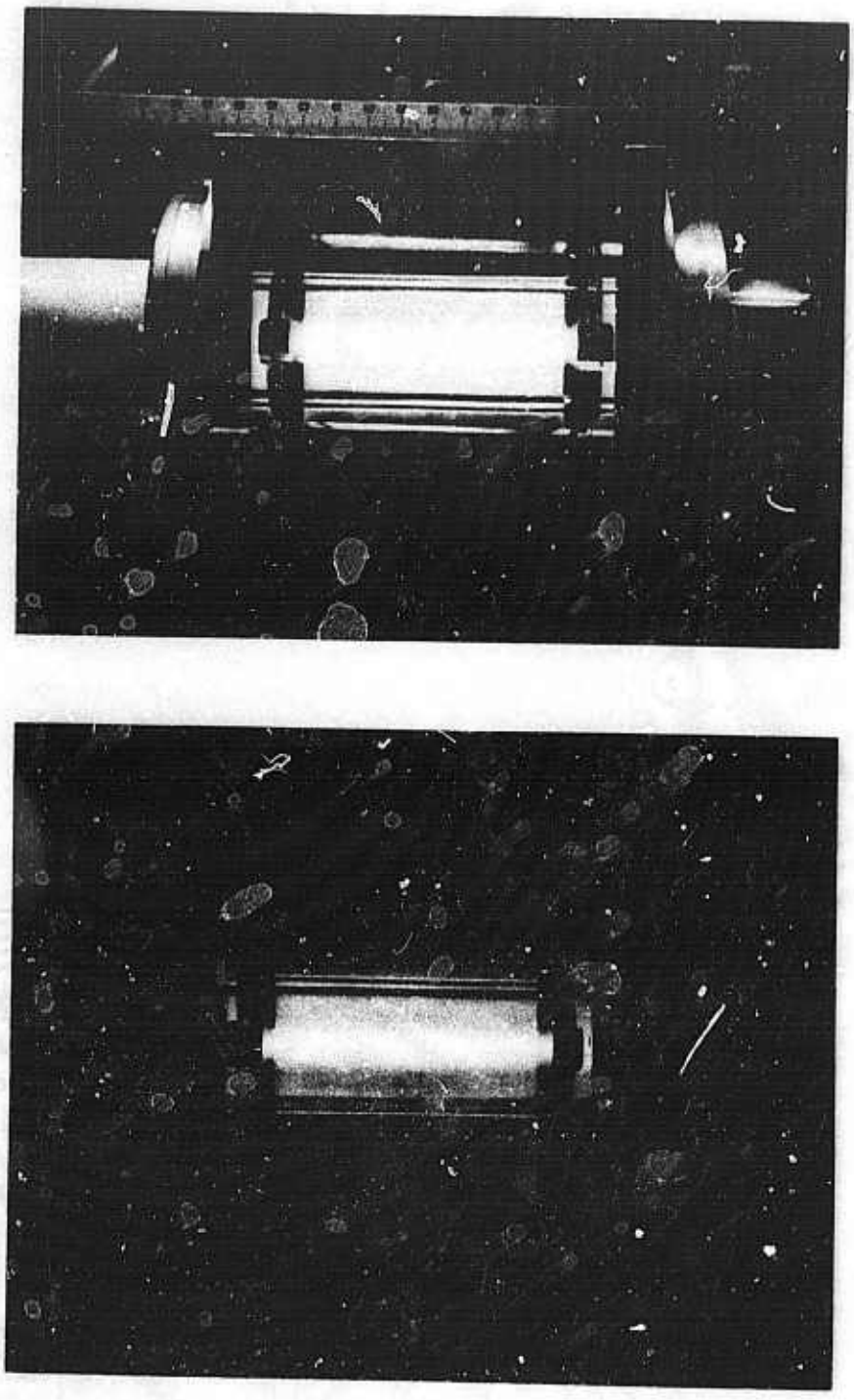

FIG. II–6

ELECTRICAL CIRCUIT FOR HIGH POWER FLASHLAMP

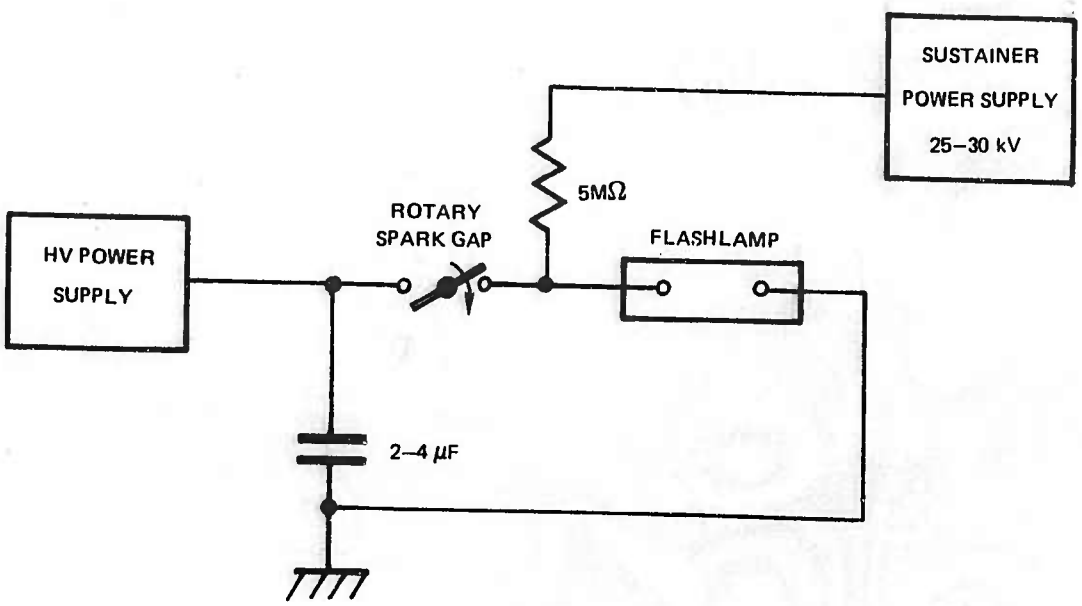

ROTARY GAP SCHEMATIC

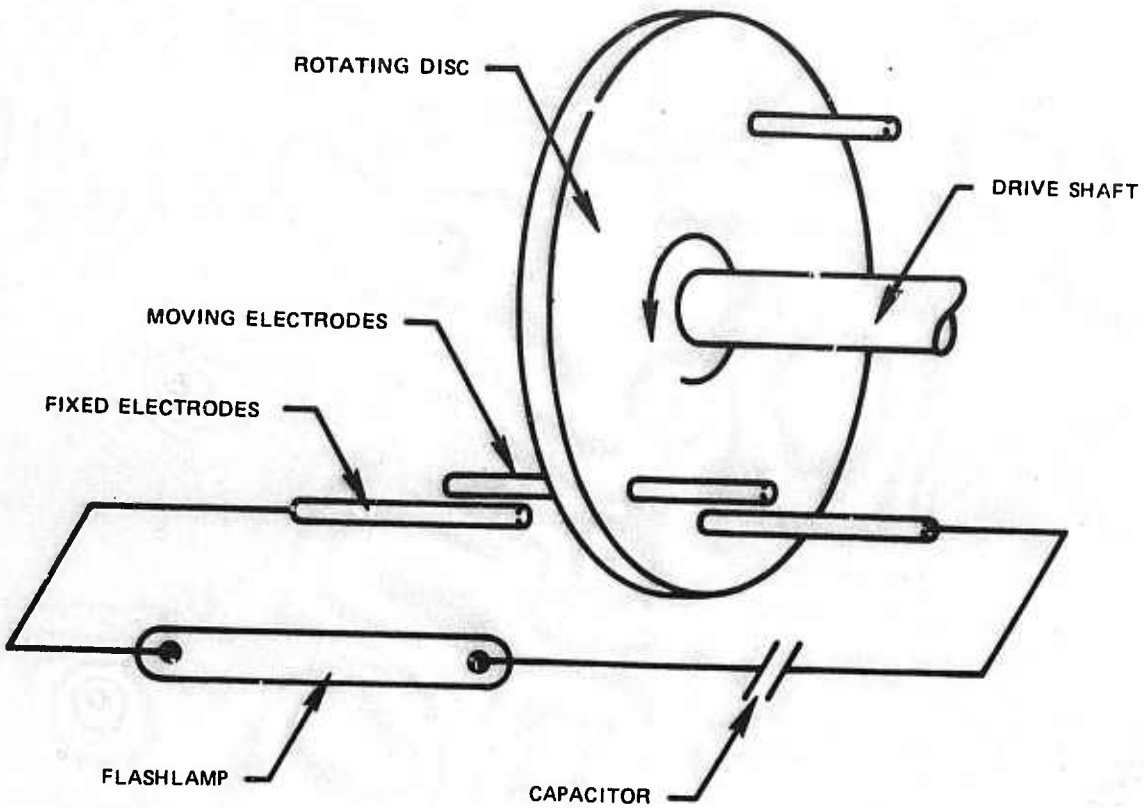

ROTARY SPARK GAP AND STRIP LINE ASSEMBLY

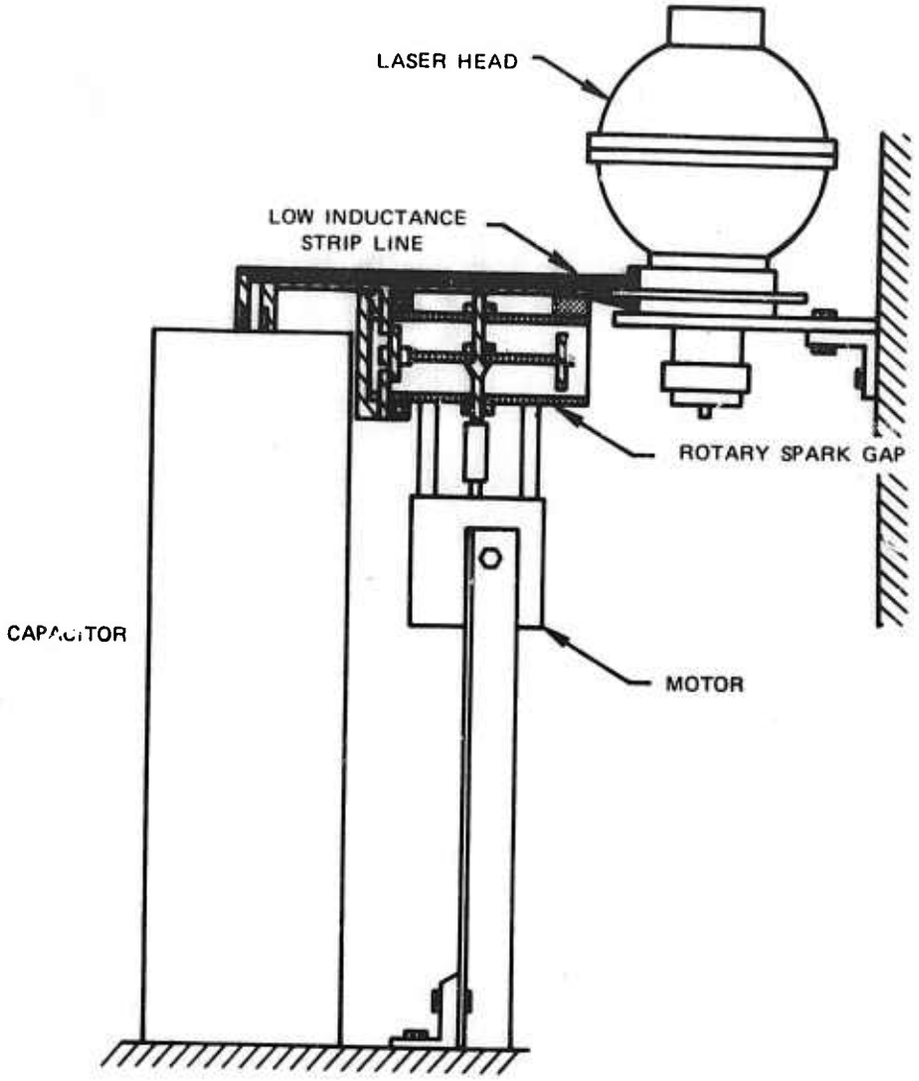

FIG. II-9

10 CM FLASHLAMP VOLTAGE AND CURRENT WAVEFORMS WITH 4 μF CAPACITOR DISCHARGING 200J

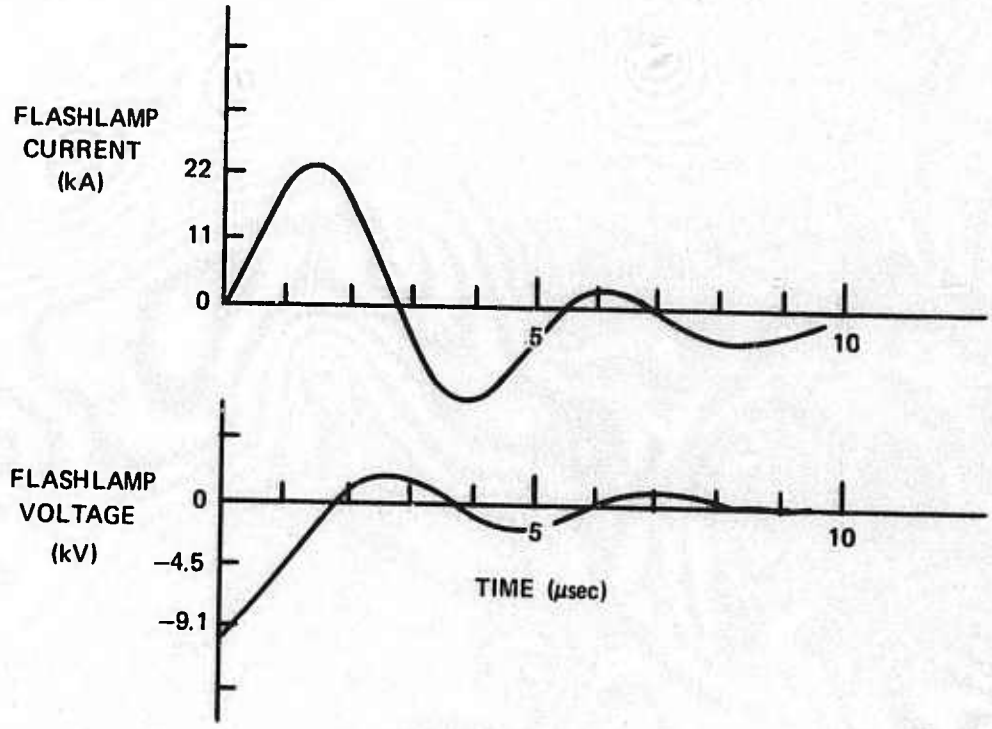

FIG. II–10

FLASHLAMP PRESSURE GRADIENT CREATED BY VORTEX FLOW

ℓ = 6 CM

r_e = 0.35

r_o = 2.0 cm

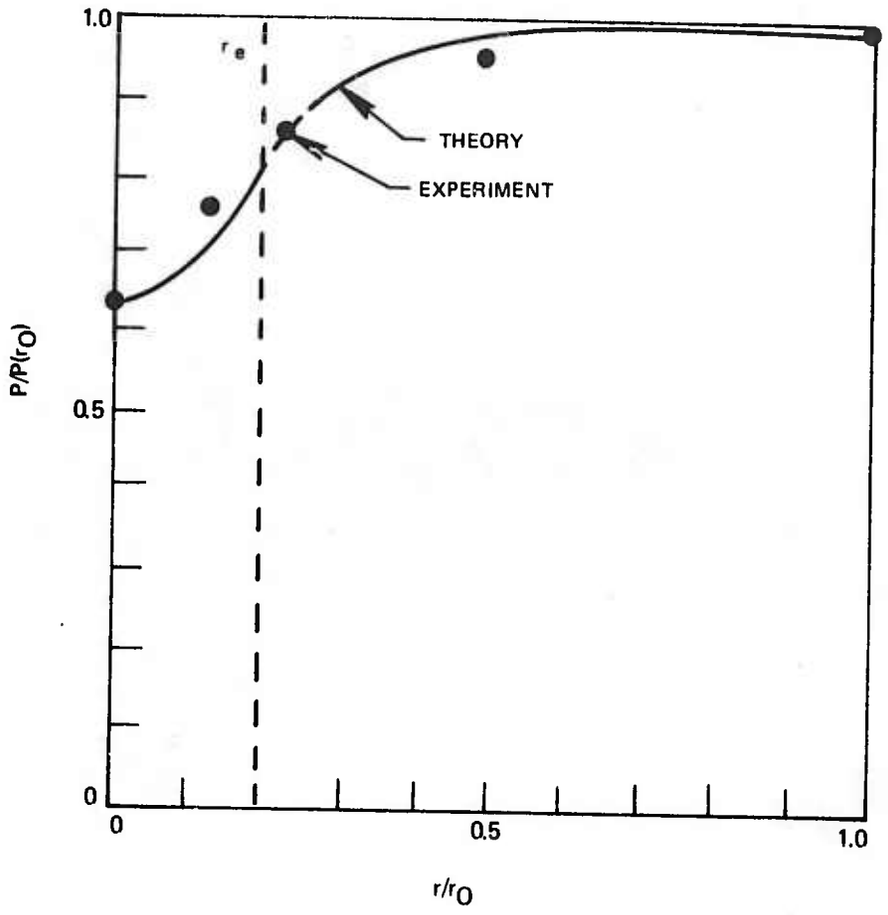

FIG. II-11

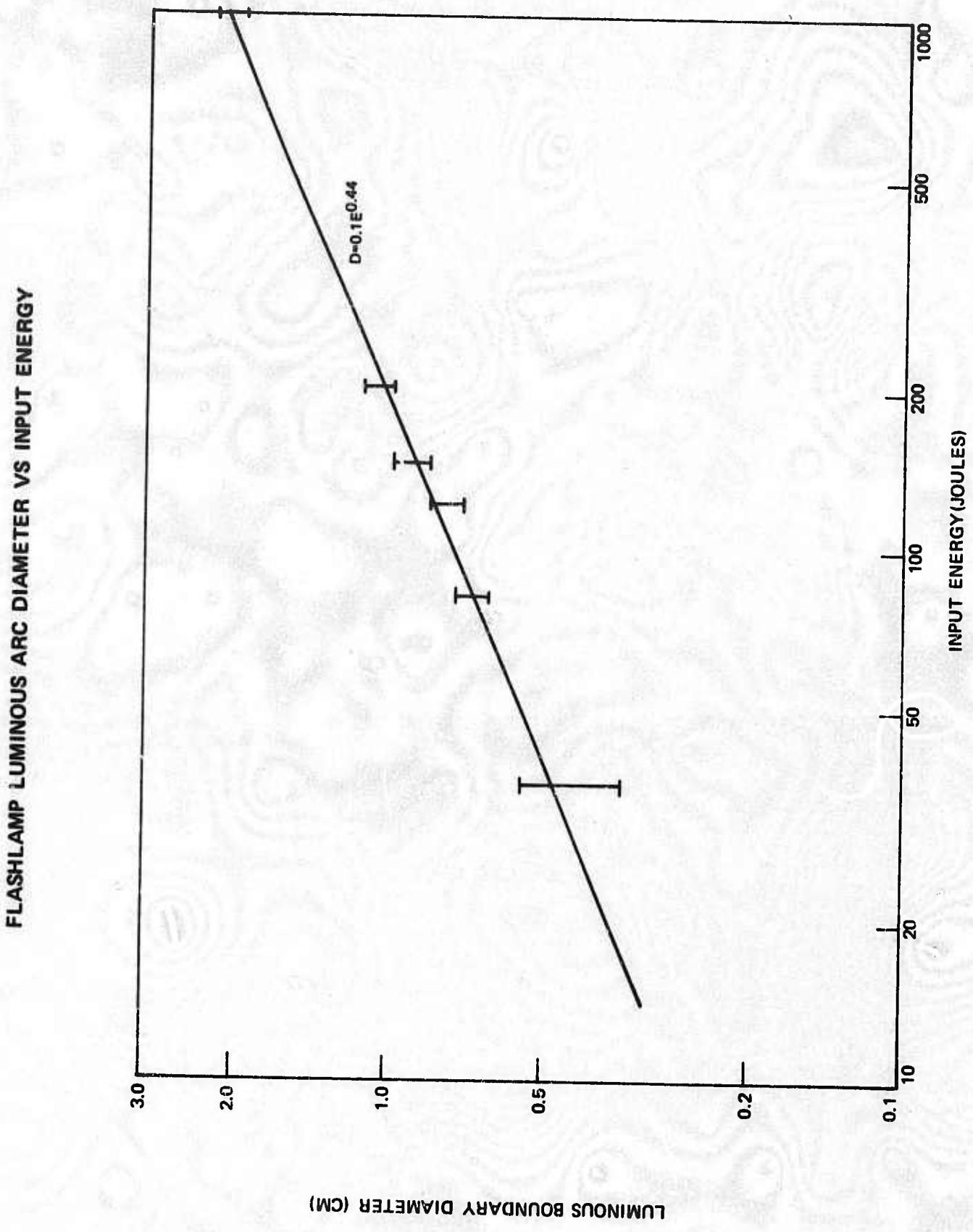

R10-74-14

FIG. II–12

EXPANSION OF ARC

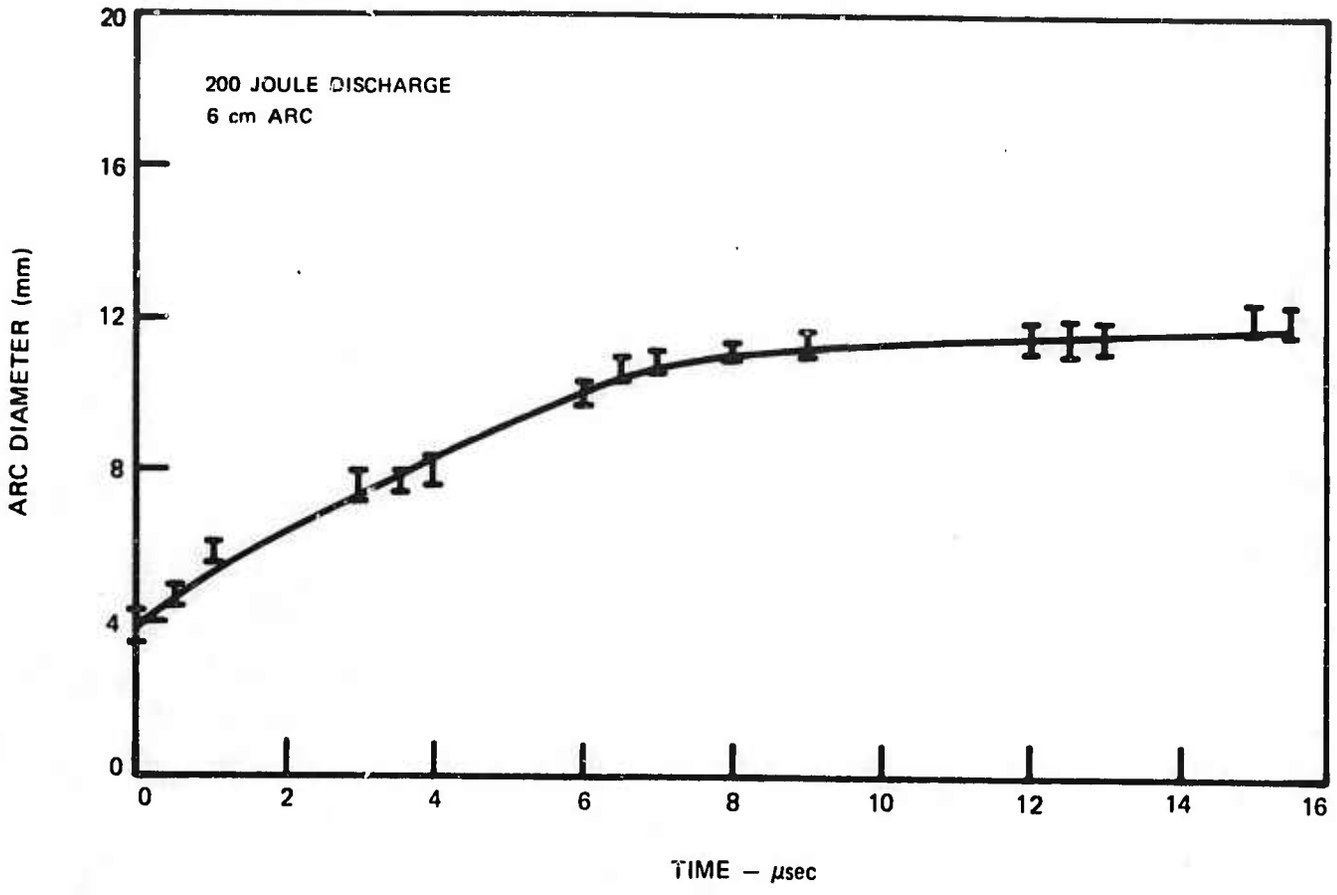

R10–74–26

FIG. II-13

SHOCK WAVE IN FLASHLAMP

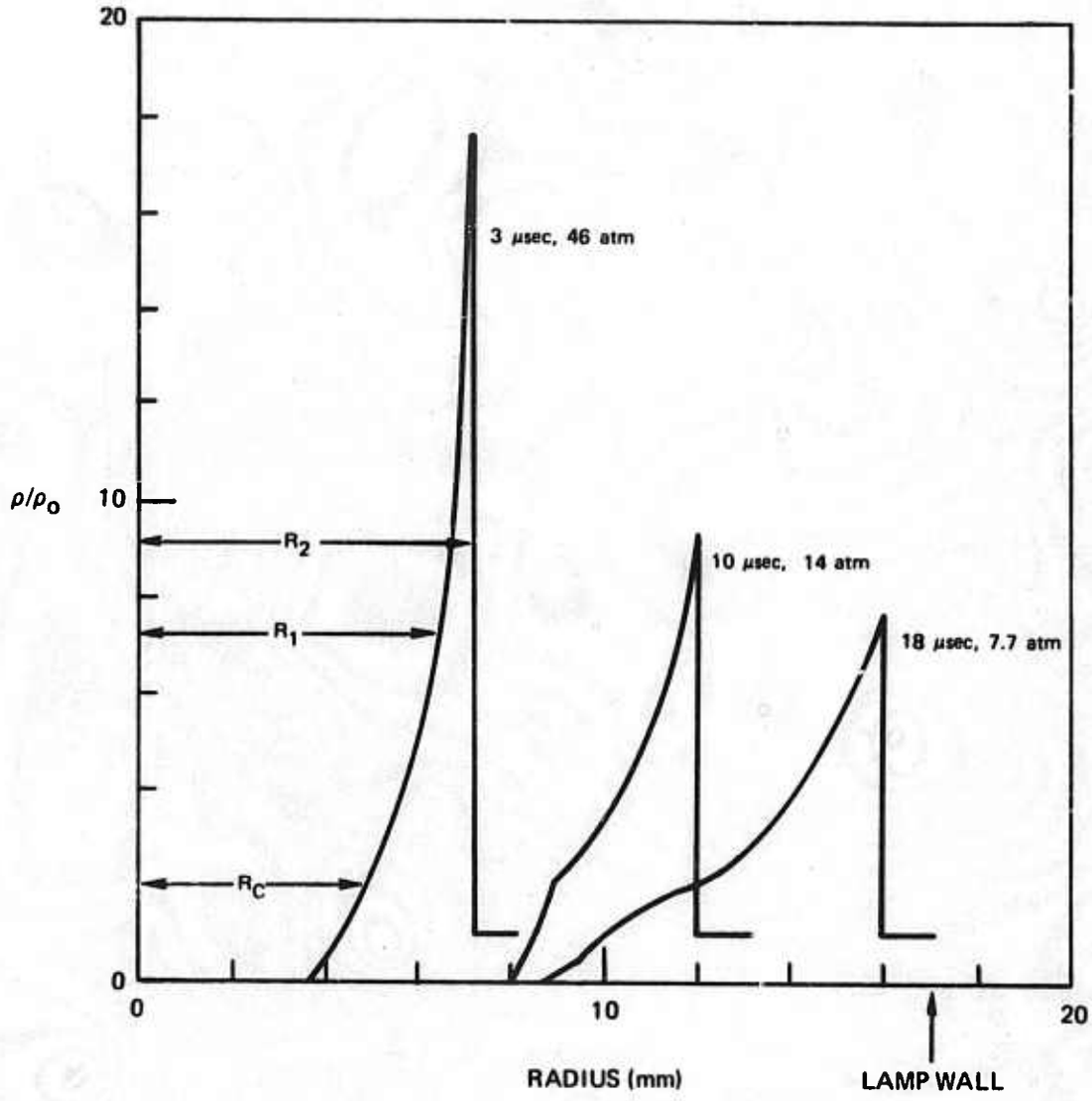

R10-118-1

FIG. II-14

ENVELOPE VIBRATION

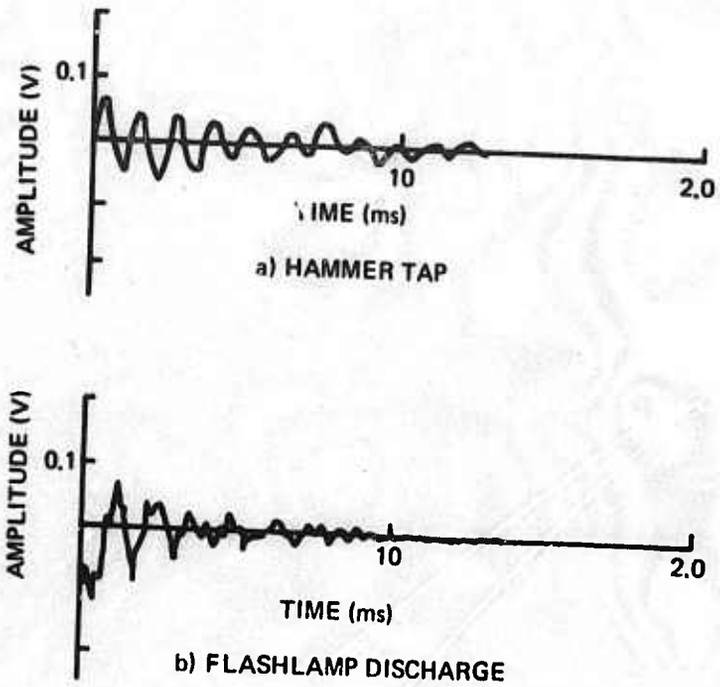

FIG. II-15

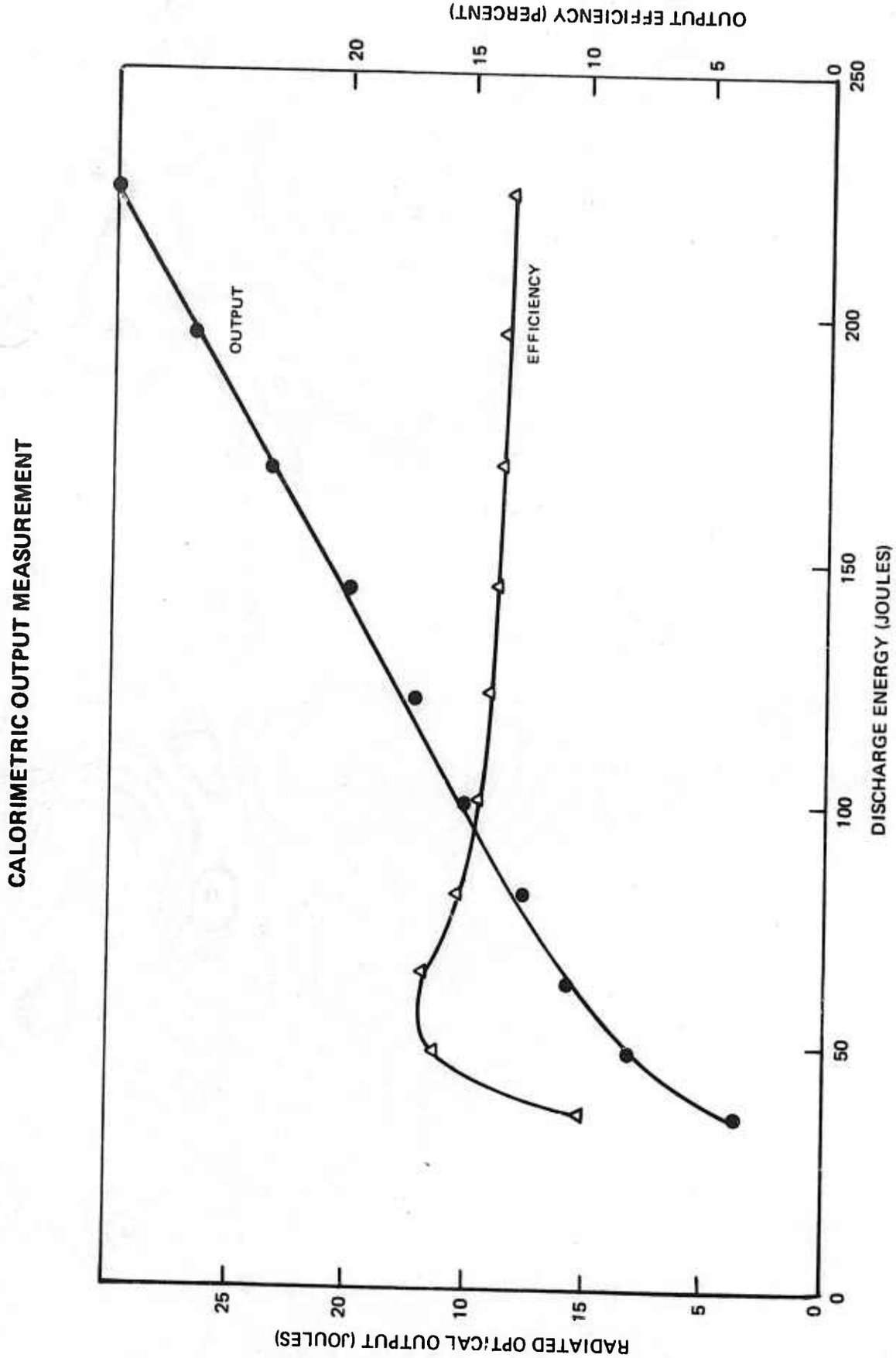

R10-74-6

FIG. II-16

FLASHLAMP EXHAUST GAS TEMPERATURE RISE

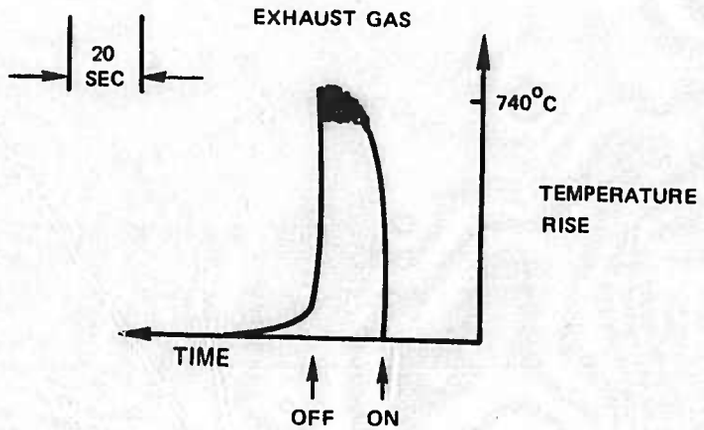

5750 WATTS INPUT

N09-162-9

FIG. II–17

ENERGY BALANCE FOR VORTEX DRIVEN FLASHLAMP

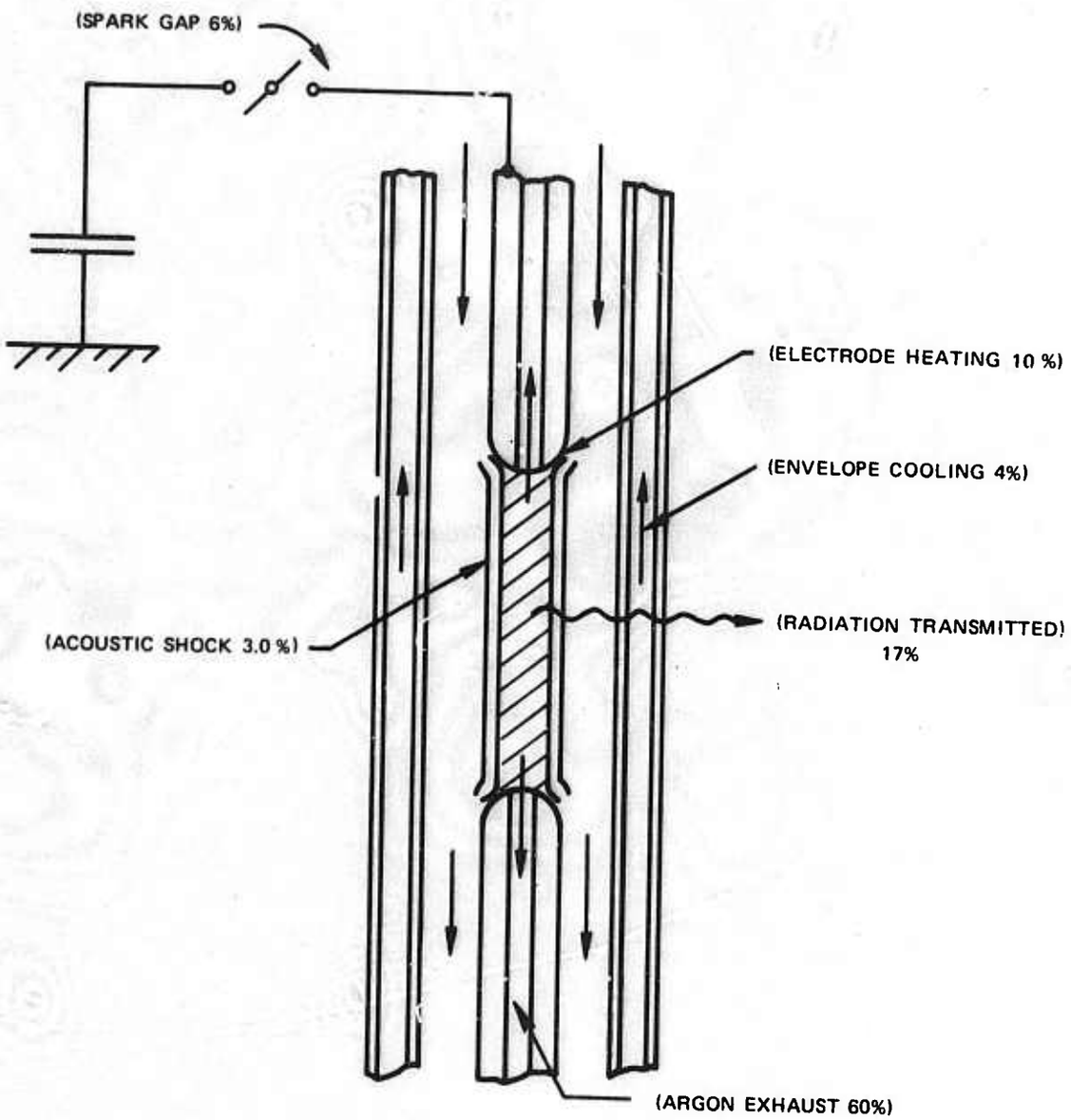

FIG. II-18

FLASHLAMP COOLING SYSTEM

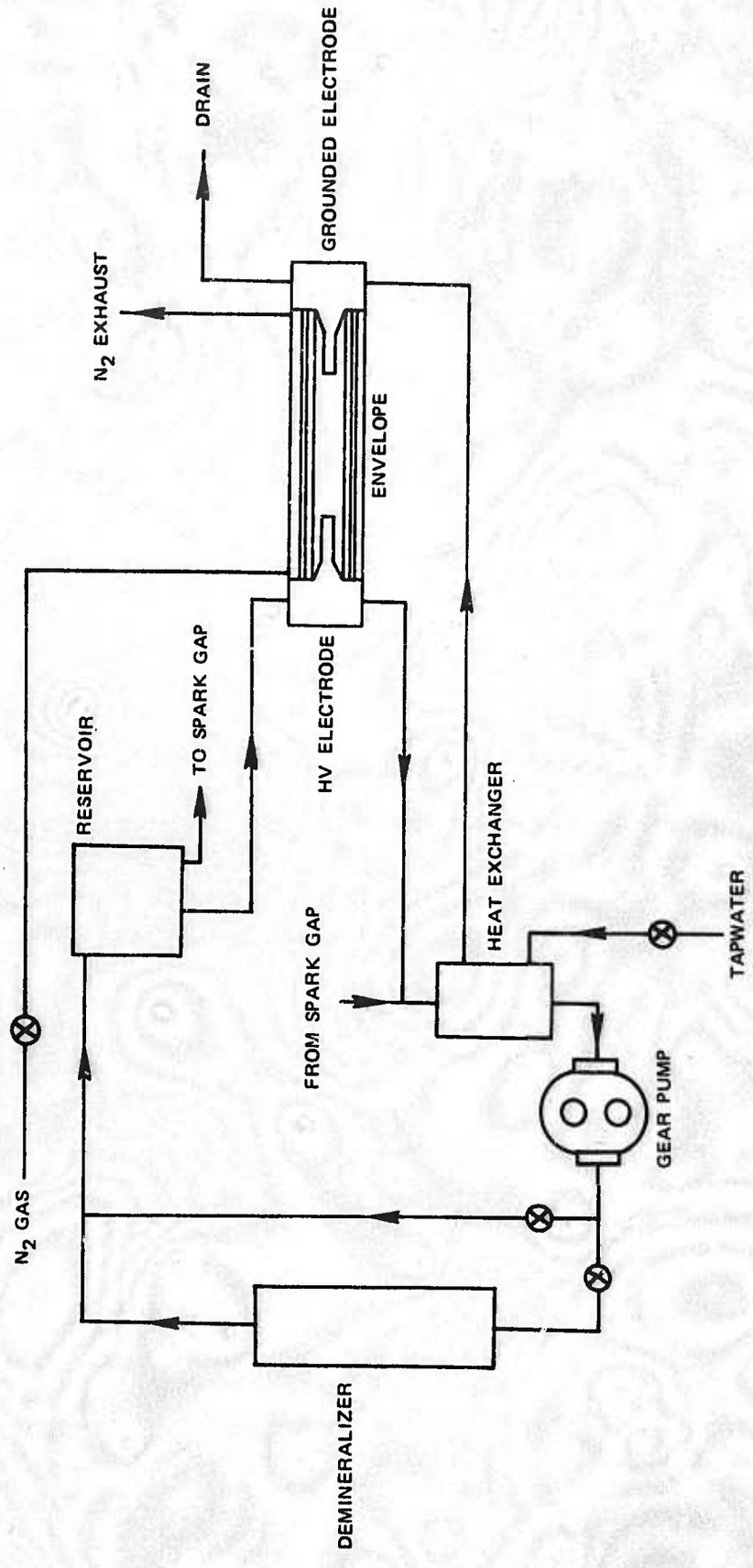

R10-74-21

FIG. II-19

THERMAL STRESS IN FUSED SILICA TUBES

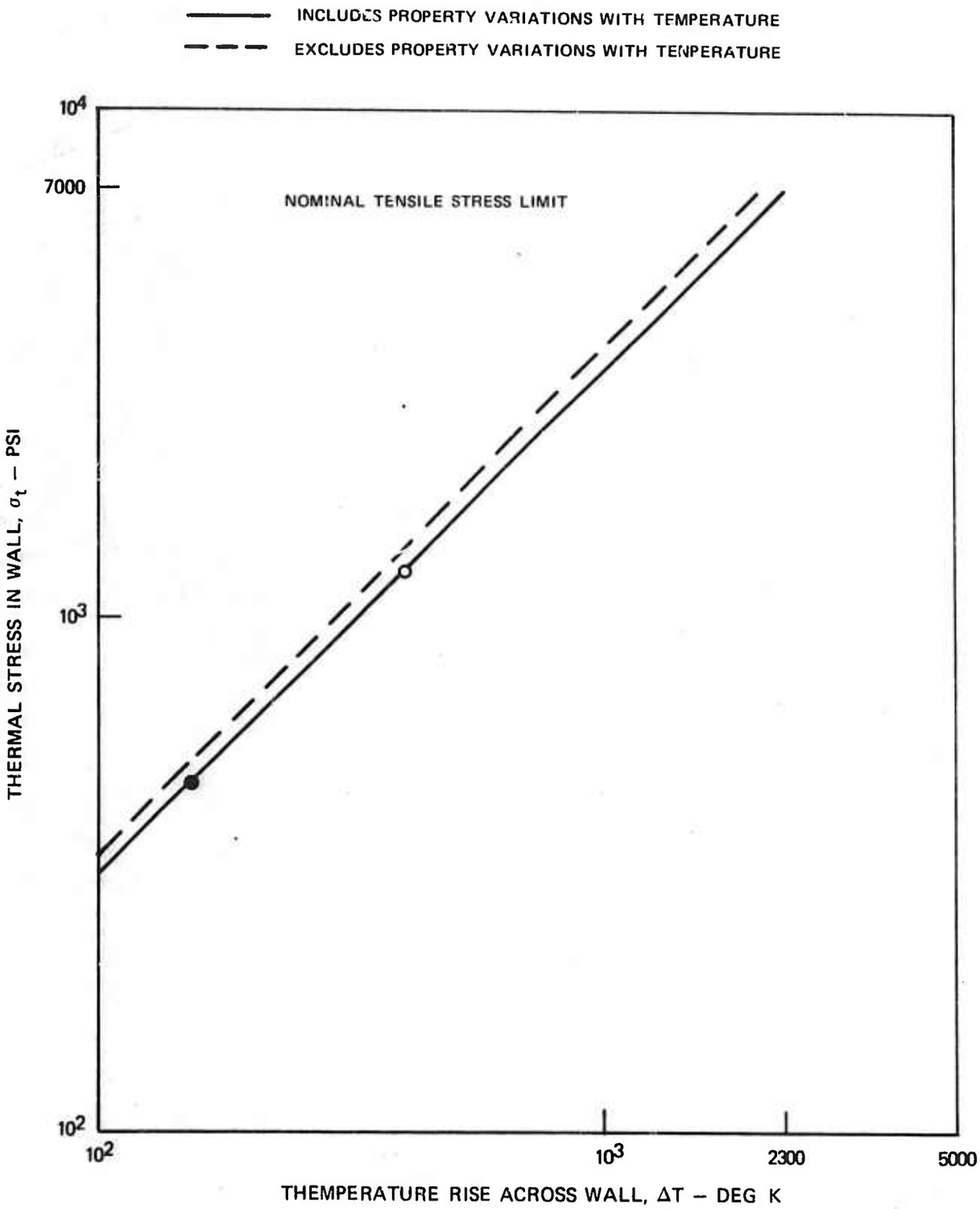

R10-74-44

PLOT OF HOOP STRESS VERSUS BURST PRESSURE

SYMBOL	TUBE DIMENSIONS
○	2.26–IN.–ID. X 2.38–IN.–OD
△	2.22–IN.–ID X 2.38–IN.–OD
□	1.95–IN.–ID X 2.15–IN.–OD
◇	1.76–IN.–ID X 2.85–IN.–OD
◺	2.54–IN.–ID X 2.85–IN.–OD
D	0.05–IN.–ID X 0.06–IN.–ID

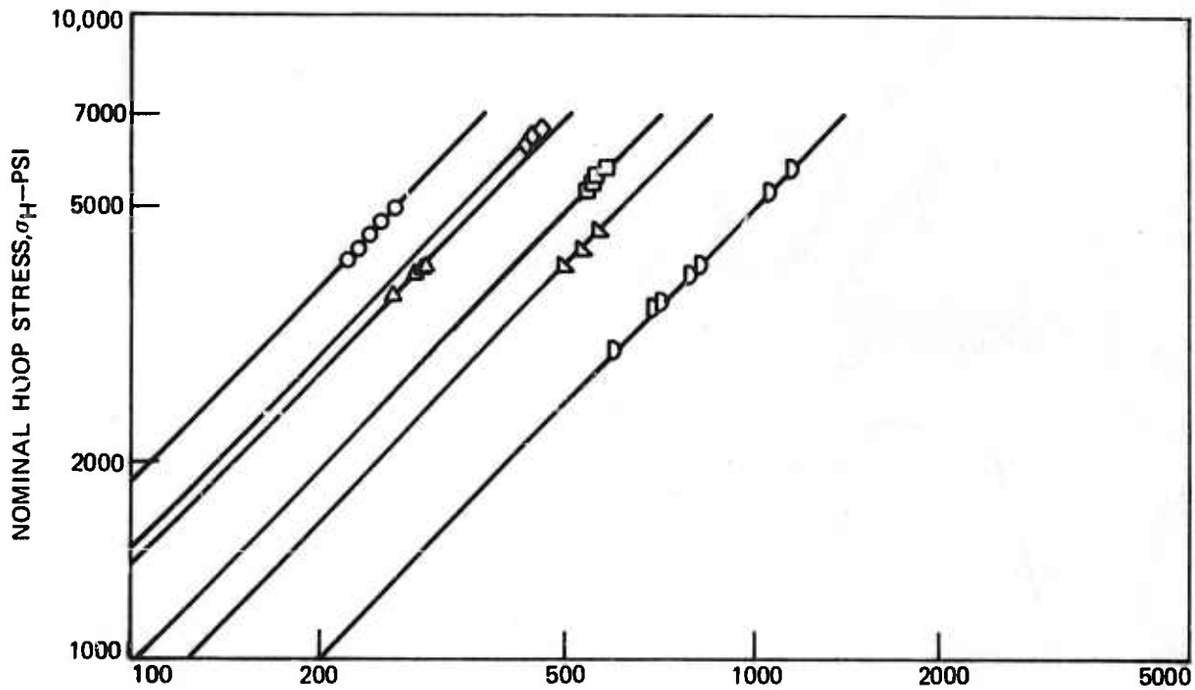

LIGHT INTENSITY FROM DIFFERENT PULSED ARC SOURCES

202J DISCHARGES (14.2 KV)

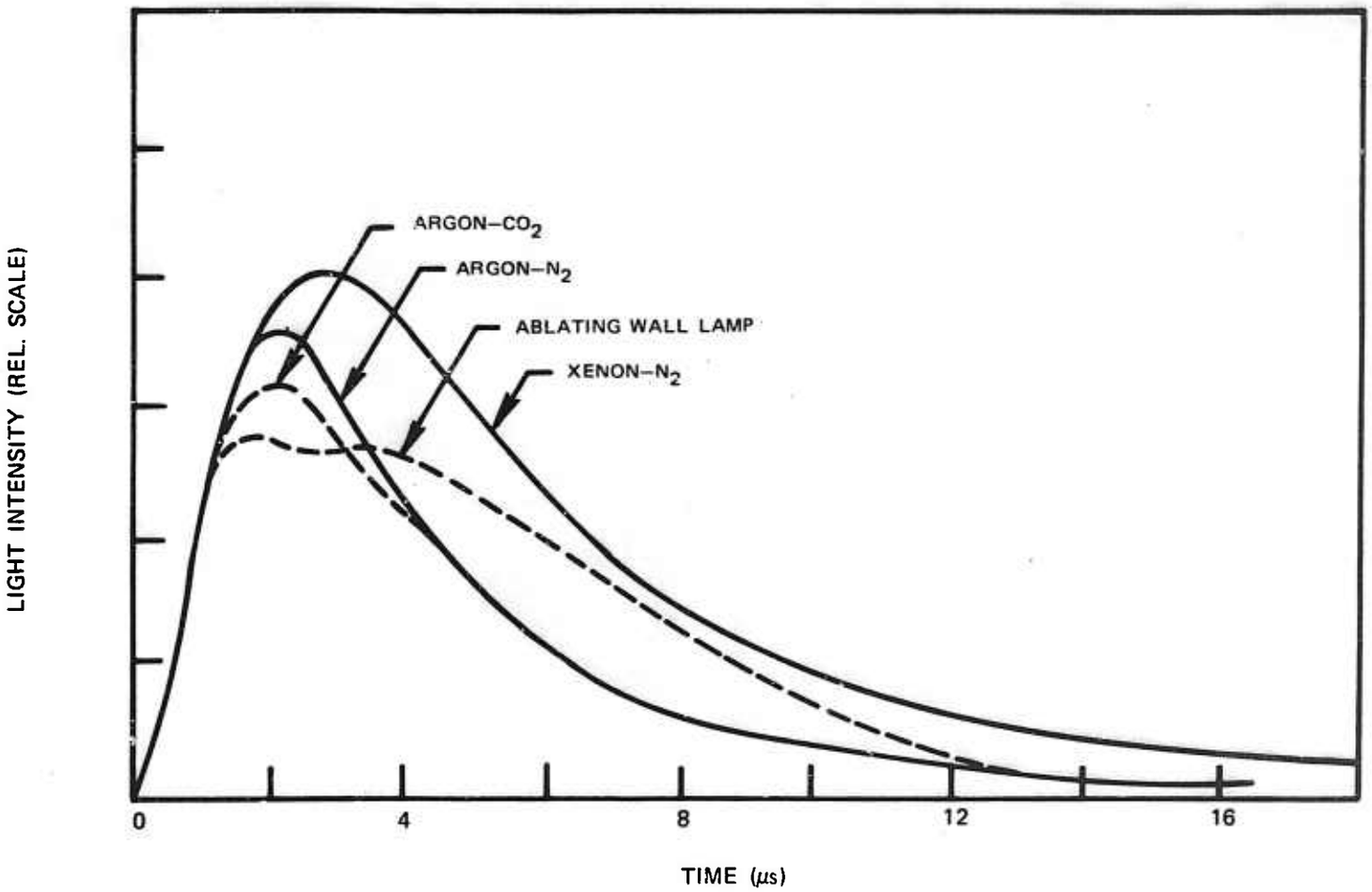

FIG. II-21

FIG. II-22

RELATIVE FLUORESCENCE EXCITED BY 200 JOULE DISCHARGE IN SEVERAL GASES

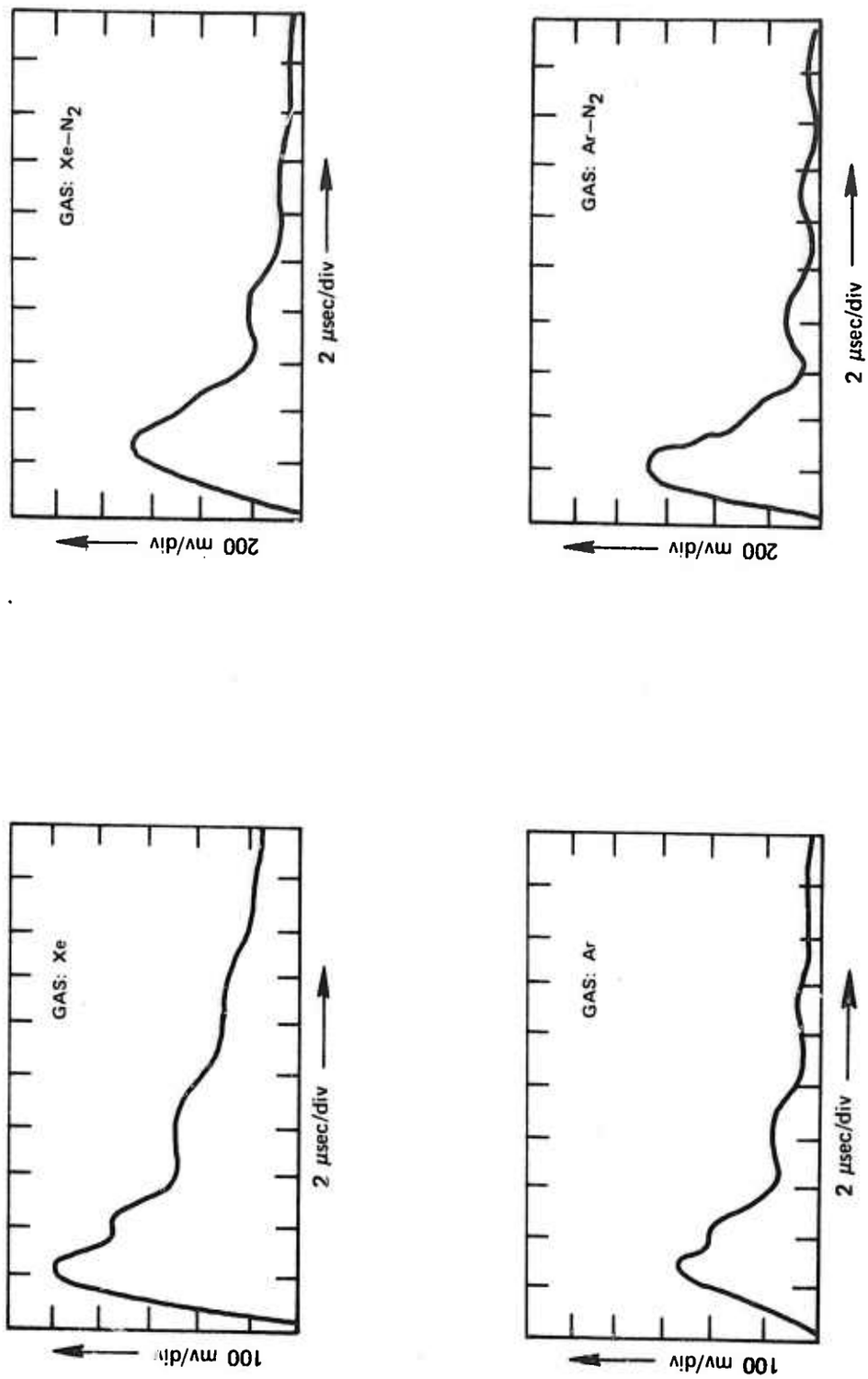

R10-74-35

FIG. II-23

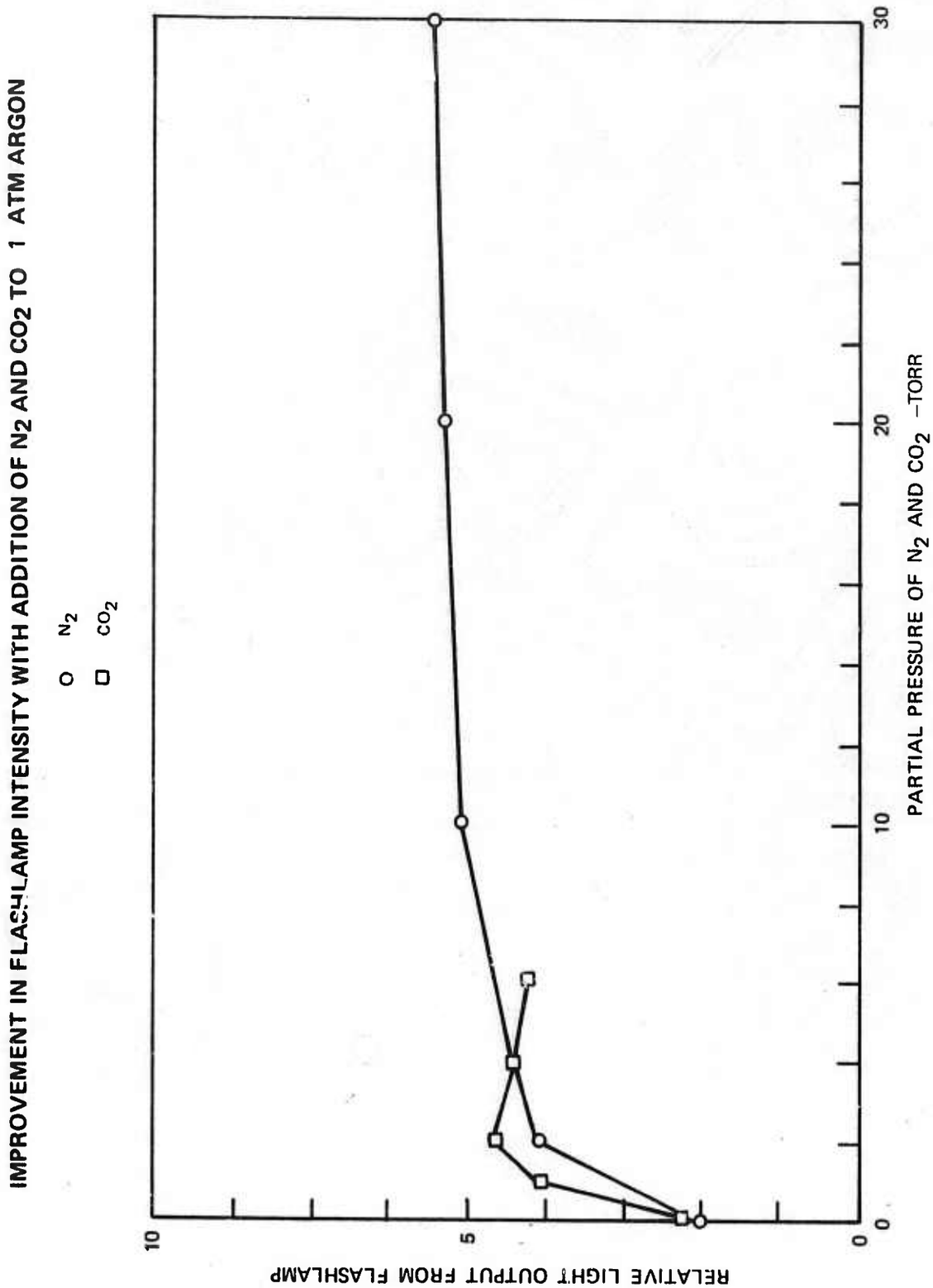

R10-74-7

FLASHLAMP OPTICAL POWER AND ENERGY VS INPUT ENERGY AT λ 500 nm

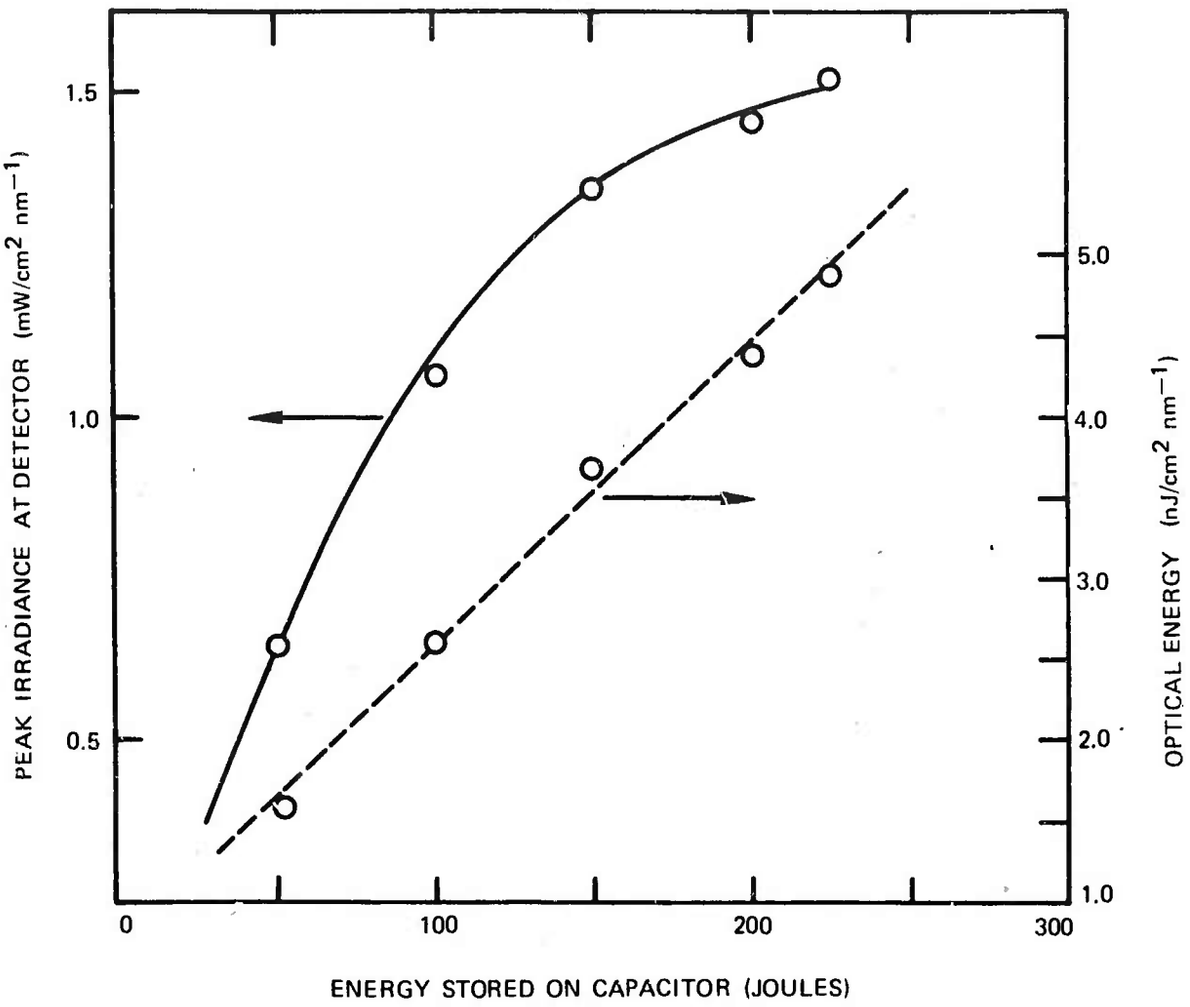

FIG. II–25

IRRADIANCE FOR 1 MM OF ARC LENGTH MEASURED 1 METER FROM ARC AXIS WITH 150 J DISCHARGE INTO 6 CM GAP

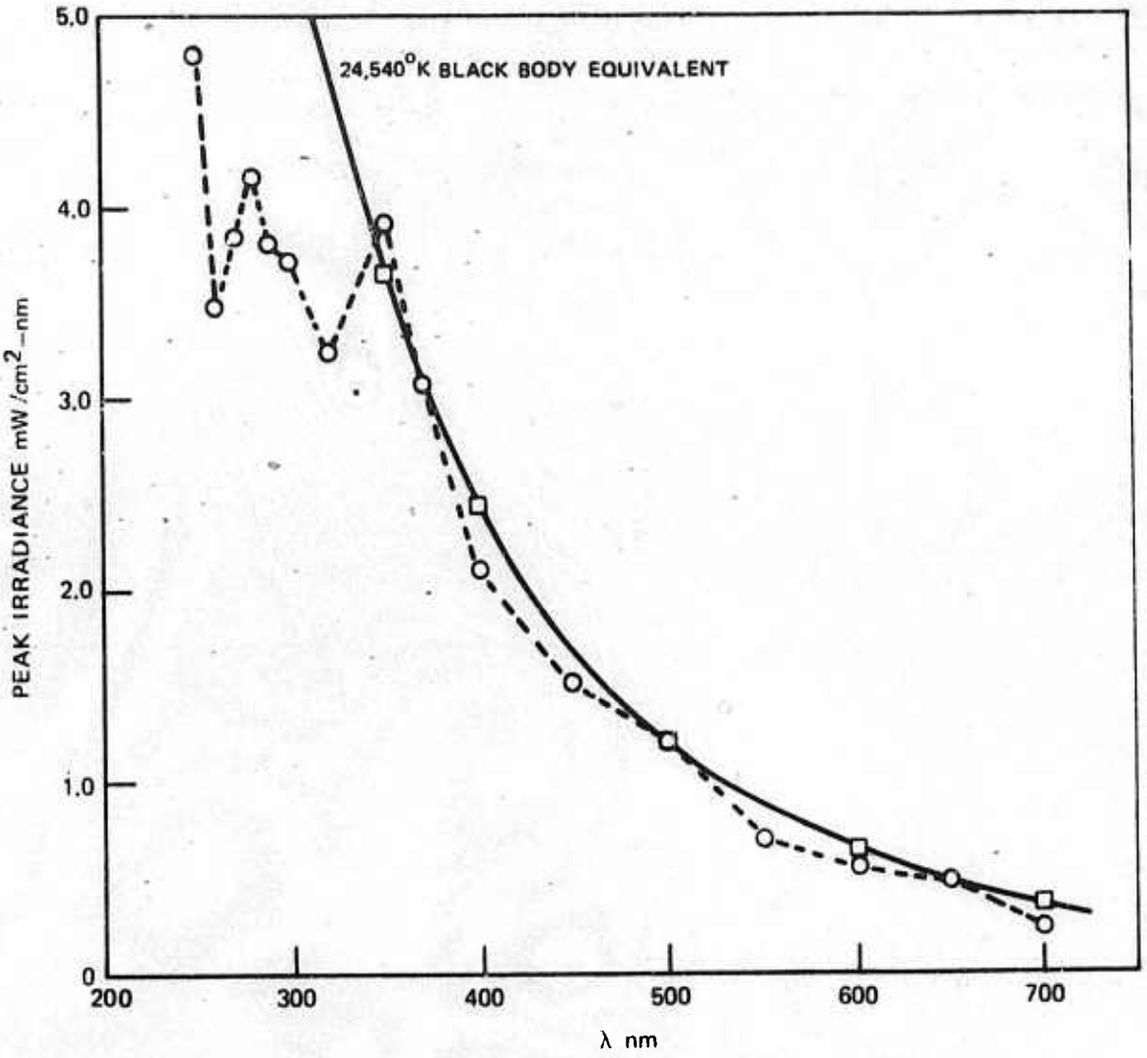

R06–251–6

FIG. II-26

VORTEX FLASHLAMP SPECTRUM WITH 100J DISCHARGE

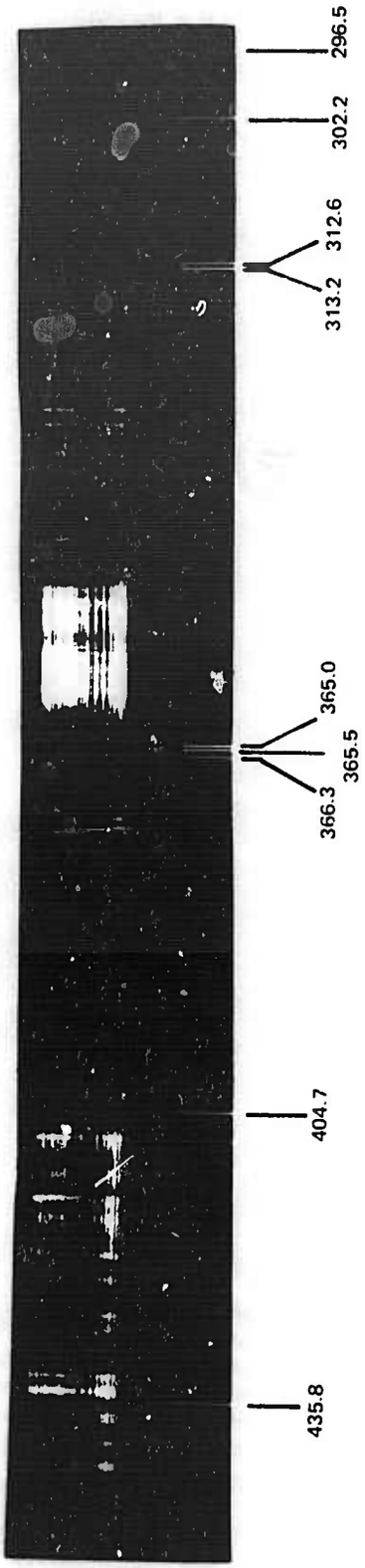

FLASHLAMP INTENSITY FALL OFF

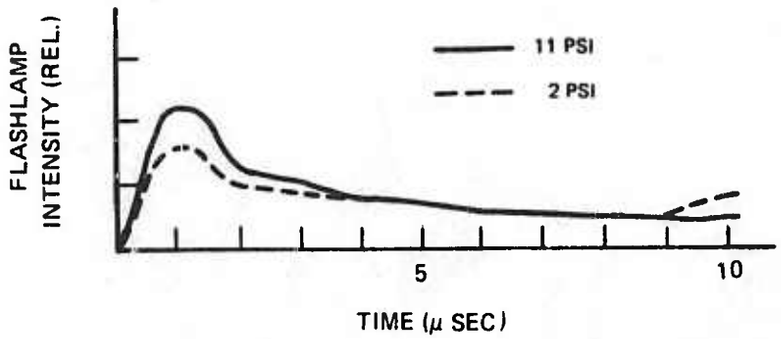

A) FLASHLAMP INTENSITY
AT 200J/PULSE, 100 Hz

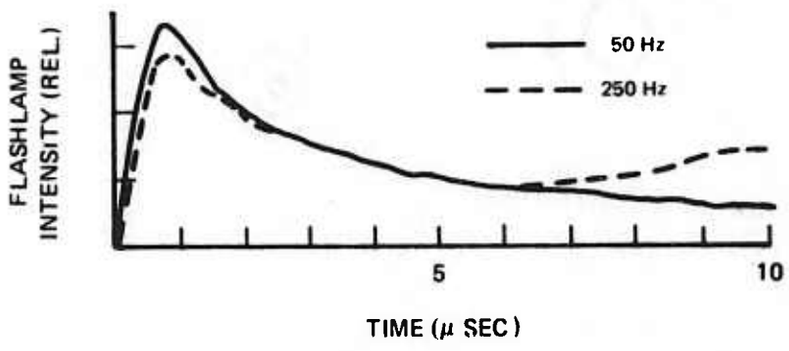

B) FLASHLAMP INTENSITY AT 200J/PULSE,
11 PSI LAMP PRESSURE

FIG. II-28

SECOND LIGHT BURST FROM FLASHLAMP

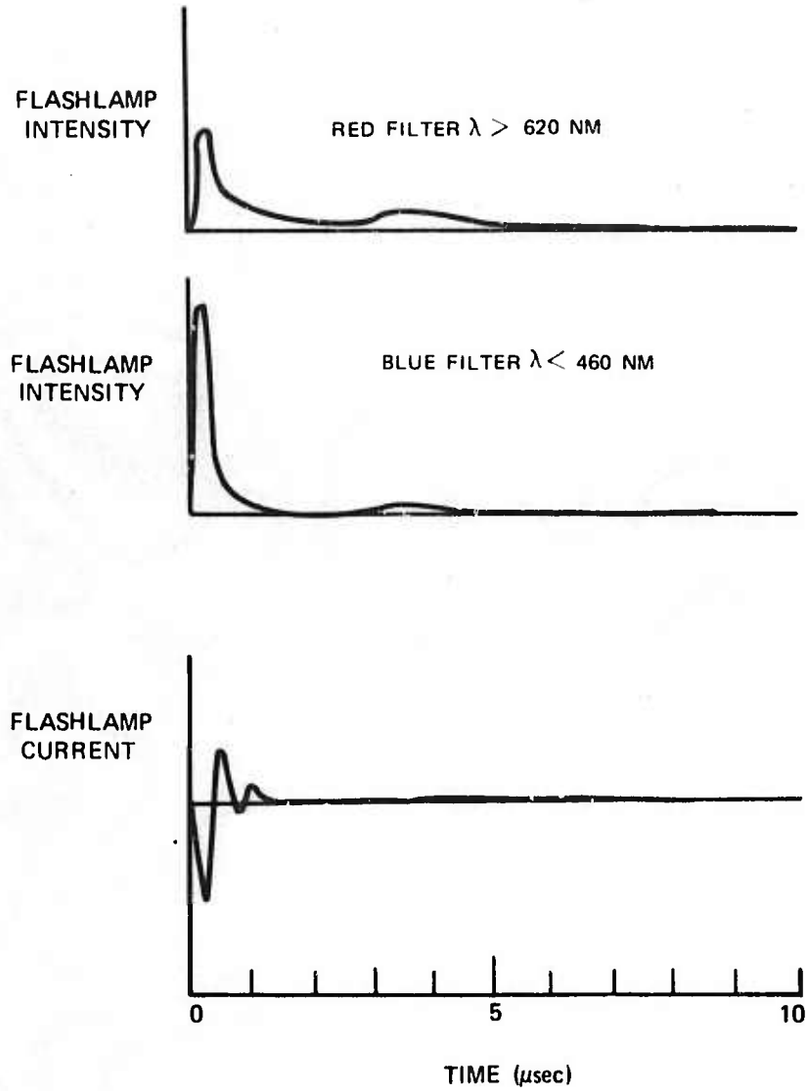

R10-74-38

III. AXIAL FLOW DYE LASER

Introduction

It was originally felt that in order to stablize the flashlamp discharge on the electrode axis a symmetrical environment is required. As a consequence, a spherical reflecting cavity was used to focus the light from the flashlamp discharge along one hemisphere axis into the dye cell which is placed along a joining hemisphere axis as shown in Fig. III-1. This system gives a symmetrical environment to the flashlamp, and, as our ray tracing program shows in the next section, the spherical reflector is an efficient light focusing geometry. The spherical reflector also provides symmetrical pumping for the dye cell.

The dye solution flows into a manifold chamber mounted on the top of the hemisphere as shown in Fig. III-1 and along the axis of the hemisphere where the flashlamp arc is focused (hence axial or longitudinal flow). The dye solution exits the dye cell from the center of the hemisphere along four equally spaced structs. A high reflectivity mirror for the laser resonator is mounted in the small holder at the end of the dye cell where the four struts come together. An antireflection coated window is mounted in the input chamber at the opposite end of the dye cell.

Three axial flow dye lasers were built. The first one used a 2μF tubular capacitor that was found to be unsatisfactory in repetition rate operation. The second system used a larger 2μF capacitor that was capable of operation at the higher power loadings required for repetition rate operation. This system used a short parallel plate strip line to connect the capacitor to the flashlamp housing. The third axial flow dye laser included an extensive modification of the flashlamp housing and capacitor connections from the second design. The dye cell part of the laser was essentially unchanged between the three systems, however.

The first axial flow dye laser was kept intact and used extensively on a single shot basis to test various materials for compatability with the dye solution, various dyes and solvent, and optical distortion. This laser system was convenient in that it used only a liter of dye solution compared with 32 liters for the high repetition rate laser.

In the next section we will describe the results of a ray tracing program for the spherical reflector, then, in the following section discuss the dye solution pumping system and its limitations. Following this the results of laser average power measurements will be given. There were two major problems with this dye laser: a fall off in laser output at repetition rates exceeding 50 Hz, and optical distortion that occurred on a single laser shot. The optical distortion causes early termination of the laser pulse and reduces the beam quality. The last two sections will deal with these topics.

Ray Tracing Program

A computer program was developed to calculate the efficiency of the laser pumping cavity and to determine the distribution of energy within the dye cell. This program provides a guide to optimize the dye cell and arc diameters. Knowledge of the energy distribution within the cell can be used to determine the thermo-optical distortion and the dye concentration can be adjusted for the best compromise between the power output and the thermal distortion.

An idealized model of the pumping cavity is shown in Fig. III-2. The dye cell is located on the axis of the cavity. The arc is assumed to be cylindrical and it is assumed to radiate from its surface as a black body. The symmetry of this configuration allows a considerable simplification in the calculation of the ray paths from the arc to the dye cell. Because of the symmetry, the efficiency for the cylindrical arc is the same as that for a line source that is displaced off the axis by an amount equal to the arc radius. Rays from this line source can thus be calculated rather than rays from the entire arc. This greatly reduces the number of rays that must be traced to obtain an accurate measure of the efficiency. The line source will, of course, provide an extremely asymmetric illumination of the dye cell. If we compute the power deposited by the line source in a given annular region of the dye cell, however, we will obtain the same radial distribution as would be produced by the actual cylindrical arc. This is illustrated in Fig. III-3.

The computer program picks a number of points along the line source. From each point a bundle of rays is emitted with a Lambertian intensity distribution as shown in Fig. III-2. The trajectory of each of the rays is traced, accounting for the losses on reflection from the sphere. Each ray is followed until it either hits the dye cell, the arc (where it is assumed to be reabsorbed) or decays below a specified intensity by multiple reflections from the sphere. If the ray hits the cell, the Fresnel losses are calculated and the direction cosines of the ray after refraction into the cell are computed. The trajectory of the ray is then traced within the dye cell and the power deposited in each annular region and axial region of the cell is computed. This process is repeated for the desired number of points along the line source and results in the determination of the power deposited in the cell as a function of r and z in the cell. The lengths and radii of the arc and dye cell are inputs to the program and may be chosen at will.

Typical results for the efficiency are shown in Fig. III-4. In this case, the arc radius was held fixed at 3mm and the radius of the dye cell was varied. The efficiency initially increases with the dye cell radius and levels off, as one would expect, at a value approximately equal to the arc radius. In this case it was assumed that all rays incident upon the cell were absorbed.

From the efficiency, we may compute the optimum dye cell diameter. Initially, we will simplify the problem by assuming that the energy deposition within the dye cell is uniform. The gain coefficient of the laser, α, will then be proportional to the pumping power per unit volume, i.e.,

$$\alpha = cp$$

where p is the pumping power density and c is a constant of proportionality. The gain of the laser will be

$$e^{\frac{\alpha}{1 + I/I_s}\ell}$$

where I_s is the saturation intensity and ℓ is the length. When the laser is oscillating, the gain must equal the loss, i.e.

$$e^{\frac{\alpha \ell}{1 + I/I_s}} R_1 R_2 = 1$$

or

$$\frac{\alpha \ell}{1 + I/I_s} + \log R_1 R_2 = 0$$

The output intensity is thus

$$I = T I_s \left[-\frac{\alpha \ell}{\log R_1 R_2} - 1 \right]$$

Where T is the transmission of the output mirror. The total power out is the intensity times the area A of the beam

$$P_{OUT} = T I_s \left[-\frac{\alpha \ell A}{\log R_1 R_2} - A \right]$$

Since

$$\alpha = cp,$$

$$\alpha \ell A = \alpha v = cpv = cP_{pump}$$

i.e. $\alpha \ell A$ is proportional to the total pumping power. We have then

$$P_{OUT} = T I_s \left[- \frac{c P_{pump}}{\log R_1 R_2} - \pi r^2 \right]$$

$$= K \left[\beta P_{pump} - r^2 \right]$$

where K and β are constants of proportionality, $K = \pi T I_s$, $\beta = - c/(\pi \log R_1 R_2)$.

We may now plot the output power as a function of the pump power and the dye cell radius. Such a plot is shown in Fig. III-5. These plots show that there is an optimum dye cell size and that this size increases with increasing pumping power (or correspondingly with decreased cavity loss or increased laser gain cross section). This is in agreement with experimental observations.

The pumping density is, of course, nonuniform and the computer program provides a detailed description of the pumping power density within the cell. An example of this is plotted in Fig. III-6. The function plotted is the power per unit volume at a fixed axial position and the dye absorption coefficient is a parameter. In this case the dye cell radius and the arc diameter were both taken as 3 mm. The parameter on the curves is the number of absorption lengths in the dye cell radius, i.e., 3 corresponds to an attenuation of e^{-3} in transversing the cell radius. For low values of the absorption coefficient, a peak in the power distribution is observed within the cell. This is a result of the imaging of the arc. In the absence of the cell, the point on the arc would be imaged at the conjugate point in the sphere. For equal arc and dye cell radii, this would correspond to a point on the cell radius. Because of the refraction of the cell, however, it acts as a positive lens and images the arc at a point within the cell rather than at the radius of the cell. At higher dye absorption coefficients most of the power is absorbed at the outer edges of the cell before it can propagate to the image point.

Dye Pumping System

If the dye solution is left stationary in the dye cell after a laser shot it takes several minutes before a second laser shot can be fired that gives the same laser pulse energy. This arises because of an unavoidable deposition of heat in the dye solution by the absorption of flashlamp light. The heat is nonuniformly deposited, and in addition convection currents are set up that create a distortion that can take minutes to settle out. We are thus required to flow the dye solution and completely replace the heated volume with fresh solution before a succeeding shot is taken. If we want to run at high repetition rates a high capacity pump is required, and if there are sufficient constrictions the pump must also be able to generate a reasonable pressure head.

Figure III-7 shows a schematic of the dye flow system. A liquiflo gear pump with a capacity rating of 20 gallons per minute (GPM) was used to circulate the dye solution around the closed loop. The gear pump is a positive displacement pump so that the volumetric flow rate is directly proportional to the shaft rotation rate. A large Wallace-Tiernan flowmeter was placed at the output of the pump to monitor the actual flow rate. After the flowmeter the solution was filtered by a 22 inch cartridge type. 1μm filter. In addition to removing small particulate matter, the filter acts as a site for the coalescence of tiny bubbles. These bubbles are continually generated by the pump and would remain in solution for hours without the filter. After passing through the filter, the solution goes into a large reservoir, the dye cell, and then back to a second reservoir. Three quarter inch ID polyethylene tubing connected the pump, filter, and reservoirs. Four leads of half inch ID tubing connects the reservoirs with the dye laser head. The system was filled using an aspirator to pull a vacuum on the reservoirs while the dye solution was let in through special inlet ports. Once the system was filled, pressure could be applied directly to the top of the reservoirs or to an expansion bellows in order to keep the solution degassed. If desired, the solution could be equilibrated with one atmosphere of oxygen.

The dye flow system was very versatile in allowing us to adjust the pressure or amount of dissolved gas in the dye solution. A variable speed motor ran the pump so that data could be taken with different flow rates. There were two major drawbacks to this system. After about 5 to 10 minutes of accumulated running time at full speed (a much longer time at lower speeds) the 1μm filter would clog. The pressure would then increase rapidly causing the pump seals to leak. The filters were expensive and the clogging often frustrated data taking. The gear pump had a dense polyethylene gear and a stainless steel gear. Examination of the shaft and gear wear on the pump led us to believe that the stainless steel was wearing off and producing a gray sludge to clog the filter. The rate of wear was much faster as the speed was increased because of the increased back pressure on the wearing ports of the pump. The gear pump was replaced with a centrifugal pump for the transverse laser discussed in Section IV, and the filter clogging problem was eliminated.

The second major problem was a physical limitation on the flow rate of dye solution. When the flow was increased to about .5 ℓ/sec cavitation occurred in the dye cell at points where the fluid turned to enter or exit the dye cell. If the system was pressurized to 20 psig, the cavitation would not start until a flow of .63 ℓ/sec (10 GPM) was reached. The cavitation was barely visible as an optical distortion at the onset, but the distortion increased in intensity and spread out to cover a greater percentage of the dye cell area when the flow was further increased. Several different dye cell sizes and designs were tested but no significant improvements could be made in the flow rate without cavitation.

The pump seals invariably leaked at pressures greater than 50 to 60 psig. With the first run on a new filter element we could achieve about one ℓ/sec without pump seal leakage and severe cavitation in the dye cell.

At .63 GPM the dye solution has a flow velocity of about 12.5 m/sec in the dye cell. The Reynolds number for this flow is 66,000, and the flow is well into the turbulent regime. For turbulent flow the pressure drop across the channel is proportional to the square of the average flow velocity. Figure III-8 shows the pump outlet pressure for various pump speeds. The pump speed is proportional to the flow rate in the dye system. We reduced the pressure on the dye solution to see if we could increase the flow rate for a given pressure drop across the pump. This would allow a larger flow rate before the pump seals would leak. At about 50 psig, however, the solution strongly cavitated in the pump and the flow rate remained at the same level. This is shown by the square data points in Fig. III-8. Another problem we encountered with lowering the pressure, even slightly, was that many bubbles were generated in the dye cell and observed in the outlet reservoir when the flashlamp was discharging. This undoubtedly was caused by the acoustic impact of the energy deposition of flashlamp light in the dye cell.

Laser Tests

A 1.5×10^{-4} molar solution of Rhodamine 6G tetrafluoroborate in ethanol was filtered and pumped through the 8 mm ID by 75 mm long active dye cell volume at various controlled rates up to 0.63 liters per second. In these tests the laser power supply was set for a fixed nominal output voltage of 14 kV. This supply charged a 2 mfd capacitor which was then periodically discharged into the flashlamp via the series spark gap. Although no external charging resistance was used, the internal impedance (non-linear) of the power supply caused some reduction of the charging voltage at high pulse rates. For example, although the lamp input energy remained nearly constant at about 196 joules per pulse up to 80 pps, it dropped by about 5 percent at 100 pps and by an estimated 30 percent at 150 pps. The drop could be compensated by increasing the supply voltage

setting, but this was not done for the tests reported in this section. The power supply was later modified to overcome this problem and allow charging the capacitor to its full voltage in 2 m/sec. Output power was extracted from the laser through a 42 percent transmitting dielectric-coated mirror and was measured using a Coherent Radiation Laboratories Model 201 Laser Power Meter. Extraneous meter indications due to electrical noise and to dye fluorescence other than lasing were always smaller than 0.2 watts. A fast photodiode was used to observe the laser output pulse waveform.

The operating procedure in these tests was to choose a dye flow rate and laser pulse rate, snap-start the power supply for immediate laser operation at full power, continue operation long enough to allow the power meter to respond fully, and then immediately stop operation to allow cooling of the laser components before commencing another run with new operating conditions. This short burst operation was necessitated primarily be a lack of flashlamp electrode cooling, which leads to melting of the electrode structure if high power operation is continued for more than a few seconds. The electrode assembly was later extensively redesigned to permit long term operation.

Results of the laser tests are shown in Fig. III-9 and III-10. The laser pulse waveform is similar to that observed in earlier tests without the series spark gap. As in the earlier tests, the duration of the laser output pulse (1.7 microsecond, FWHM) is substantially less than that of the corresponding flashlamp output (approx. 2.3 microsecond) due apparently to a quenching of the laser oscillation toward the end of the pulse. This quenching is thought to result from thermo-acoustic distortion. Total energy in the laser pulse is about 10 to 12 percent less than that obtained without a series spark gap, under otherwise identical conditions.

Figure III-9 shows the dependence of average laser output power on dye flow rate for repetitive pulsing at various repetition rates. Input energy was 196 joules per pulse at low pulse rates, dropping off by about 5 percent at 100 Hz as described above. In general the laser output is seen to increase with increasing dye flow rate over the flow range employed here. At low pulse rates the output increase levels off at moderate flow rates, suggesting nearly complete interpulse replacement of dye in the active region. However, at 100 Hz the laser output is still increasing substantially with increasing dye flow rate even at the highest available flow rates. Although the maximum dye flow (0.63 liter/sec) corresponds to a nominal dye change rate of about 166 sec^{-1} in the 3.8×10^{-3} liter active dye cell volume, it appears that even faster flow is required to clear dye from the cell wall boundary layers.

Figure III-10 shows the average laser output power as a function of pulse repetition rate at the maximum dye flow rate of 0.63 liter/sec. The power increase vs pulse rate departs somewhat from linearity even at relatively low

rates but still increases substantially with increasing rate up to about 100 Hz. At higher pulse rates the laser power actually begins to decrease with increasing rate due to the previously noted power supply limitations as well as the inadequate dye flow rates.

Figure III-11 shows the laser power output at repetition rate with 100 J per pulse input energy. Two curves are shown in the figure: one for an oxygen equilibrated solution, the other for a degassed solution. Oxygen acts as a triplet state quencher for rhodamine 6G and reduces the losses caused by excited triplet state absorption of the laser light (Ref. III-1). At repetition rates of 50 Hz and below we get twice as much power from the oxygenated solution as from the degassed solution. The oxygenated solution, for example, gives slightly over 20 watts output with 5 kW input for an electrical efficiency of 0.4 percent. The output from the degassed solution, however, saturates at a slightly higher repetition rate. The best laser performance we observed with the system was 42 watts at 100 Hz in an oxygenated alcohol solution.

We note from Figs. III-10 and 11 that the output power is linear with repetition rate up to about 50 Hz. Beyond this point the laser energy per pulse starts to drop significantly. Since the flow is limited to about .6ℓ/sec in this laser system, we can expect that to get any significant improvement will require a prevention of the pulse energy fall off and/or an improvement in the laser pulse energy. These topics will be taken up in the next two sections.

Figure III-12 shows the results of single shot laser pulse energy measurements made with various mixtures of alcohol and water. Water-alcohol solutions tested in the high power laser always gave a smaller output than a pure alcohol solution. The beam quality with the alcohol-water mixture is slightly better, however (see Section III-6).

Laser Output Fall Off

The laser output was monitored with a photodiode detector and oscilloscope. The oscilloscope sweep speed was set on 0.5 sec/cm so that the envelope of the peak power of the laser pulses was traced out on the scope face. The baseline was suppressed to avoid saturation and overexposure of the polaroid film. Using this technique, we could determine how the output falls off in time. The results were surprising. Figure III-13 shows a trace taken with a repetition rate of 100 Hz and 200 J discharges in the flashlamp. The laser output fell 33 percent immediately after the first pulse. The output continues to fall off another 14 percent but more gradually, and reaches a steady value in about 1 sec. We also simultaneously monitored the flashlamp intensity and found that the flashlamp output deteriorates about 10 percent after the first five or six shots.

The 10 percent deterioration in the flashlamp light, however, does not explain the sudden drop in laser output immediately after the first pulse. A great deal of effort was spent trying to determine the cause of this effect. If this problem could be solved then we could expect a good deal more average laser power.

We first found that the sudden drop in pulse intensity was related to the dye solution flow rate. This is shown in Fig. III-14 where we have expanded the time scale to give more resolution between shots. With a PRF of 53 Hz and about half the maximum flow rate of .32 ℓ/sec we see a significant drop after the first pulse. This is shown in the top trace in Fig. III-14. If the flow rate is doubled the sudden drop in pulse intensity disappears. If we then double the repetition rate the pulse intensity again makes an initial drop as shown in the last trace in Fig. III-14. Presumably, if we could flow the dye at 1.26 ℓ/sec, we could eliminate the initial drop in pulse intensity at 100 Hz.

We first suspected that the dye solution was not changing over fast enough in the active region. The dye cell has an ID of 8 mm and a length of 7.5 cm that is exposed directly to the flashlamp light. Using this volume and a flow of .63 ℓ/sec, we get an average change-over-rate of 167 sec^{-1}. If we include extra length of the dye cell that is not directly exposed to the flashlamp light, however, we get an average change-over-rate of 107 sec^{-1}. We saw from Fig. II-9 that a flow rate of .63 ℓ/sec is barely adequate for a repetition rate of 50 Hz. That is, we have to change the dye solution in the dye cell 2 to 3 times faster than the laser repetition rate.

A boundary layer is created in the flowing dye cell that contains dye solution that is changed over at a slower rate than the solution in the central core of the cell. For turbulent flow through circular tubes the boundary layer builds up along the length of the tube axis according to the relation

$$\delta = .37D\ (R_e)^{-.2}\ (\chi/D)^{.8}$$

where δ is the thickness of the boundary layer from the edge of the wall, D is the tube diameter, R_e the Reynolds number and χ the distance along the tube axis (Ref. III-2). For a distance, y, inwards from the tube wall greater than δ ($y > \delta$), the flow velocity is uniform. For distances less than δ, the flow velocity drops off as the one seventh power of the ratio of y to δ. That is,

$$V/V_c = (y/\delta)^{1/7} \text{ for } y \leq \delta$$

where V is the flow velocity at y and V_c is the flow velocity of the core ($y > \delta$).

Using the above formula for δ we can compute the size of the boundary layer at the extreme end of the tube (x = 10 cm). For a flow velocity of 12.5 m/sec (.63 ℓ/sec), the Reynolds number is 6.6×10^4, and δ = 0.243 cm. If we then compute the distance from the wall where the flow velocity drops to 1/2 the core velocity, we get

$$y_{1/2} = \delta/2^7 = 19\mu m$$

This represents the maximum distance that the half velocity streamline extends from the wall. For a velocity of 75 percent of centerline flow, $y_{3/4}$ = 0.32 mm.

In order to determine the fraction of the laser pulse energy that comes from the boundary region, we placed apertures of different diameters over the end of the dye cell to block off different amounts of the dye cell boundary. In this way we could determine what fraction of the laser pulse energy comes from a given cross sectional area of the cell. Figure III-15 shows the results of the experiment. From this figure we see that a 20 percent drop in the laser pulse energy requires an obstruction of .65 mm from the tube wall. The streamline that is .65 mm from the wall has a flow velocity of 83 percent of the center line or core flow velocity. Thus, if we change the fluid in the core over at a rate of 107 sec^{-1} then the fluid at .65 mm will change over at 89 sec^{-1}. The fluid at distances closer to the wall change over even more slowly.

Figure III-16 shows the results of a distortion measurement we made on the high power dye laser. A HeNe laser beam was sent down the cell and retroreflected from the high reflectivity mirror at the end of the dye cell. A beam splitter separated the return beam which was then focused through a pinhole and detected with a photomultiplier. A 632.8 nm spike filter was used to block all radiation except the HeNe beam. When an optical distortion occurred in the dye cell the HeNe beam would be deflected away from the pinhole. In Fig. III-16 the photomultiplier current level with no distortion is listed as 0 percent distortion. When the flashlamp fires the beam is immediately deflected away giving 100 percent distortion. As the solution moves out of the dye cell the beam slowly recovers to its undistorted level as shown. The optical distortion measurement was not very accurate in this experiment because of pump vibration of the high reflectivity mirror at the end of the dye cell. The mirror is spring loaded against an "o" ring and in direct contact with the dye solution. Pump fluctuations from the gear pump would move the mirror slightly. This action generated a certain amount of noise making it hard to tell exactly where the distortion settled out. In Fig. III-16 the distortion recovered in about 21 msec for a flow of .32 ℓ/sec (5 GPM) and 15 msec for .63 ℓ/sec (10 GPM). At this latter flow rate, which is the maximum for the system, the dye recovery rate is 67 sec^{-1}. This is 62 percent less than the calculated change over rate based on the entire length of the dye path. It could be that some of the light is getting into the

end bells where the fluid enters the dye cell. Allowing for this extra volume reduces the change-over-rate to 77 sec^{-1}. In addition, the boundary layer must break up at the turning point of the dye flow when it leaves the cell. This action too could give a longer time for some of the exposed dye solution to remain in the cell. We tried several different ways of flowing the dye solution through the laser tubes, but we were unsuccessful at reducing the recovery time.

The fall off in the laser output is therefore caused by a smaller than expected recovery rate of the solution in the dye cell coupled with a fall off in the flashlamp intensity. The fall off in flashlamp intensity was more severe with the 10 cm long arc flashlamp built for the transverse flow laser. This problem was remedied by increasing the pressure and flow in the flashlamp as discussed in Section II.

Single Shot Optical Distortion

In addition to a distortion that remains between succeeding laser shots, there is a distortion that occurs during the laser pulse. This has been referred to before. The second and third trace in Fig. III-17 show the laser intensity and flashlamp intensity taken at the same starting point. The laser intensity reaches its peak value before the flashlamp, and the laser pulse is terminated before the flashlamp has decreased to 1/2 of its peak value. The reason for the early termination of the laser pulse is a nonuniform deposition of heat by absorption of the flashlamp light. This action generates an acoustic wave which deflects the laser light from the resonating cavity (Ref. III-3). As previously discussed, the excited triplet states of the dye molecules are effectively quenched so that if there were no rapid time varying distortions, the dye theoretically could lase cw (at present there is no arc lamp that can maintain the required brightness level to run cw, however).

We performed an experiment that clearly demonstrated the generation of a flashlamp induced, photoacoustic wave. Figure III-18 shows the experimental set up. A HeNe laser beam was sent through a 60 x 60 x 20 mm spectrophotometer cell filled with rhodamine 6G dye solution. The beam was then focused through a pin hole, spectrally filtered to pass only the 632.8 nm wavelength of the HeNe laser, and detected with a photomultiplier. An ablating wall flashlamp was placed under, but not touching, the spectrophotometer cell, in order to avoid the transfer of a mechanical shock from the flashlamp. Aluminum foil was placed around the bottom and sides of the flashlamp to help contain the light. The HeNe beam transits the cell parallel to the bottom so that the passage of an acoustic density wave would register by deflecting the focused light beam across the pinhole. The HeNe beam is focused half way into the upper half of the pinhole so that an upward deflection gives a decrease in photocurrent and vice versa. A

concentrated dye solution was used so that the flashlamp light would be absorbed in a thin layer at the bottom of the cell. Figure III-19 shows the results with a flashlamp discharge, and indeed, a photoacoustic wave is launched that intercepts the beam in its upward travel, totally reflects from the surface of the liquid and then returns to give a second deflection. The acoustic wave is then partially reflected from the bottom of the cell and repeats the above deflections. The time of travel between deflections divided into the distance agrees with the sound velocity in ethanol at 20.5°C (1213m/sec).

A similar process might be occurring in the dye cell. The upper trace in Fig. III-17 shows the optical distortion in the dye laser cell on a 2 μsec/div. time scale. This trace was taken with a courmarin dye in the dye cell so as not to affect the HeNe laser beam. The experimental set up was similar to that described in Section III-5 for the recovery rate measurements on the high power dye laser. The retroreflected HeNe beam was focused through a pinhole and detected by a photomultiplier detector. Complete distortion occurs at the level marked with an arrow; optical homogeneity occurs when the level is at the base line of the trace. The distortion increases from the start of the laser pulse until about 2 μsec. At this time the distortion appears to be reduced for about one μsec and then increases again. Successive openings are again seen at later times. This result was repeatable and could represent a reverberating acoustic wave. Using the 2 μF capacitor with the laser we frequently observed a second rise in the laser intensity occurring at the same time as the opening in the optical distortion. This is shown in Fig. III-17. A program had been initiated to analyze the acoustic wave disturbance in the dye cell but due to time restrictions the program was not completed. It is clear that if the early termination of the laser pulse could be avoided, while not affecting other laser parameters, a sizeable increase in the pulse energy and electrical efficiency could be obtained.

Figure III-20 shows the results of a beam quality measurement made on the dye laser. For these results the laser beam was examined in the far field of a 1 meter focal length lens. We measured the laser power coming through apertures of different sizes. Using the focal length of the lens, the detected signal was calibrated in the acceptance angle of the aperture. This procedure gives a direct measure of the laser beam divergence. The signals were normalized to the widest aperture of 25 milliradians which passes the entire beam.

REFERENCES FOR SECTION III

III-1. Marling, J. B., D. W. Gregg, and S. J. Thomas: Effect of Oxygen on Flashlamp-Pumped Organic-Dye lasers. IEEE JQE, Sept. 1970, p. 570.

III-2. Discussions with Olof L. Anderson, Gasdynamics Section, United Technologies Research Center.

III-3. Ewanizky, T. F., R. H. Wright, Jr., and H. H. Theissing: Shock Wave Termination of Laser Action in Coaxial Flashlamp Dye Lasers. Appl. Phys. Lett. 22, 521 (1973).

HIGH POWER DYE LASER

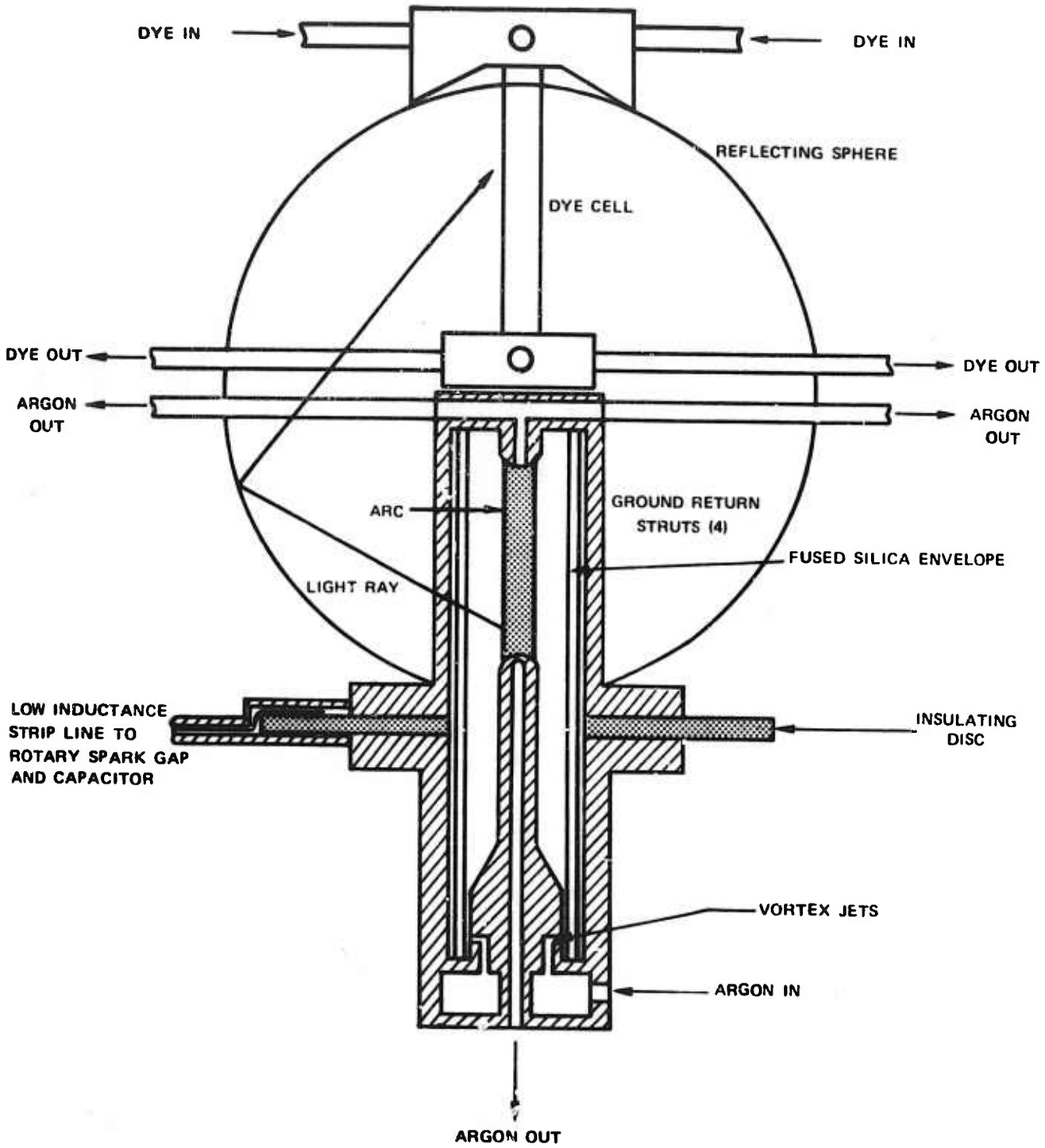

IDEALIZED CAVITY MODEL

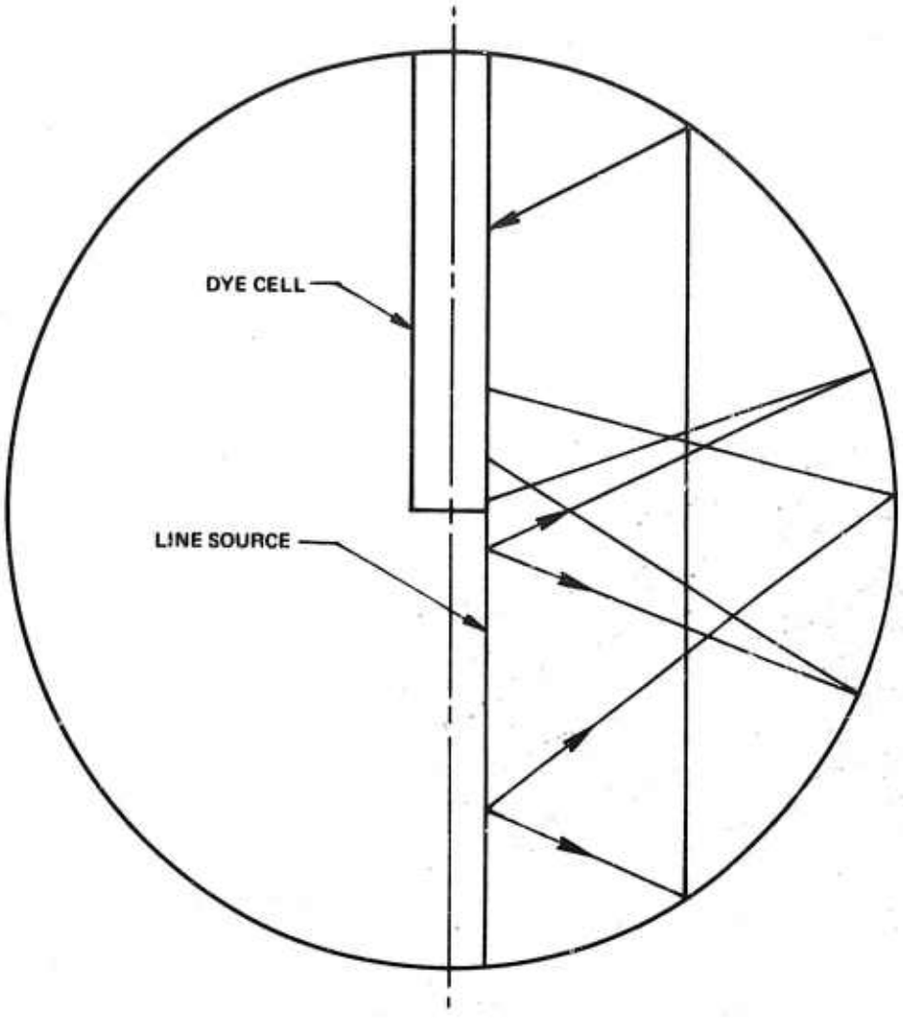

TOP VIEW OF LINE SOURCE

SIDE VIEW OF LINE SOURCE

LAMBERTIAN EMISSION

POWER DEPOSITION IN CELL

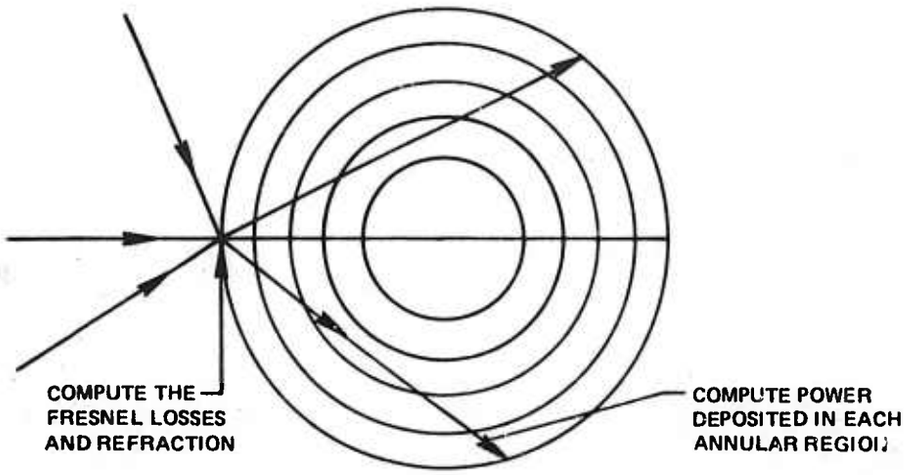

TOP VIEW

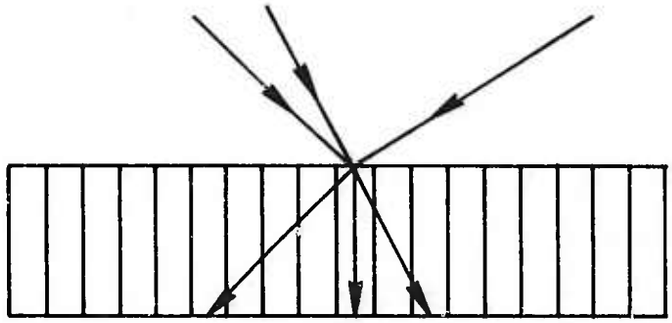

SIDE VIEW

FIG. III-4

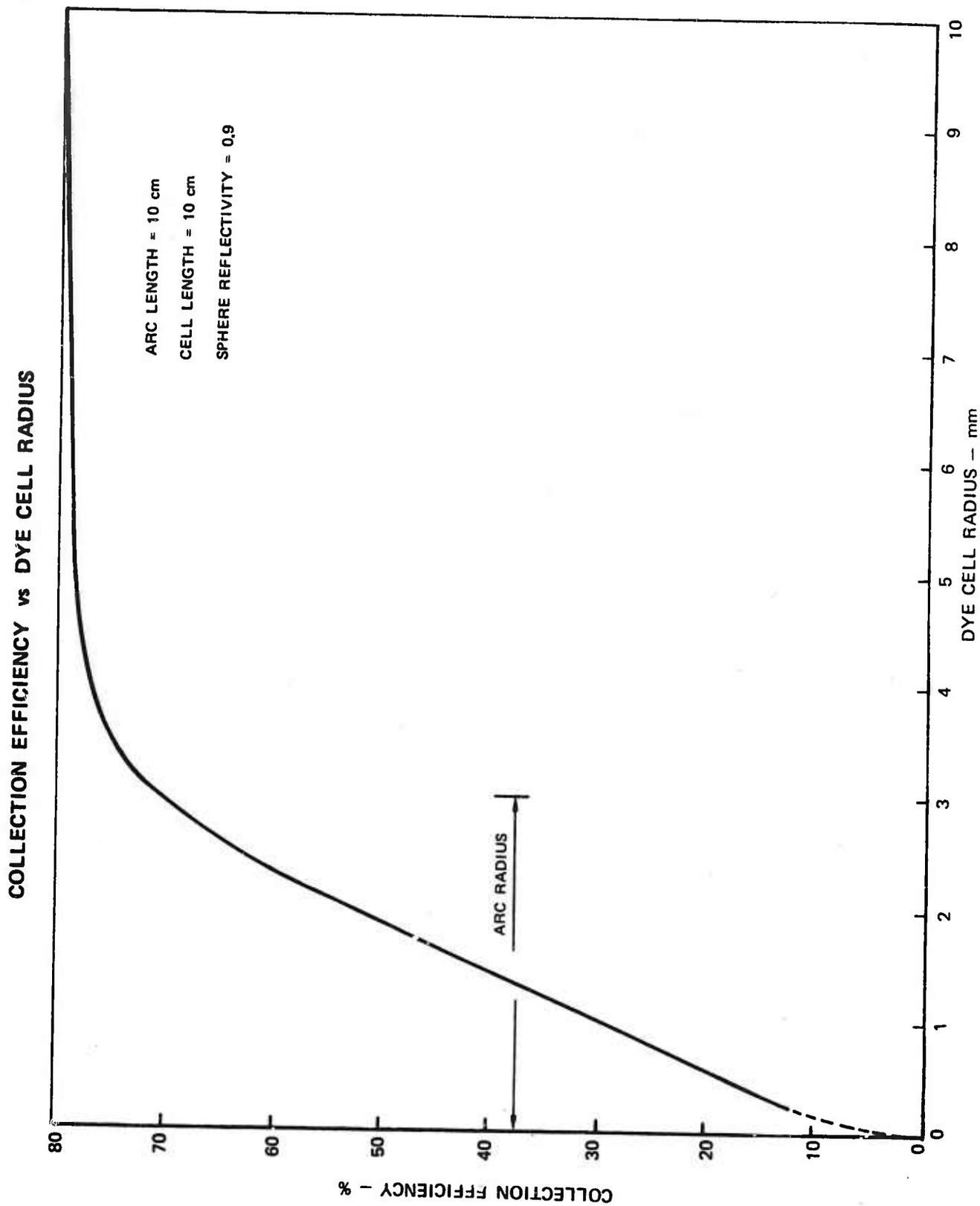

N09-134-1

FIG. III-5

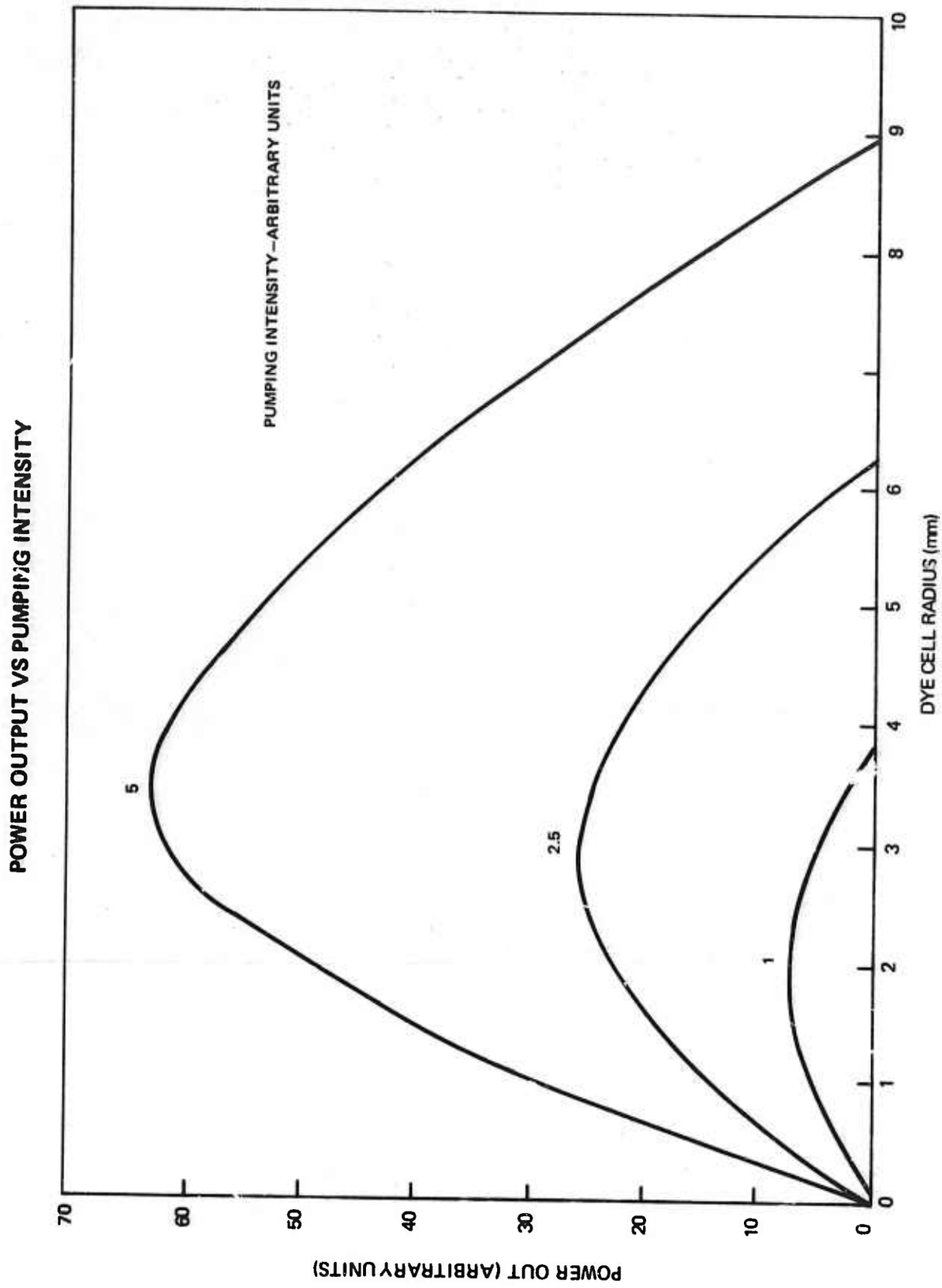

N09-184-1

FIG. III–6

POWER DISTRIBUTION IN DYE CELL

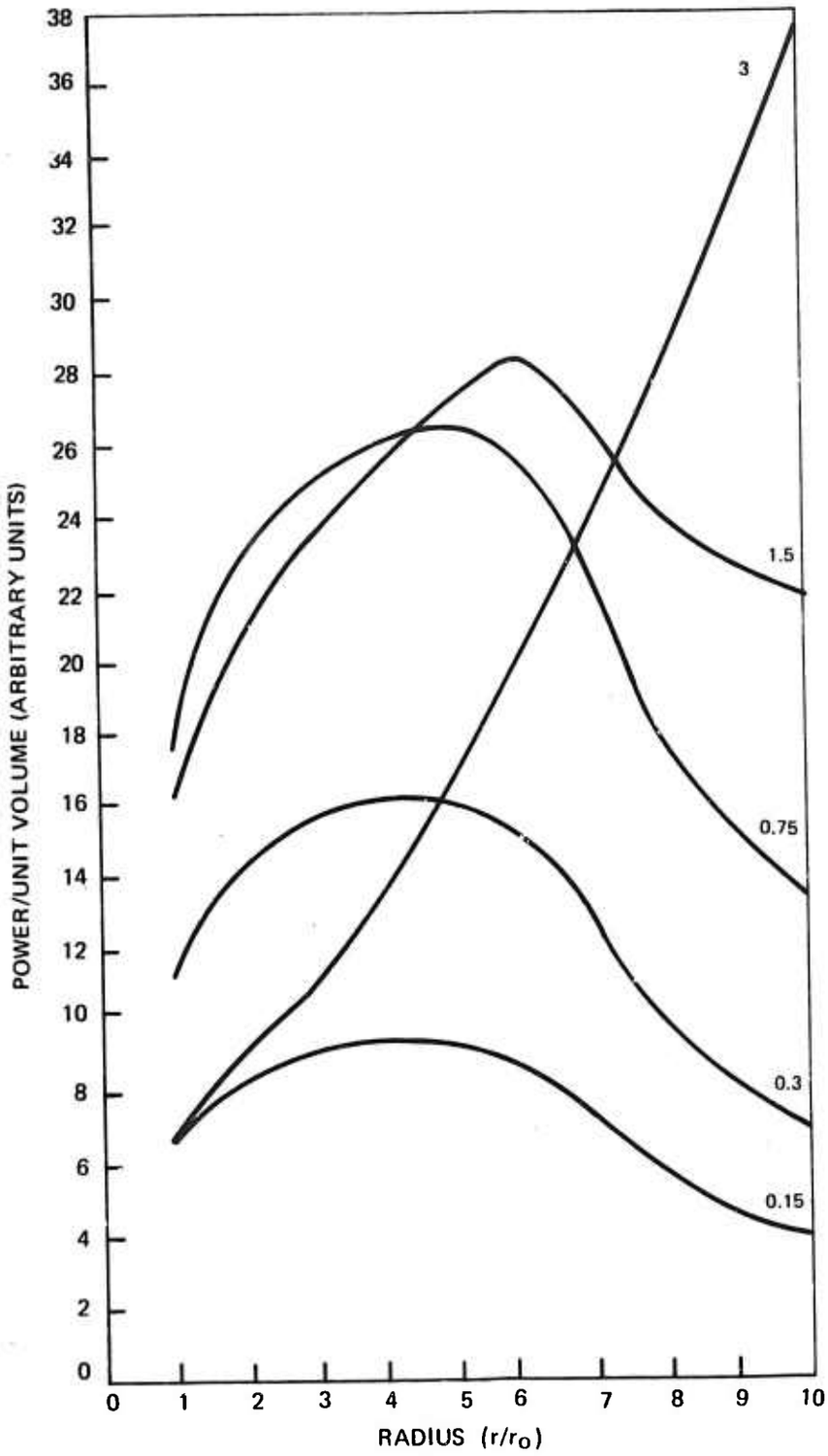

N09–184–2

FIG. III-7

DYE FLOW SYSTEM FOR AXIAL PUMPED DYE LASER

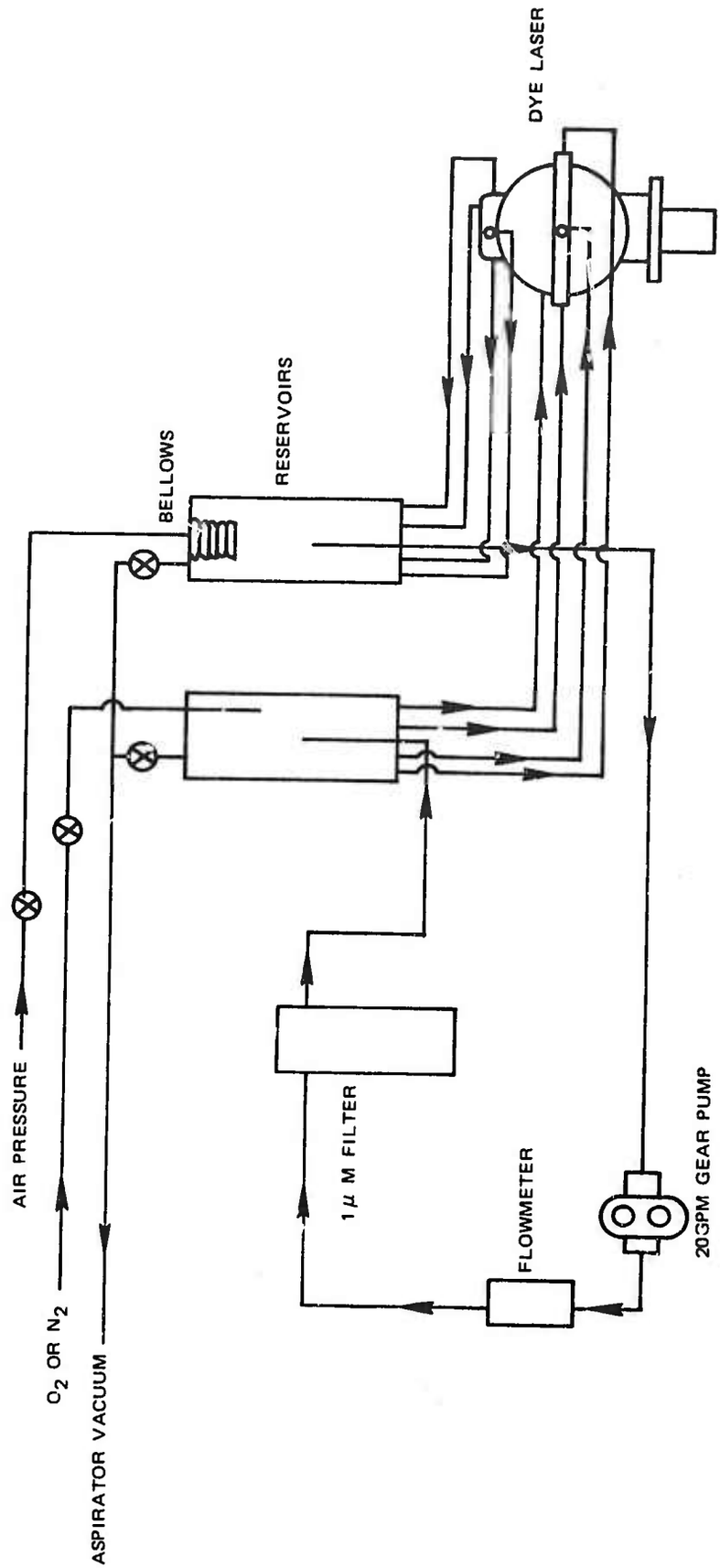

PUMPING CHARACTERISTICS OF AXIAL FLOW DYE LASER

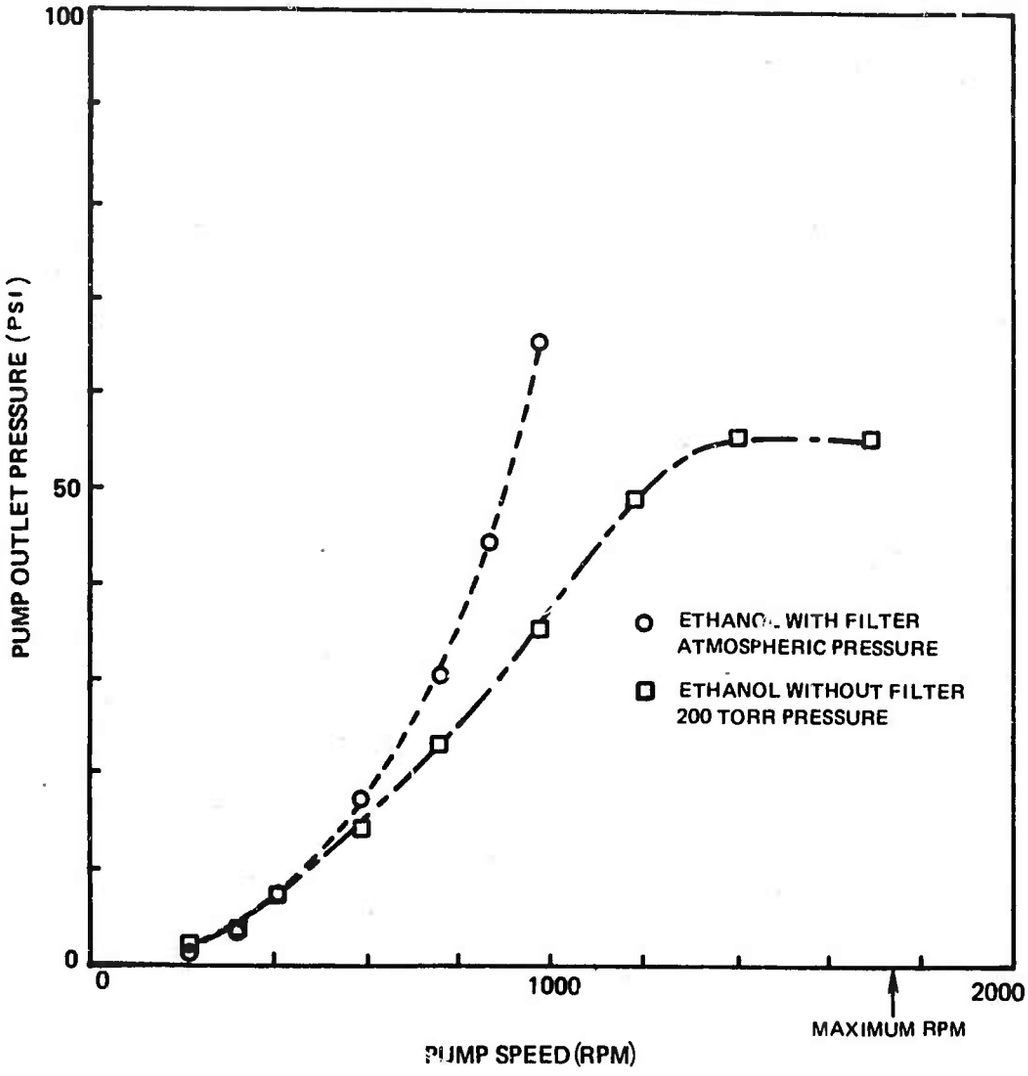

FIG. III-9

LASER POWER OUTPUT VS DYE FLOW RATE

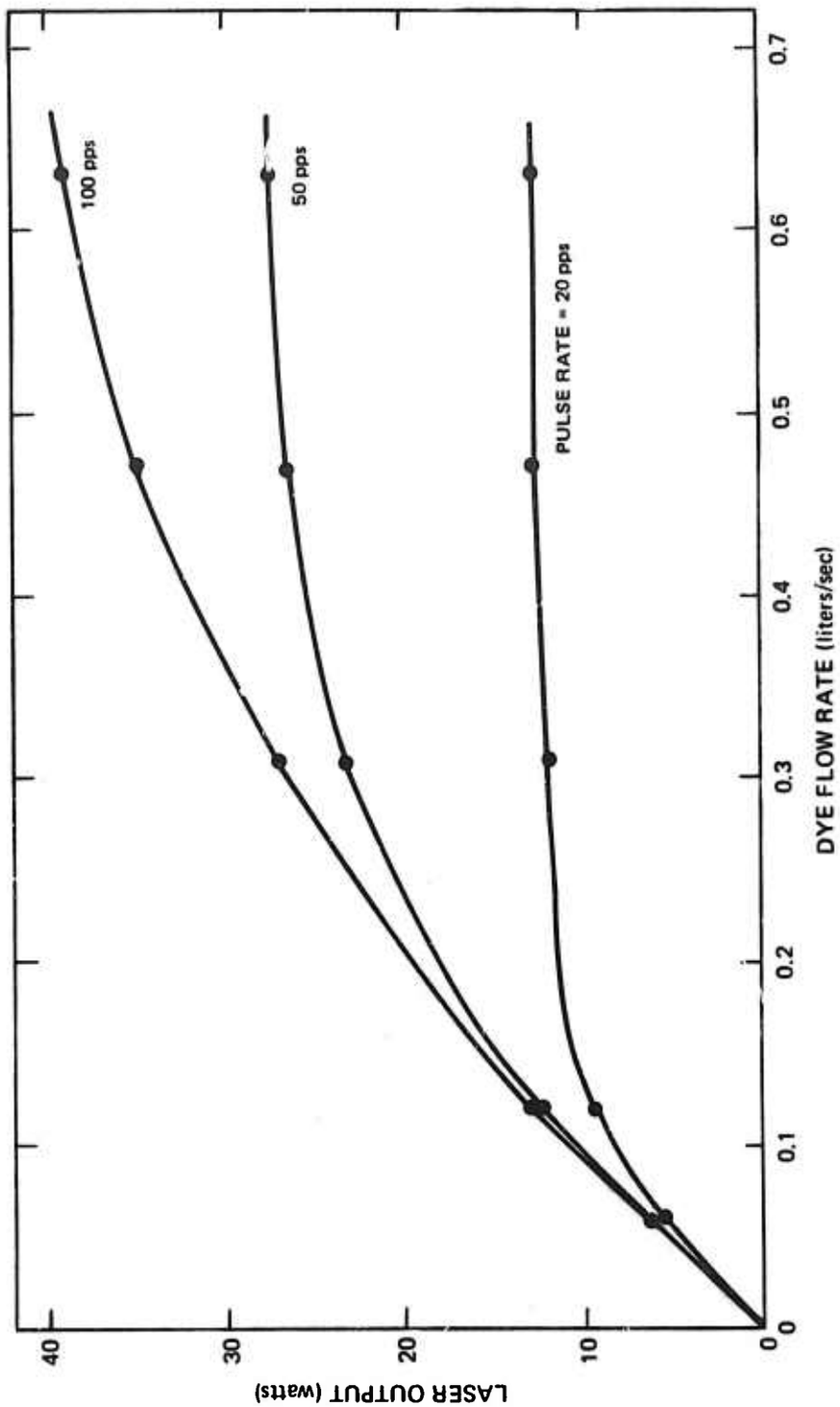

N02-144-1

FIG. III-10

LASER POWER OUTPUT VS PULSE REPETITION RATE

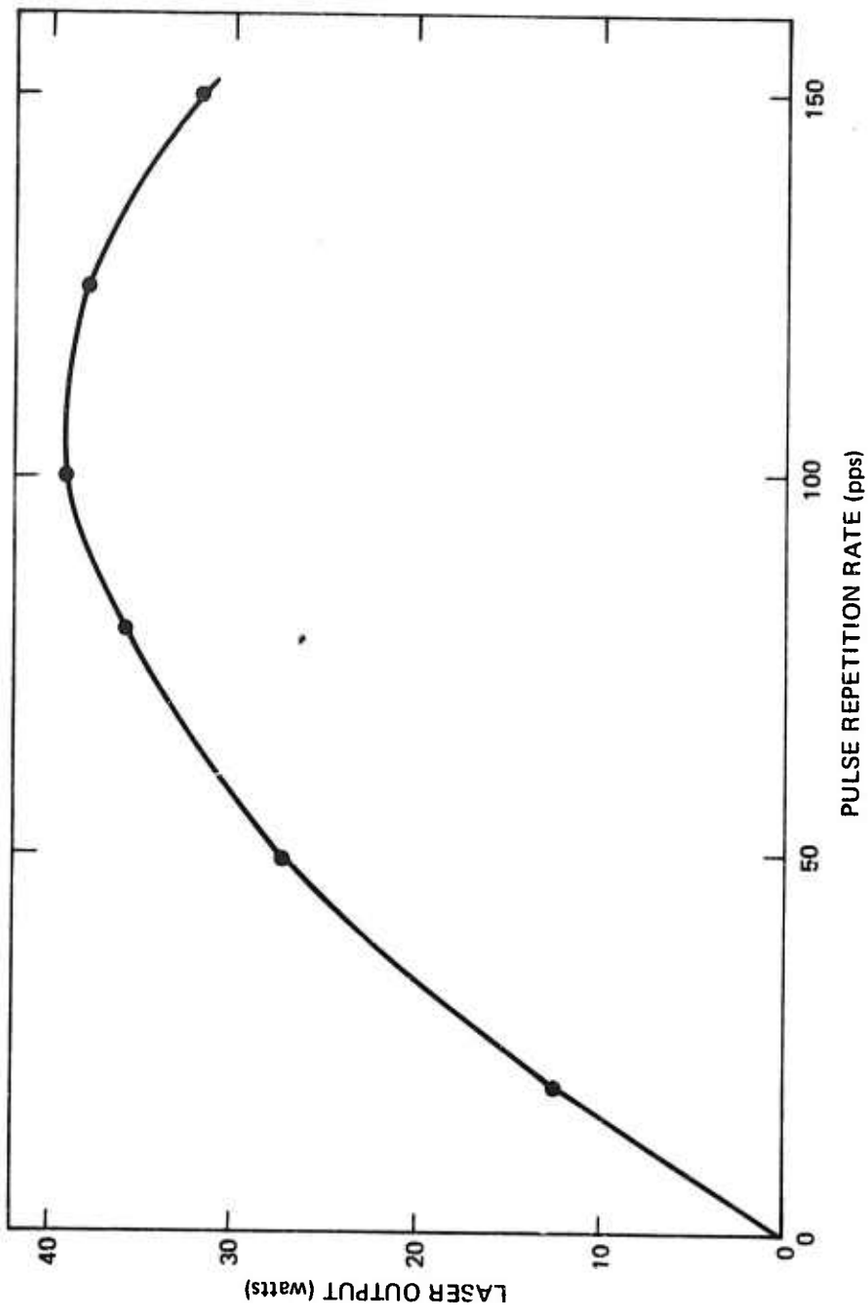

N02-144-5

FIG. III-11

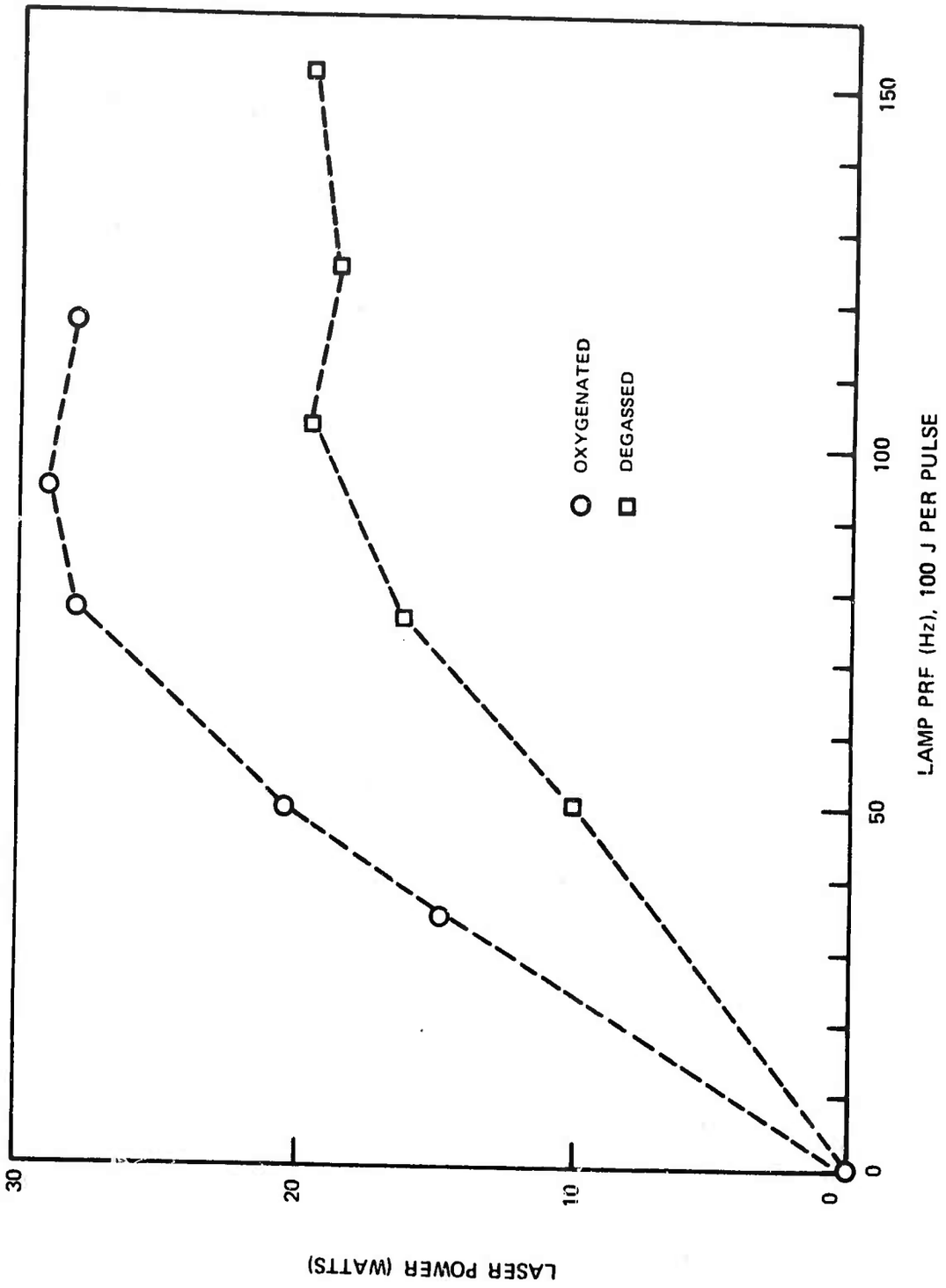

R10-74-36

FIG. III–12

LASER OUTPUT COMPARED TO FRACTION OF H_2O IN DYE SOLUTION

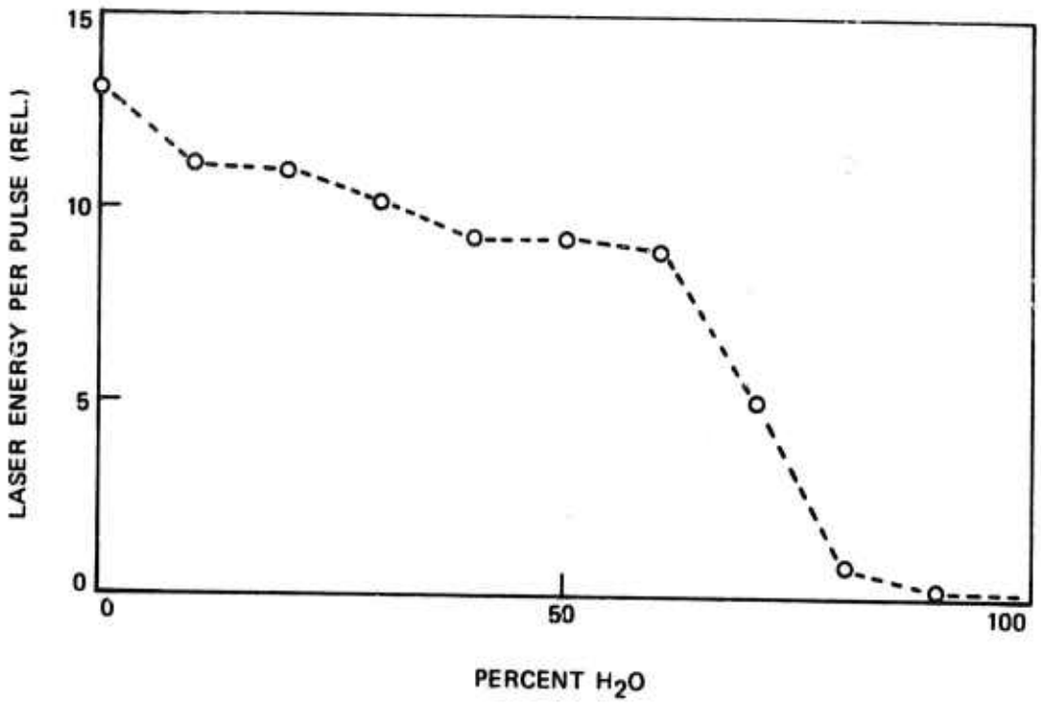

FIG. III–13

LASER INTENSITY FALLOFF AT 100 Hz REPITITION RATE

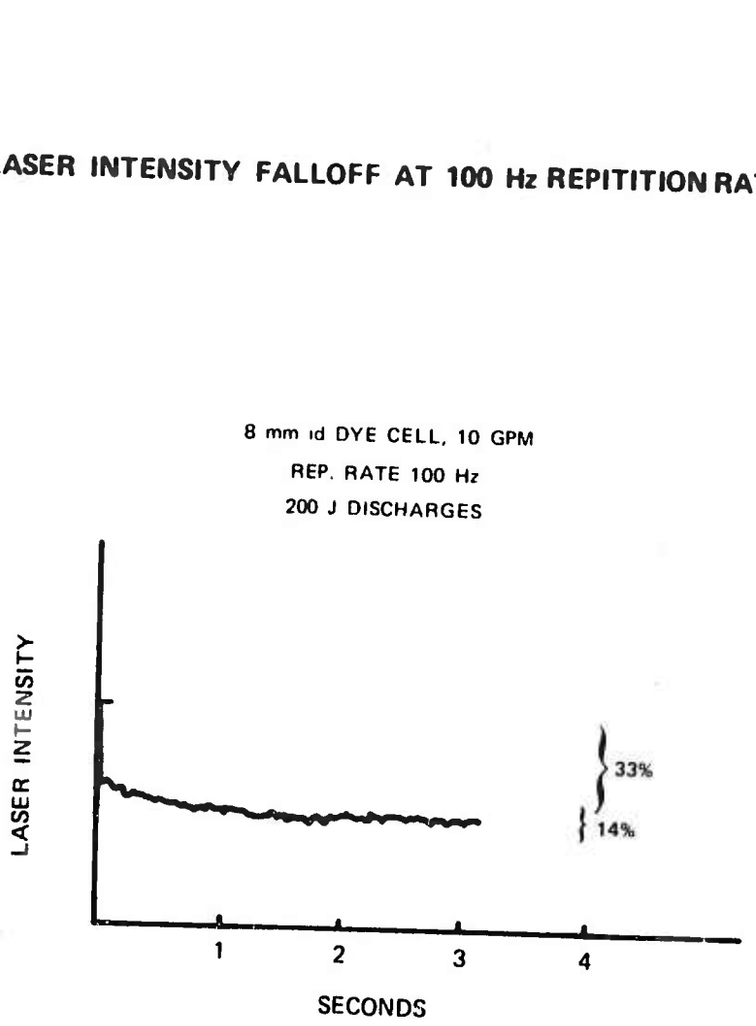

FIG. III–14

FLOW LIMITATION OF PULSE ENERGY

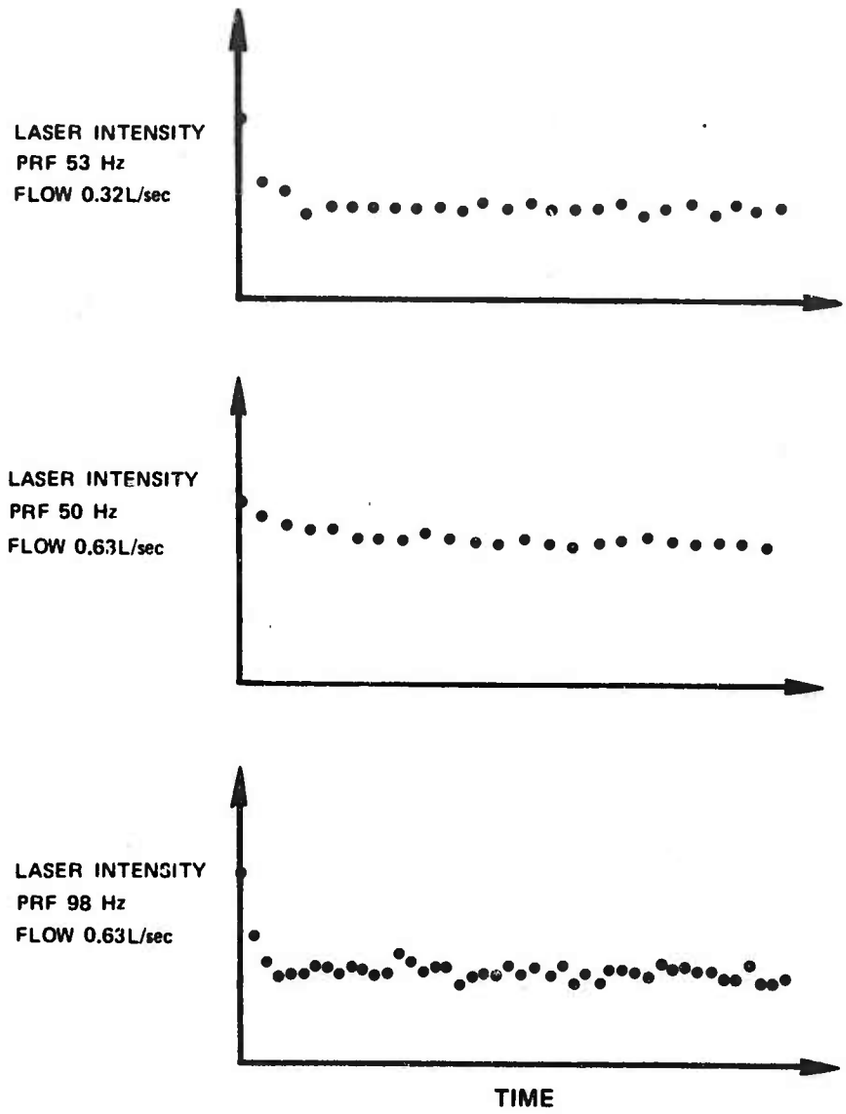

LASER OUTPUT FOR A GIVEN CROSS SECTION AREA OF DYE CELL EXPOSED

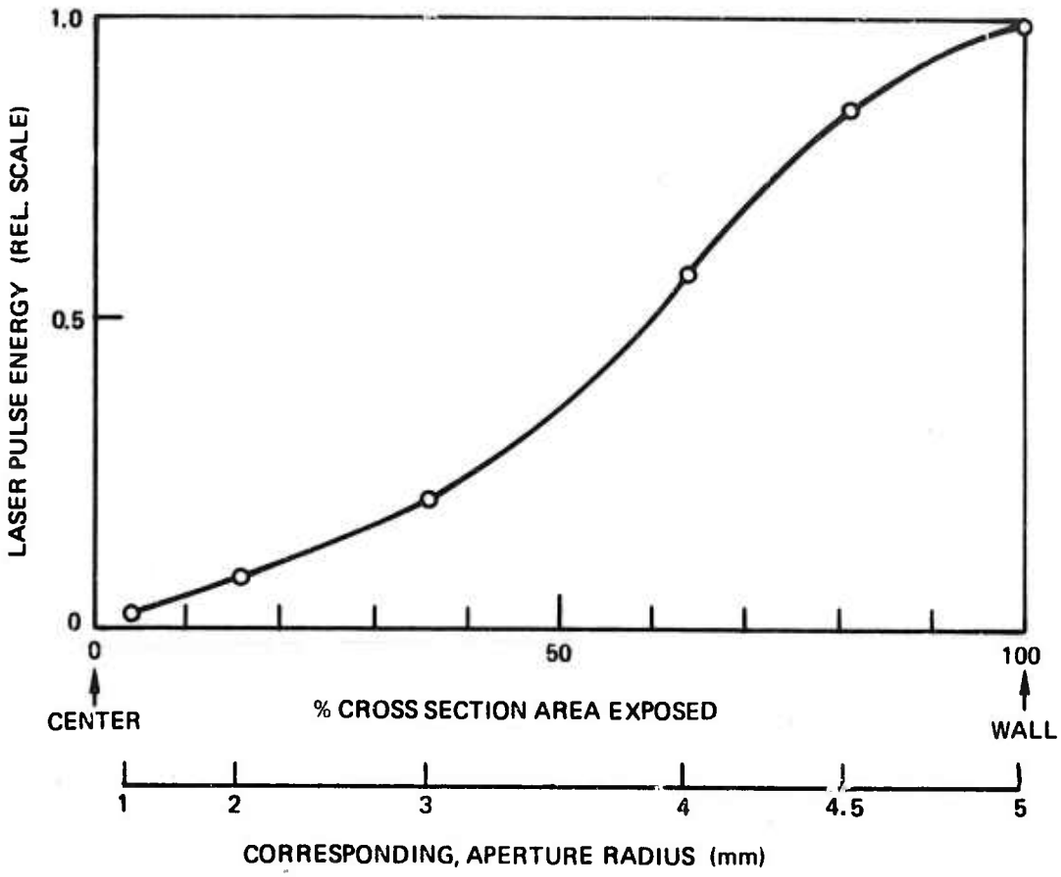

FIG. III–16

RECOVERY FROM FLASHLAMP INDUCED OPTICAL DISTORATION

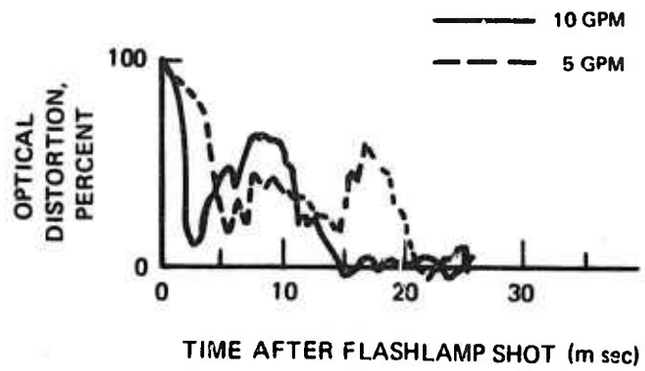

FIG. III-17

ACOUSTIC WAVE DISTORTION IN DYE CELL

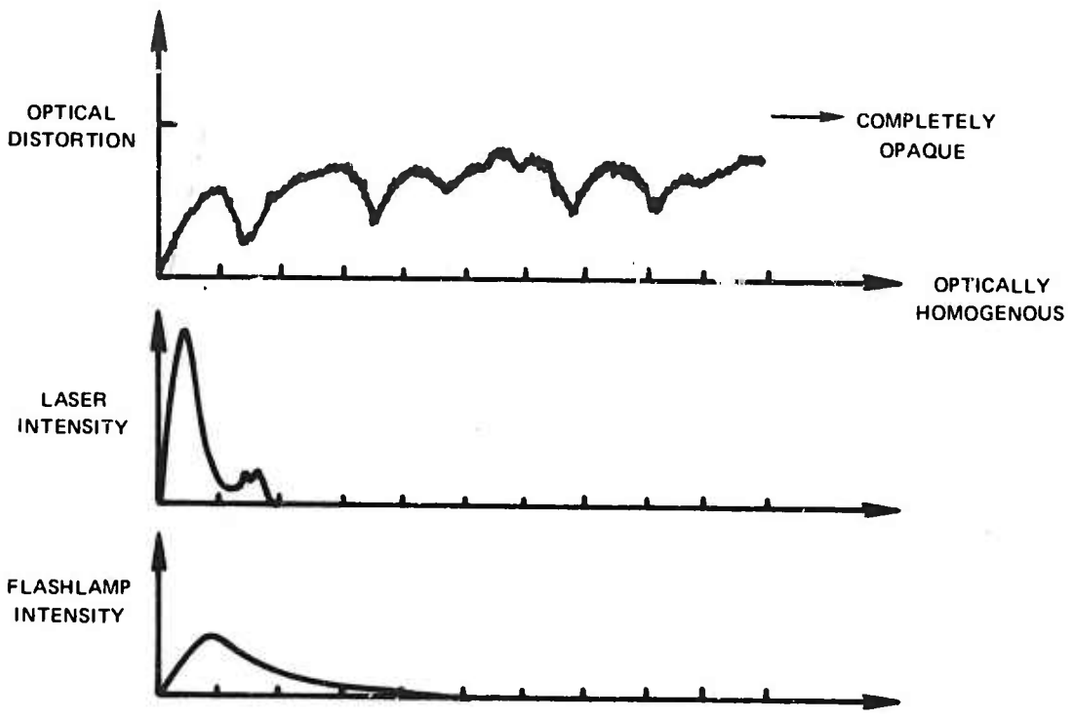

FIG. III–18

FLASHLAMP INDUCED PHOTOACOUSTIC WAVE

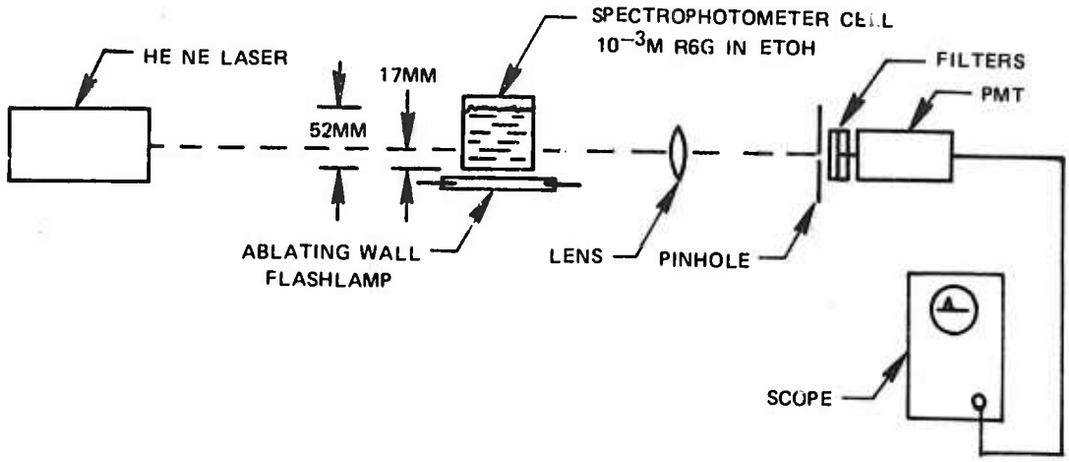

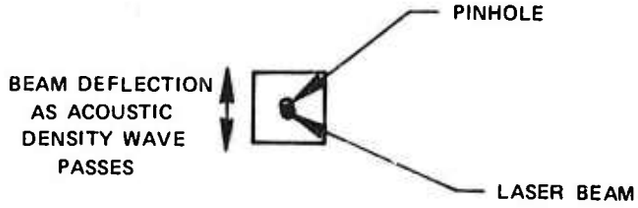

FIG. III-19

PHOTO ACOUSTIC WAVE TRAVEL IN SPECTRO PHOTOMETER CELL

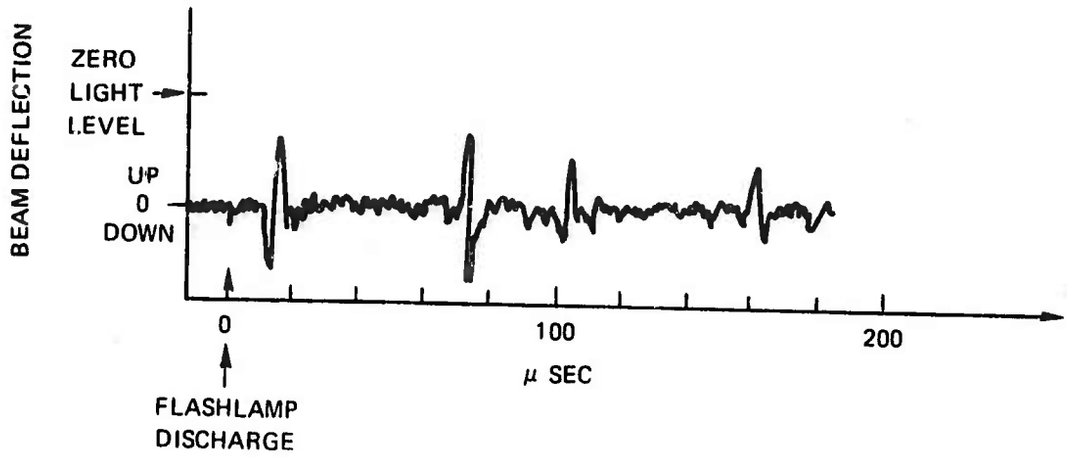

FIG. III-20

LASER BEAM QUALITY FROM SINGLE SHOT LASER TESTS

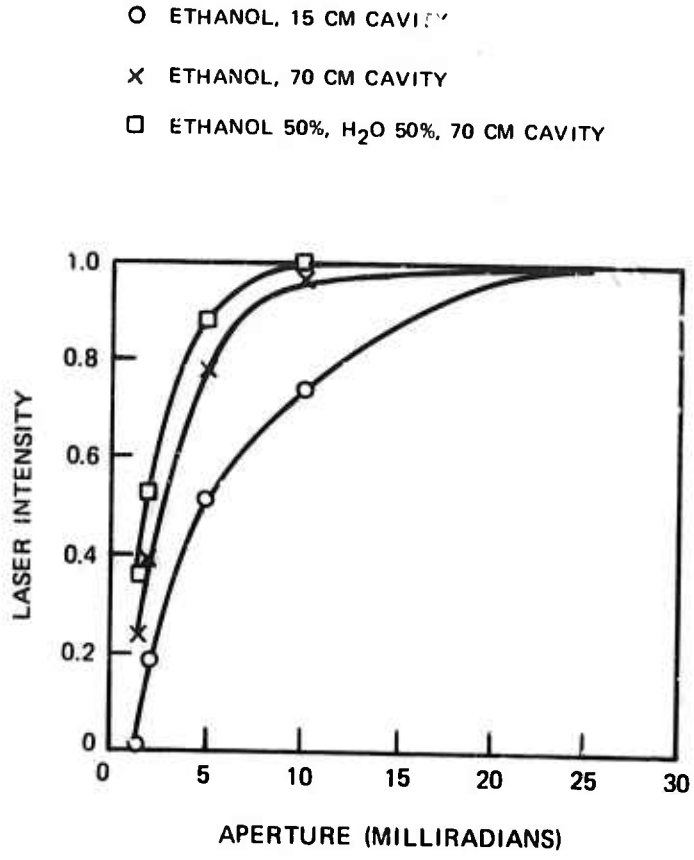

IV. TRANSVERSE FLOW DYE LASER

Introduction

From the discussions in Section III, it is apparent that the principal limitation to obtaining higher average laser power is the fluid flow rate through the dye cell. For laser repetition rates larger than about 60 Hz the fluid is simply not being replaced fast enough. The use of a bigger pump was not the answer either, since the limitation in the flow velocity in the dye cell (12m/sec) and the pressure limits of the pump seals (60-70 psig) have been reached. Clearly a completely redesigned flowing dye cell is needed to permit lower pressures and higher flows. Experimental results of S. G. Varnado (Ref. IV-1) indicated that larger flow velocities will degrade the laser output by the production of small bubbles in the dye solution. We had to pressurize the fluid system for the axial flow laser in order to avoid the generation of bubbles when the flashlamp was fired. It is clear, then, that probably only small gains at best could be achieved in laser average power by redesigning the axial flow system for a faster flow rate

A system that flows the dye solution transverse to the flashlamp pumping axis would give a gain in the dye replacement rate of the length to diameter ratio of the flashlamp. In addition, we can make a transverse flow system narrow so that the dye volume is smaller. A transverse flow system, then, would allow us to run the laser to a much higher pulse repetition frequency without the sudden fall off in pulse intensity observed with the axial flow laser. The disadvantage of a transverse flow system is the inability to focus the flashlamp light into the dye cell as efficiently as with an axial flow system. It will be shown in the following sections that the repetition rate advantage of the transverse flow outweighed the loss in efficiency to give us a much higher average laser power.

We considered two designs for a transverse flow system. The first one is shown in Fig. IV-1. Two grooves could be cut on opposite sides of the dye cell hemisphere and a channel placed through the hemisphere as shown . In order to avoid severe reflection loss for high angle of incidence light rays cylindrical focusing lenses would have to be used for the dye cell pumping windows. The light collection efficiency with the flow channel placed in the reflecting sphere is greatly reduced when compared to the axial flow dye cell. This is because the focusing optics can only direct light from a limited angle into the dye cell.

The second design considered was to place a straight flow channel at the opposite focus of an elliptical reflector from the flashlamp. This requires cutting off the ellipse at the focus where the flow channel is to be placed. A fraction of the pumping light will then be lost by the light baffling of the flow channel. The

second design was chosen for several reasons. First, the light collection efficiency should not be any less than the transverse flow in the spherical reflector. We could improve the flashlamp design to allow both envelope end seals to be recessed from the hot arc region. Also no long, narrow struts are required to remove the hot gases from the pumping cavity. We could also easily isolate the laser resonator optics from the flowing dye channel. This avoids mechanical vibrations and gives more flexibility for inserting optics in the laser resonator.

Figure IV-2 shows a front view photo of the dye flow channel. The new flashlamp constructed for this laser ran conveniently with a 10 cm arc length. The dye channel, therefore, was made 10 cm wide to accommodate the new flashlamp. Figure IV-3 shows a side view of the dye channel. From this view we can see how the flow channel tapers down to the window section where the flashlamp light is focused into the dye solution. A water lens helps to focus the flashlamp light into the channel. The lens gives a significant increase in the laser output as demonstrated beforehand by a ray tracing program. This will be discussed in the next section. The following sections will discuss the flow system and then the results of the laser tests for both single shot and repetition rate operation.

Ray Tracing Program

As a guide in the design of the transverse flow laser, a ray tracing program was used to calculate the properties of the pumping cavity. The program that was used was a highly sophisticated, three dimensional program that was developed on another project. The program is based on a Monte Carlo method. Rays are emitted in random directions and from random points within the arc source. The history of each ray is then computed as it propagates within the cavity. Dielectric claddings of arbitrary refractive induces may be placed around the lamp and/or laser medium, and the program accounts for all the Fresnel reflections and refractions at the interfaces. The rays are followed until they are absorbed by the laser medium, the arc, or other absorbing structure in the cavity. The program can account for the reflectivity of the pumping cavity walls, and, because of its three dimensional capabilities, can account for end losses. In this project, the full capabilities of the program were not used. It was used rather to provide an estimate of the distribution of pumping intensity that would be expected in the transverse dye flow channel.

The program was applied to the idealized pumping cavity shown in Fig. IV-4. The dimensions shown in the figure are those of the elliptical cavity that was actually used for the transverse flow laser. The program was arranged to provide a ray counter in the plane of the latus rectum of the ellipse where the flow channel was located. Typical results are shown in Fig. IV-5. The results are shown for two cases, with and without an auxiliary cylindrical focusing lens of 20 mm radius. It is clear that the auxiliary lens is quite effective in increasing the pumping intensity in the transverse flow channel and reducing the excited area. The minimum in the curve with the lens corresponds to the point of contact of the lens and the flow channel. Rays incident at this point are either refracted inward toward the axis or suffer large Fresnel reflections and are reflected outward from the axis.

As mentioned above, the ray tracing program is very versatile and can model most of the properties of an actual pumping cavity. In further work, this could be used to develop a fully optimized cavity for a transverse flow system.

Flow System

The transverse flow channel and manifold chambers were constructed from 1/16 inch stainless steel metal, welded together and pacified to prevent corrosion. A rigid aluminum frame holds the manifolds and tapered boxes in place. Solarization resistant fused quartz windows were attached between the two tapered boxes to form the section where the dye solution is optically pumped by the flashlamp. The windows that form the laser cavity were antireflection coated on the outside surface and placed on the ends of the flow channel. The window opposite the pumping window was backed by a polished aluminum reflector as shown in Fig. IV-3. Without the reflector the laser output would drop 14 percent.

At first we epoxied all the windows in place. The epoxy joints and quartz windows are rigid, but the stainless steel channel is flexible. As a consequence, small channel pressures can build up large stresses at the epoxy joints and eventually cause either the quartz window or the epoxy seal to break. The epoxy was replaced with RTV which is more flexible. The RTV worked for the most part, but after a few weeks dye solution would seep out under the seals at the end windows. This might have been avoided by sandblasting the window surfaces that are joined by the RTV. The sandblasted surfaces would give the RTV more area to adhere to. In any event, a mechanically sealed design with the special cut and ground windows required would be the ultimate solution. Time limitations, however, prevented this option.

Figure IV-6 is a schematic of the circulating dye system built for the transverse flow dye cell. A 40 GPM centrifugal pump was driven by a 3 hp variable speed motor to provide the dye circulation. The pump easily gave 40 GPM with the motor speed control set to 80 percent of full speed. The 22 inch cartridge filter and housing used earlier was replaced by a larger capacity filter that could handle the 40 GPM flow with only an 8 psig pressure drop. With several hours of accumulated running time no clogging of the filter system was observed in contrast to the gear pump system. After leaving the dye cell, the solution went into a 6 inch I.D. by 2 ft high reservoir. From the reservoir, the solution returned to the pump. Two inch I.D., rigid PVC tubing was used to interconnect the pump, flowmeter, filter housing, dye cell and reservoir. The system was filled through the top of the reservoir and several drain valves were placed around the system to allow quick and efficient drainage. A second pump, filter, and reservoir system circulated distilled water for the focusing lens. Before entering the focusing lens, the water was passed through a 1/4 inch stainless steel coil immersed in the dye solution reservoir. This allowed the lens water and dye solution temperatures to equilibrate and prevent the possibility of thermo-optic distortion from heat transfer between the two fluids through the pumping window.

Figure IV-7 shows the pressure vs flow rate curve for the transverse flow system. The transverse flow system was originally hooked up with the 20 GPM pump and 22 inch cartridge filter. Data for both pumps is shown in the figure.

The velocity in the flow channel was measured by determining the transit time of entrapped bubbles moving between two parallel He-Ne laser beams separated by 4.5 mm. Light scattering from a bubble as it crossed the He-Ne beams was detected. If the density of bubbles was kept low enough we could time a single bubble transiting the two laser beams. Figure IV-8 shows a typical result. The velocity measured this way agreed with the average velocity computed from the flow meter indication and cross sectional area of the channel. This measurement served as a check on the flow meter.

Figure IV-9 shows the results of the recovery time measurements for flashlamp induced distortion in the dye channel. The experimental setup was the same as described for the measurement on the axial flow laser. In this case, however, there was no vibration noise to contend with, and the measurements were quite good. The He-Ne beam transited the channel at the center of the pumping axis. Thus, the indicated recovery time is one-half the recovery time for the exposed dye. The recovery times were in agreement with what we would calculate from the flow rate. Figure IV-9 shows the overlays of the recovery time for the three different flow rates listed.

The recovery rate was also tested with the flashlamp running at repetition rate. The results were essentially the same as the single shot recovery times. This is shown in Fig. IV-10.

The channel for the above tests had a thickness of 1.8 mm. For the laser tests, however, the channel was set at 3 mm. With a maximum flow of about 2.52 ℓ/sec, the flow velocity in the channel is 774 cm/sec. Since 1.9 cm of window height is exposed to the flashlamp, we get a maximum change-over-rate of 392 sec^{-1} for the 3 mm channel.

In another test we measured the deflection of a He-Ne laser beam that transits the flow channel. The He-Ne beam was sent through the channel along the lasing axis and reflected to a frosted glass screen. We used a high speed Dynafax 35 mm drum camera to take framing pictures of the deflection of the He-Ne beam spot when the flashlamp was run at repetition rate. Figure IV-11 shows the results of the drum camera measurement with a flow rate of 1.2 ℓ/sec. The drum camera exposed two rows of frames. The time between each frame in a given row is .4 msec. In Fig. IV-11a the He-Ne beam was sent down the center of the channel. In the bottom row, going from left to right, we see the He-Ne beam deflecting up (actually to the right on the screen which was in a direction away from the pumping light) after the first two frames. The spot then gradually settles back to normal after about 8 frames or 3.2 msec. Figure IV-11b is the same as IV-11a except the He-Ne beam was sent along the edge of the pumping window. The beam deflection takes about 9 to 10 frames to return to normal in this case. The magnitude of the deflection of the He-Ne beam is about 5 mrad for the beam in the center and about 12 mrad for the beam along the edge. The deflection is also observed with the dye laser and will be discussed again in the next section.

The results of the measurements on the recovery of the flashlamp induced optical distortion clearly indicate the we should be able to run the laser at repetition rates well over 300 Hz without affecting the laser pulse. The transverse flow system is about 6 times faster in replacement of the dye solution than the axial flow system even when using a lower flow velocity.

Laser Tests

The transverse flow laser was first tested with single shots to determine the optimum dye concentrations and output couplings. Burn patterns of the laser beam taken on black polaroid film gave a "c" shaped pattern. Figure IV-12 shows a tracing of two burn patterns. The cross hatched areas are the places where the burning was most intense. The fact that we get a "c" shape in the intense part of the laser beam seems reasonable if one considers the pump light distribution in the dye channel. The pump light is most intense just behind the window and in the center of the focused light. In these regions, the optical index of refraction is the greatest. As a consequence, during the course of the pumping pulse, the laser beam is deflected away from the window and split vertically. The distortion builds up in the channel so rapidly that the laser pulse is terminated before the flashlamp pump light has decreased to half of its peak value (see Fig. IV-14). Figure IV-12b shows the burn pattern when the laser reflectors are angulated 10 mrad towards the flashlamp. The angulation helps to counterbalance the beam deflection away from the flashlamp and produces a more rectangular burn pattern. We also get a larger laser pulse energy and higher peak intensity with the angulated reflectors.

To get maximum pulse energy the laser reflectors were placed as close to the dye channel as possible. The laser cavity was then 13 cm long. Optimum dye concentration and output coupling were found to be 2.5×10^{-4} M and 50 to 60 percent. Figure IV-13 shows data points for laser pulse energy at different discharge energies. The laser pulse energy was measured with a Science Tech model 362 power/energy meter. The single shot efficiency for the transverse flow laser (laser pulse energy/energy stored on discharge capacitor) is just over 0.2 percent. The efficiency was improved 13 percent by using a commercially purified grade of rhodamine 6G (Pilot 559).

The transverse flow laser had an efficiency of one-half that of the axial flow laser. We expected the efficiency of the transverse flow to be smaller than the axial flow because an additional 15 to 20 percent portion of the flashlamp light that strikes the flow channel is not focused by the ellipse into the dye solution. More importantly, however, the ray tracing program showed that a sizable fraction of the flashlamp light was being reflected into the flashlamp end wells from the side of the ellipse opposite the flow channel. Also, the elliptical reflector was cut out of an aluminum piece and polished by hand. The best specular reflectivity we could obtain by hand polishing was measured to be 68 percent. The reflectivity could be improved considerably by using an aluminized, kanigen coated reflector that is overcoated with a MgF layer to enhance the reflectivity at wavelengths into the uv. We estimated the collection efficiency for the transverse flow laser to be 40 percent.

In spite of the loss in the single shot efficiency, we expected the transverse flow laser to maintain the pulse energy at much higher repetition rates than the axial flow system. When we first ran the transverse flow laser at repetition rate we found, much to our surprise, that the output dropped even more severely than in the axial flow laser. This problem was later resolved as a gas flow rate that was too small for the new 10 cm flashlamp. By increasing the gas pressure in the flashlamp (and consequently the gas flow), we significantly reduced the laser falloff proglem. The flashlamp intensity falloff was discussed in more detail in Section II.

Figure IV-14 shows overlaying scope traces of the flashlamp and laser intensities taken with the system running at 52 and 249 Hz pulse repetition frequencies. The pressure in the flashlamp was 20 psig with a corresponding flow rate of 8.3 l/sec (STP). The peak laser intensity at the 249 Hz rate drops only 10 percent in this case.

Figure IV-15 shows the average laser power for repetition rates to 250 Hz. The measured data points are shown as circles, triangles, and only a small amount from linearity at repetition rates up to 225 Hz. At 250 Hz the laser power fell below the value at 225 Hz. By increasing the pressure another 5 psig we were able to recover most of this loss and obtain 102 watts average power.

Figure IV-16 shows the laser output as a function of the dye solution flow velocity. At 100 Hz PRF the output saturates at about 2 m/sec and at 200 Hz, 4 m/sec. The repetition rate, as expected, is not limited by the dye solution flow. Why the power falls off slightly at flow velocities greater than the saturation flow (see Fig. IV-16) is not currently understood. We have already run the flashlamp with a higher pressure of 26 psig. The laser, then , should be capable of delivering considerably more average power than measured to date.

In order to make the average power measurements at input power levels above 20 kW we had to limit the laser run to about a second. For longer running times, the rotary spark gap would draw a continuous arc. If this happens excessive average currents are drawn from the power supply and the flashlamp is rendered useless for pumping the dye laser. Average power measurements were first made at 50 Hz PRF using a CRL model 201 power head and meter. The power measurements required about 3 sec to allow for the time response of the power head. Using the photodetector we could then record the laser pulse shapes as shown in Fig. IV-14 for about 1 sec running times at the higher power levels. Accurate measurements of the areas under the laser pulses were then made with a planimeter. Knowing the repetition rate, we could then accurately calculate the average laser power at the higher levels.

Another reason for limiting the laser running time at high PRF is the large dye photodegradation rate. Figure IV-17 shows the results of laser pulse energy measurements taken on the low repetition rate laser system with a circulation of 485 ml of dye solution. The shots were taken several seconds apart. The pulse energy degrades to one half of its original value after 640 shots. This computes to a value of 264,000 joules of flashlamp discharge energy per liter of dye solution. Results reported by Weber (Ref. IV-2) indicate that we could extend the life of rhodamine 6G by a factor of 4 if we replace the oxygen triplet quencher by COT (Cyclooctatetraene).

REFERENCES FOR SECTION IV

IV-1. Varnado, S. G.: Degradation in Long Pulse Dye Laser Emission under Fast Flow Conditions, J. Appl. Phys. 44, 5067 (1973).

IV-2. Weber, J.: Study of the Influence of Triplet Quencher on the Photobleaching of Rhodamine-6G, Opt. Comm. 7, 420 (1973).

FIG. IV-1

TRANSVERSE DYE FLOW CELL IN HEMISPHERICAL REFLECTOR

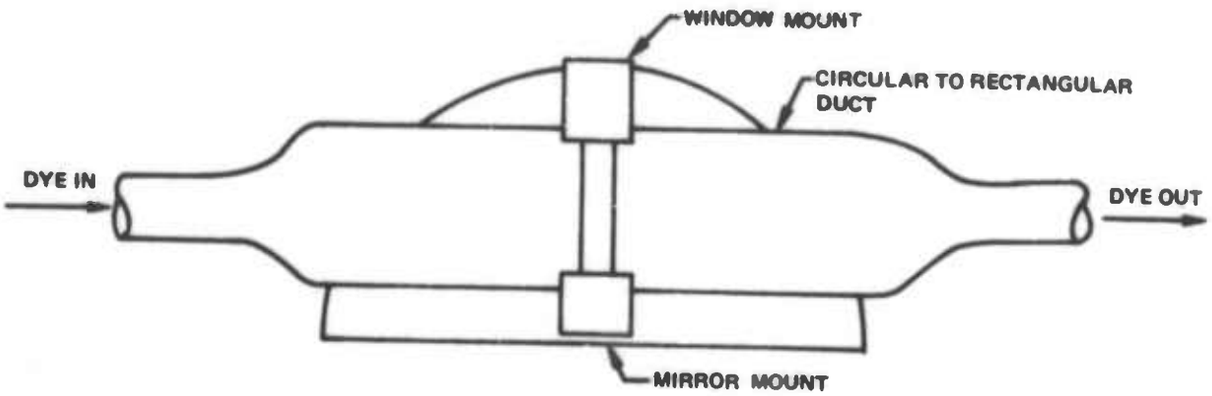

SIDE VIEW

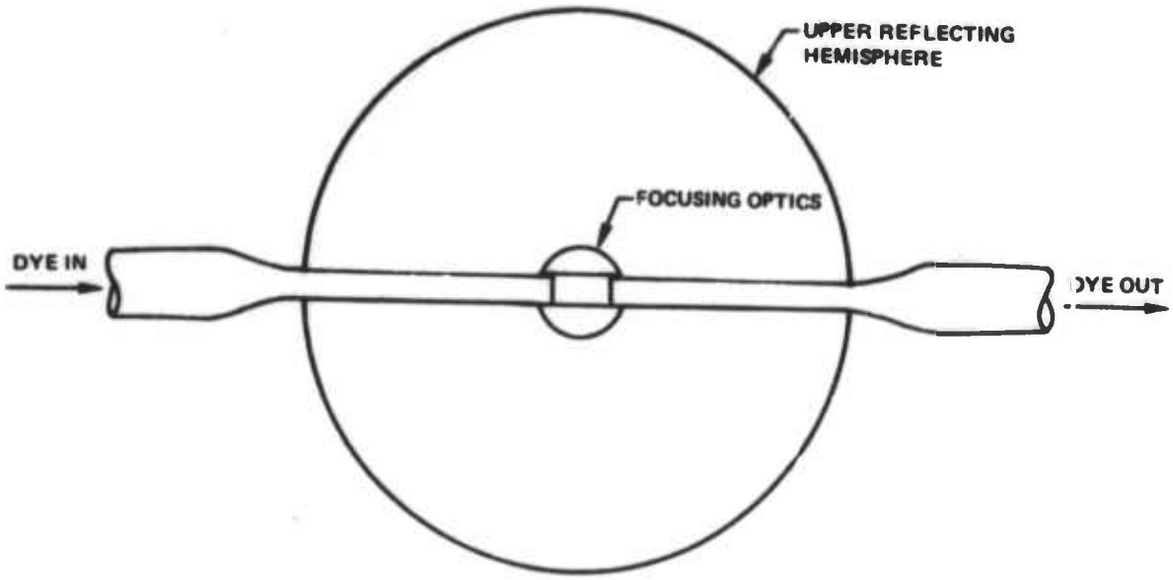

TOP VIEW

N09-162-2

FIG. IV-2

TRANSVERSE DYE FLOW CHANNEL

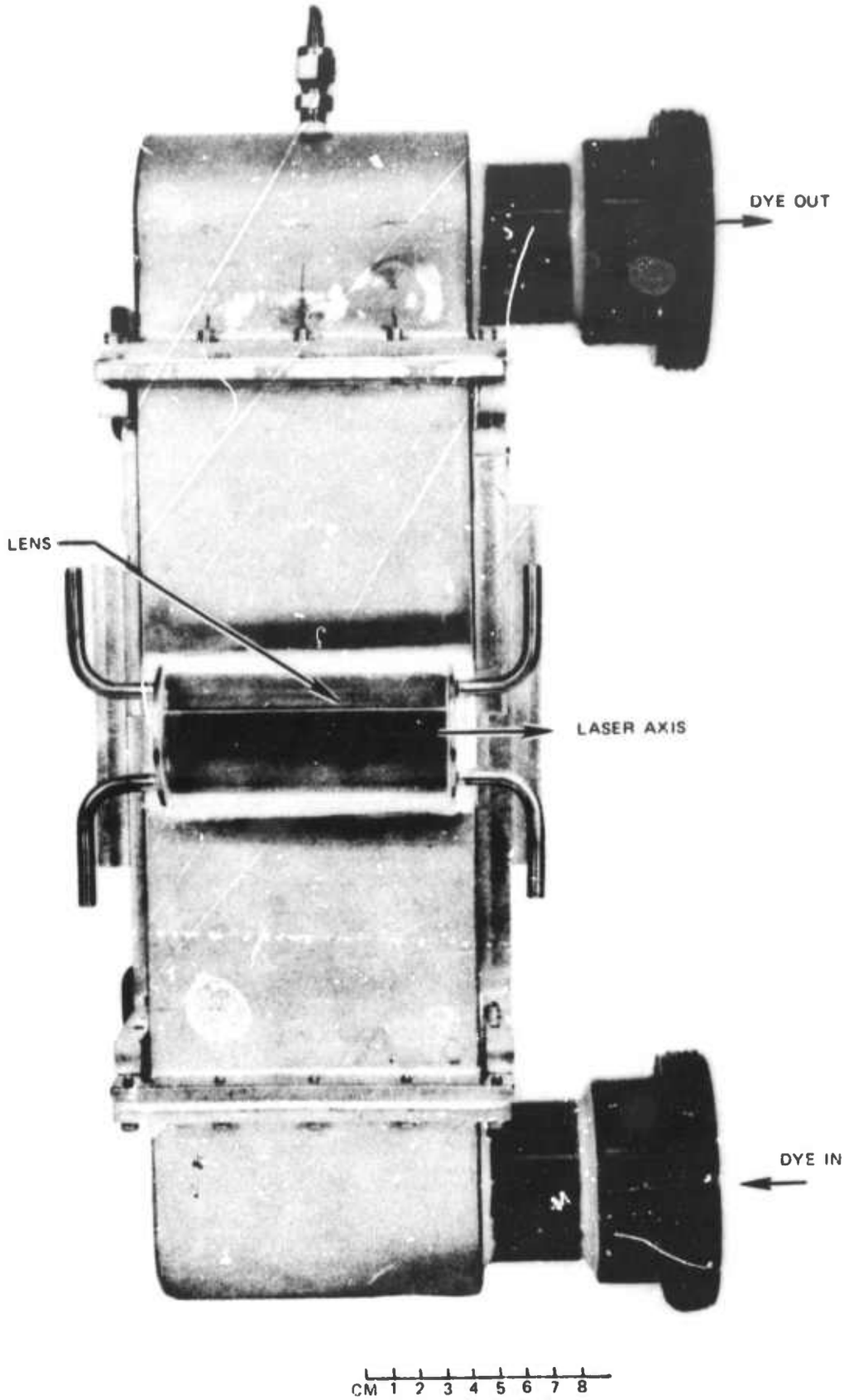

FIG. IV-3

SIDEVIEW OF FLOW CHANNEL FOR TRANSVERSE FLOW DYE LASER

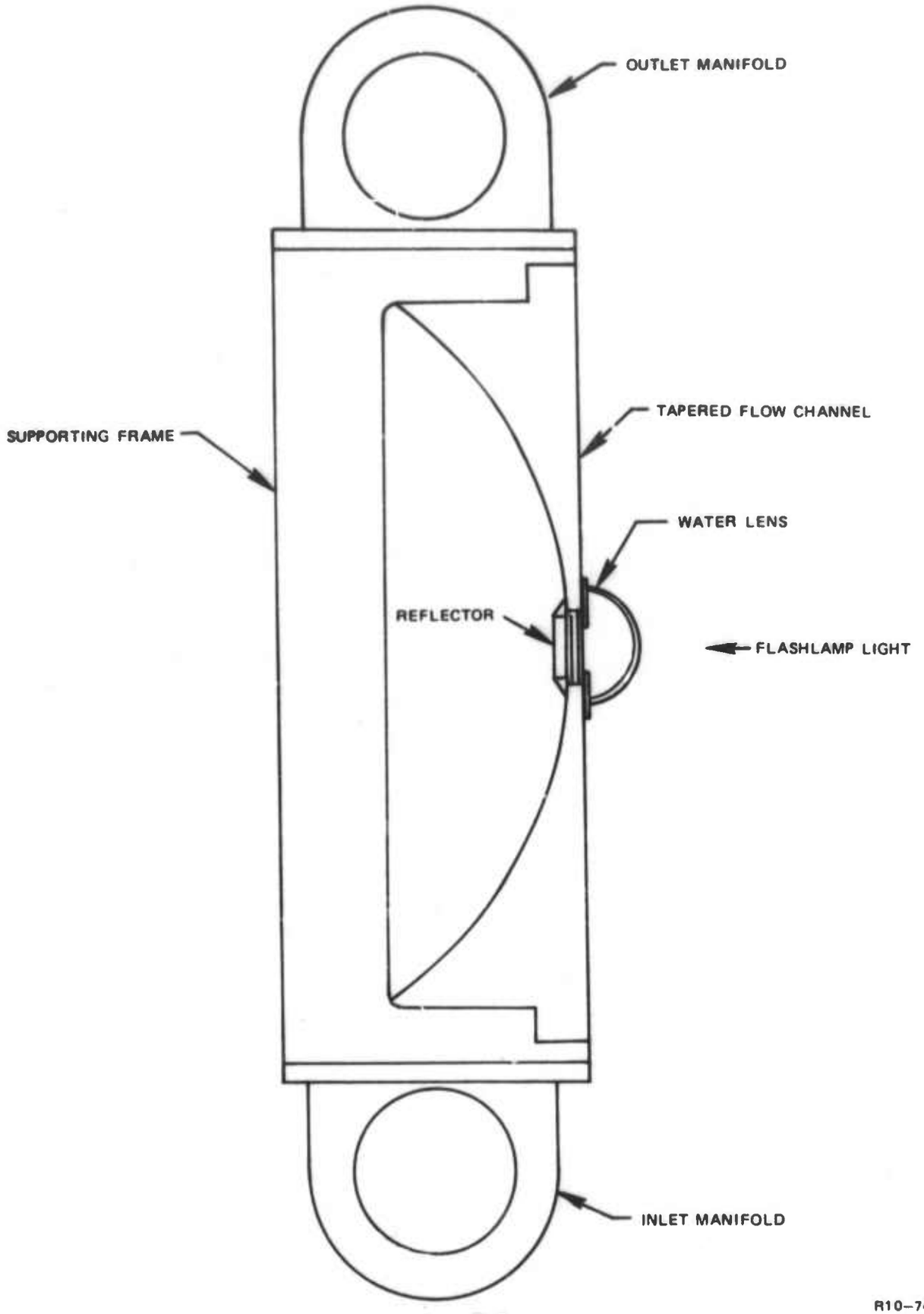

R10-74-15

TRANSVERSE FLOW CAVITY

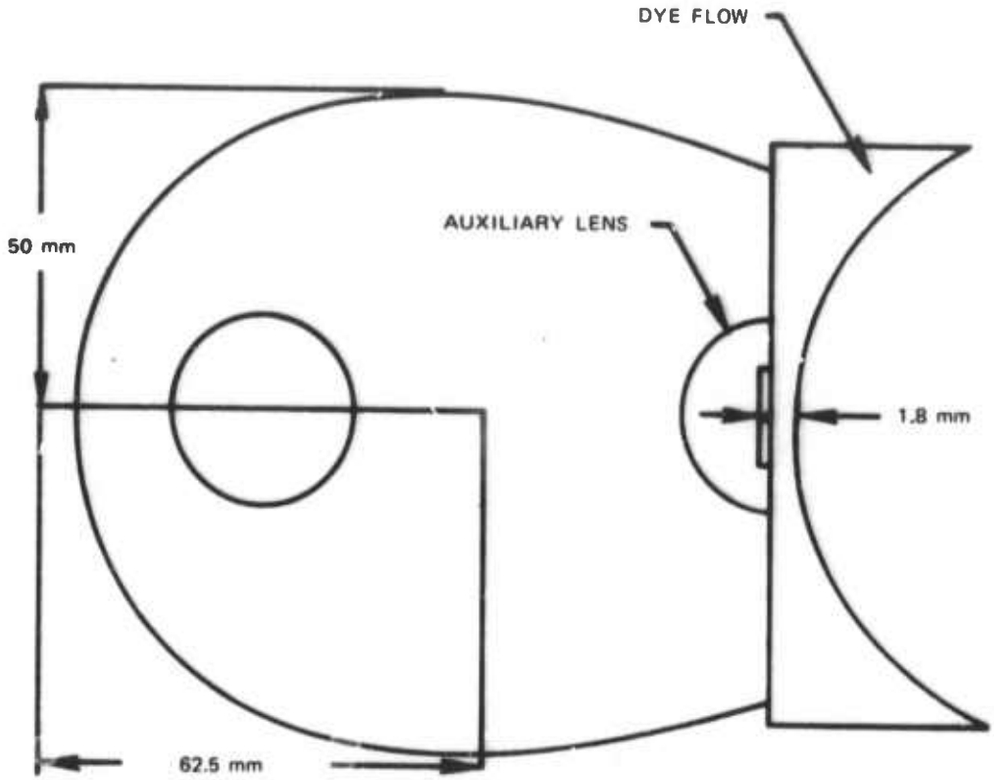

FIG. IV-5

DISTRIBUTION OF LIGHT IN FOCAL PLANE
(COMPUTED)

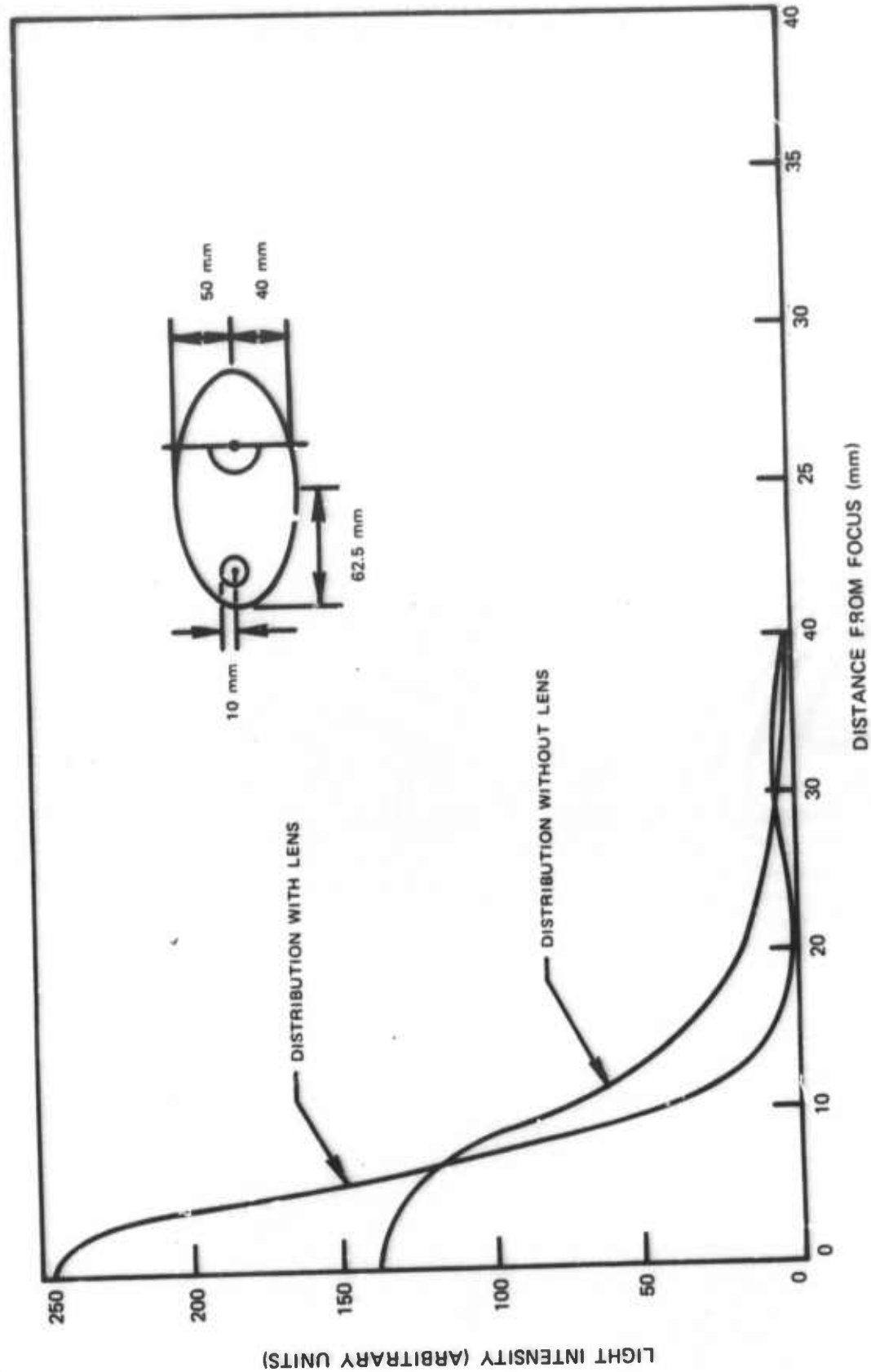

R10-74-4

FIG. IV–6

DYE FLOW SCHEMATIC FOR TRANSVERSE PUMPED DYE LASER

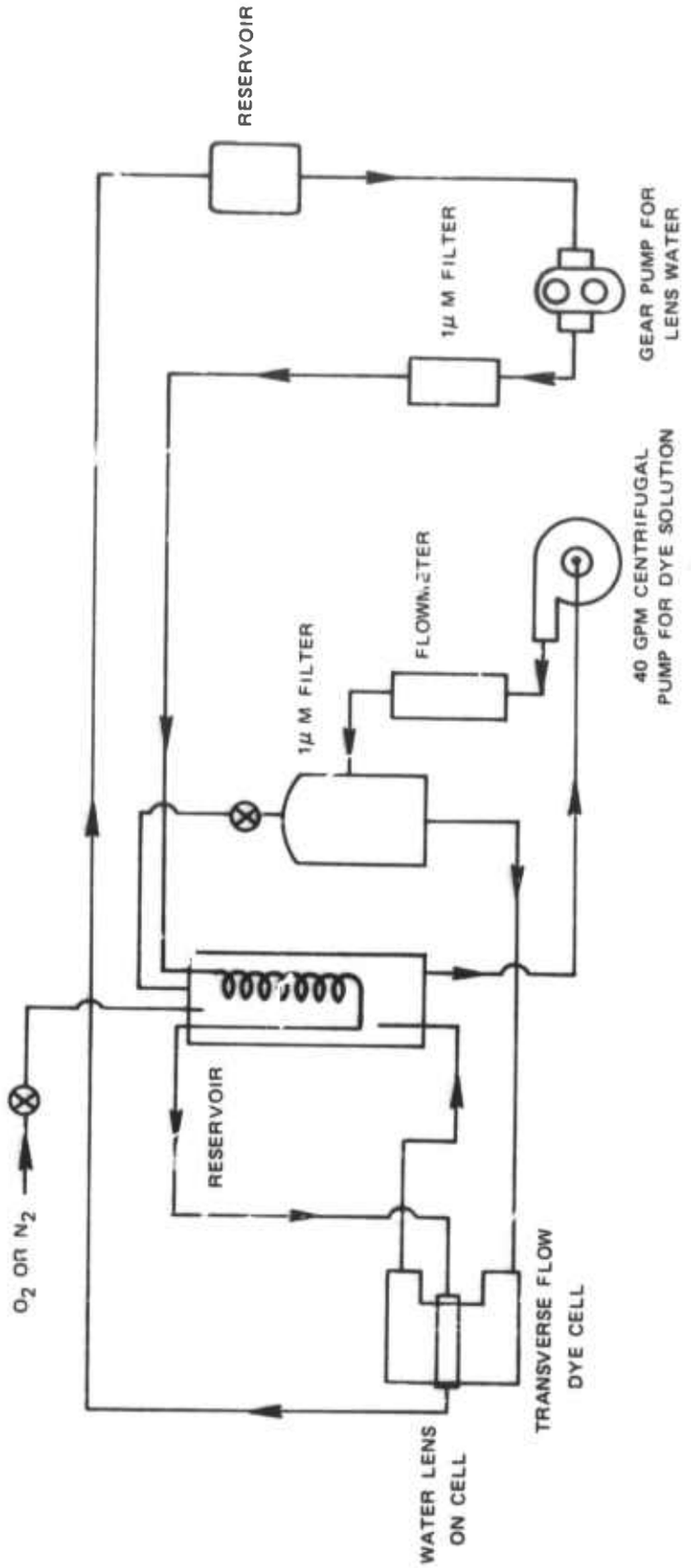

FIG. IV–7

PUMPING CHARACTERISTICS OF TRANSVERSE FLOW SYSTEM

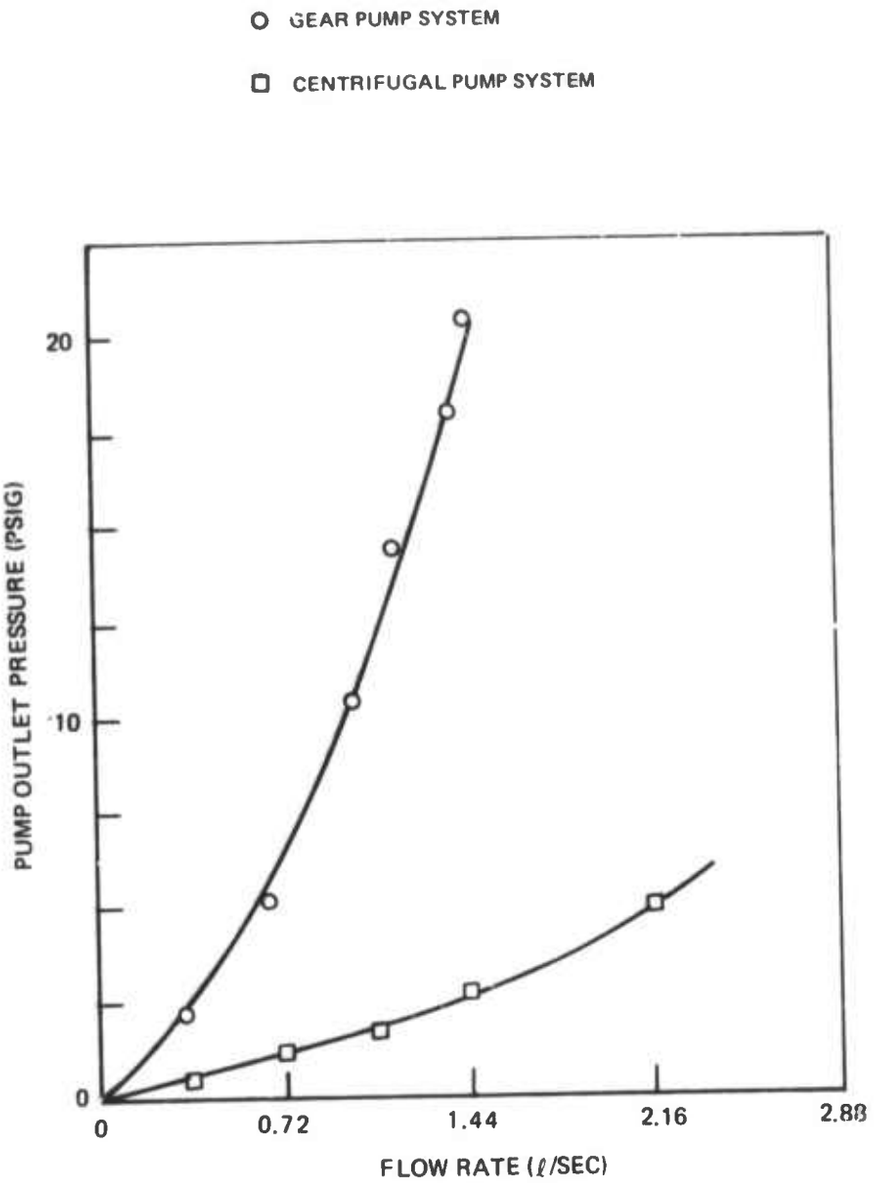

FIG. IV-8

TRANSIT TIME OF BUBBLE IN FLOW CHANNEL AT 0.72 ℓ/ SEC

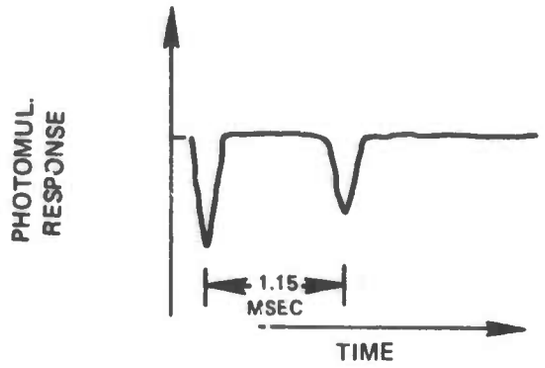

FIG. IV-9

RECOVERY FROM FLASHLAMP INDUCED OPTICAL DISTORTION IN FLOW CHANNEL,SINGLE- SHOT

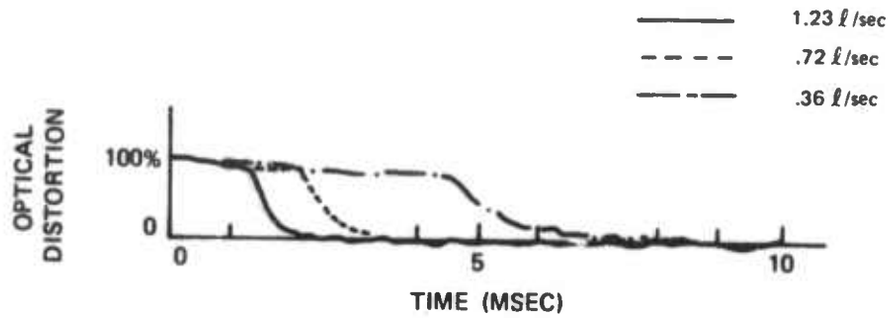

RECOVERY TIME FROM FLASHLAMP INDUCED DISTORTION AT 80 Hz REP RATE, 0.72 ℓ/ SEC FLOW

FIG. IV-10

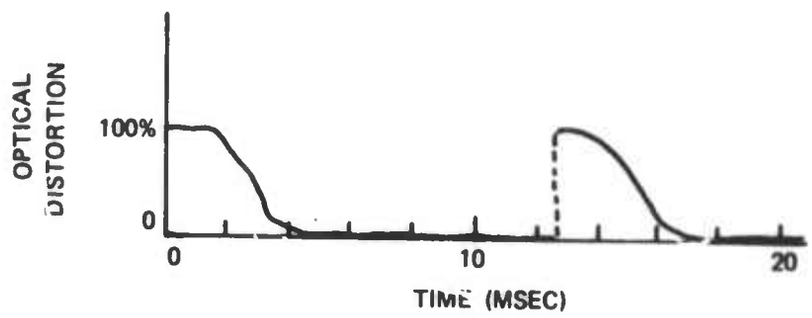

HIGH SPEED FRAMING PHOTOS OF A HE–NE LASER BEAM SPOT

THE LASER BEAM TRAVERSES THE DYE CELL.
FLASHLAMP DISCHARGING AT 100 Hz 200J/PULSE

BEAM DEFLECTION ↑

TIME ⟶

A) CENTER OF CELL

BEAM DEFLECTION ↑

TIME ⟶

B) EDGE OF CELL

BURN PATTERNS FROM TRANSVERSE FLOW DYE LASER

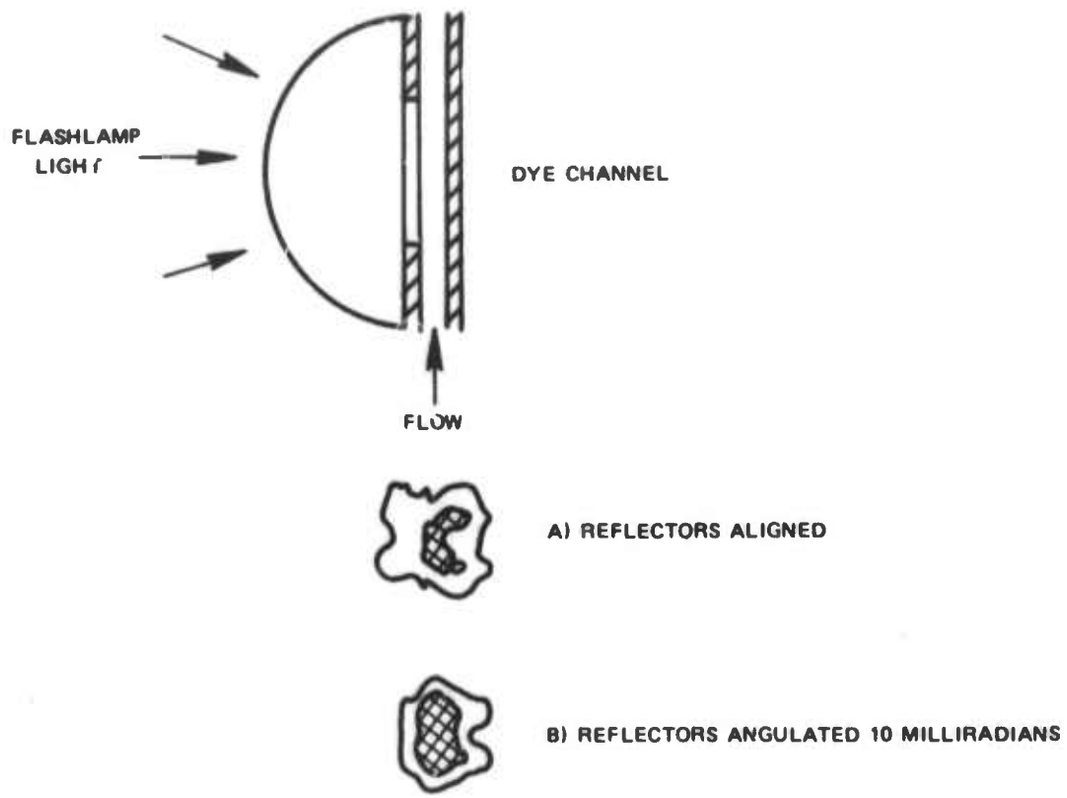

FIG. IV-13

SINGLE SHOT LASER PULSE ENERGY FOR 37% OUTPUT REFLECTOR AND DYE CONCENTRATION 2.5×10^{-4} M

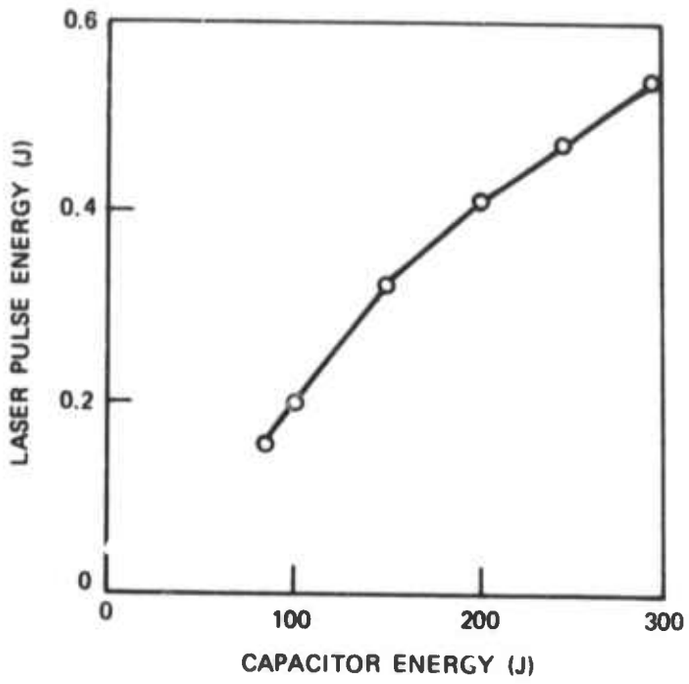

LASER AND FLASHLAMP PULSES

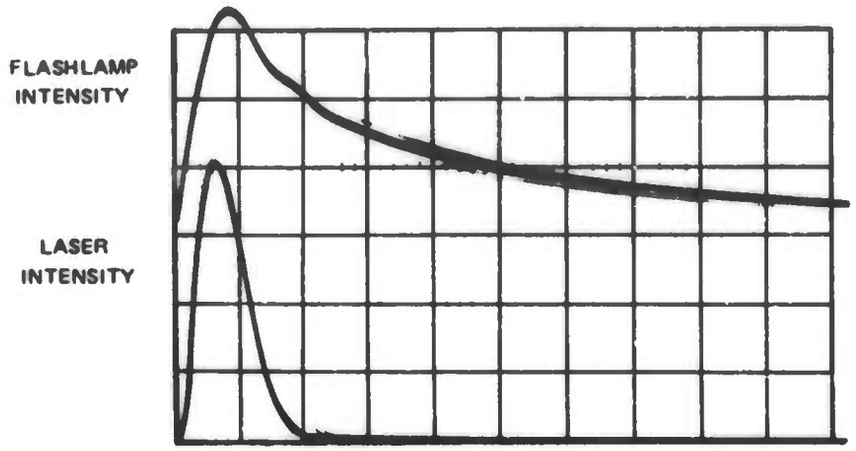

A) 52 Hz PRF ; 0.47 J/PULSE

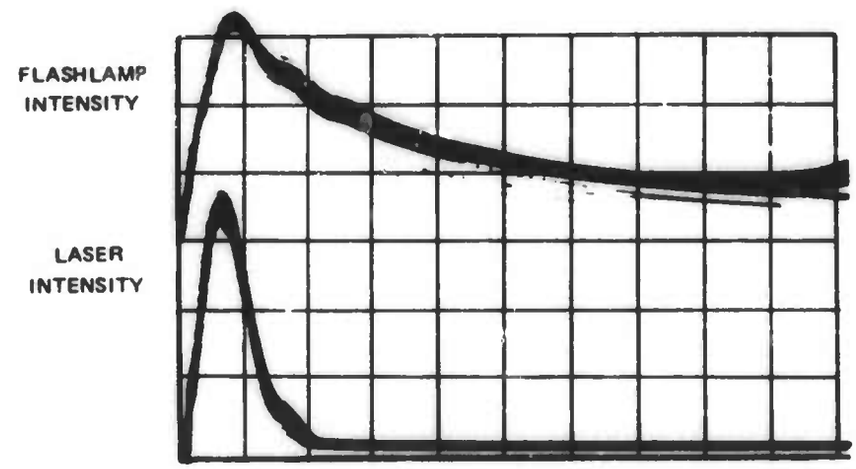

B) 249 Hz PRF

FIG. IV–15

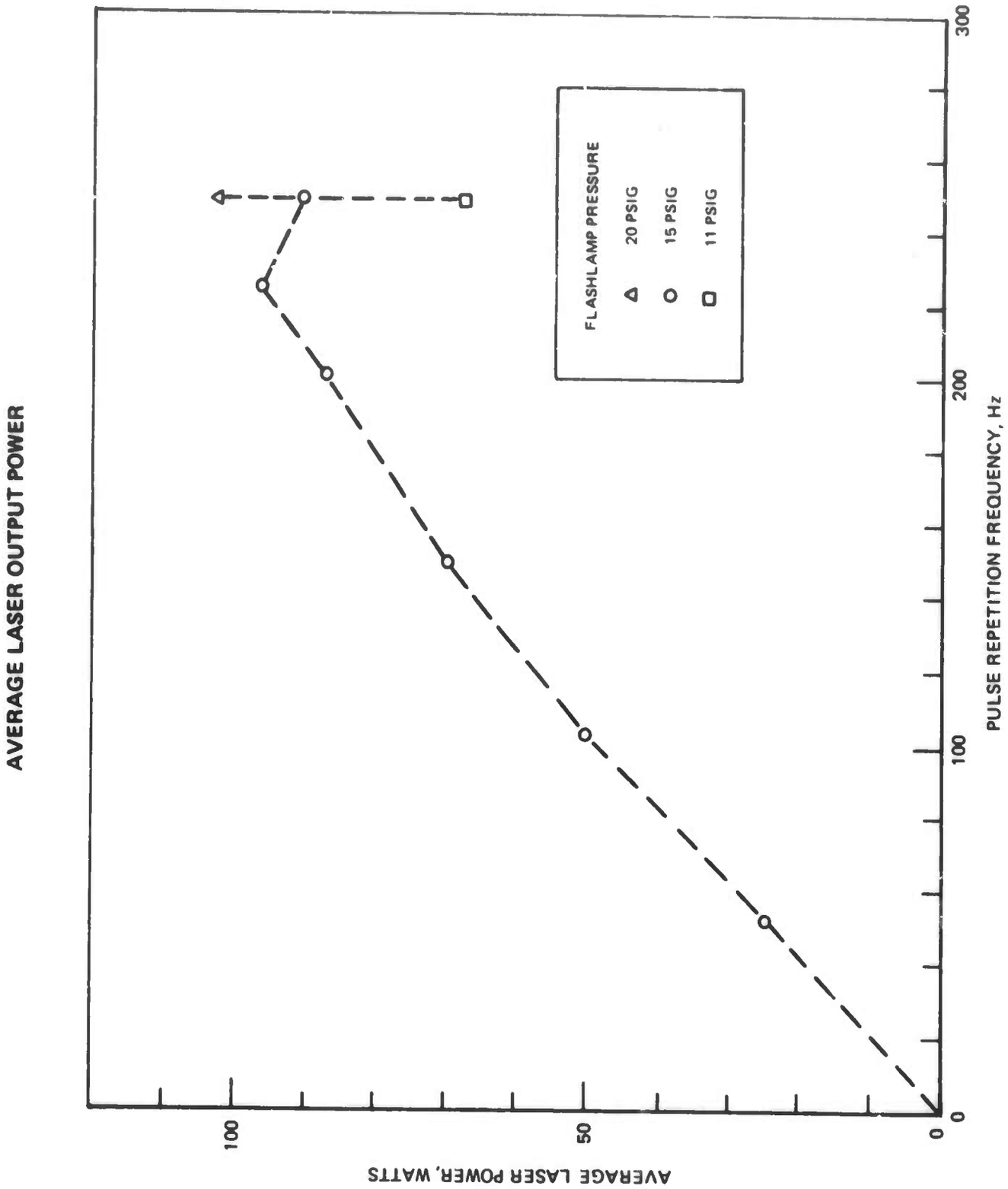

R10–74–49

FIG. IV-16

EFFECT OF FLOW VELOCITY ON LASER OUTPUT

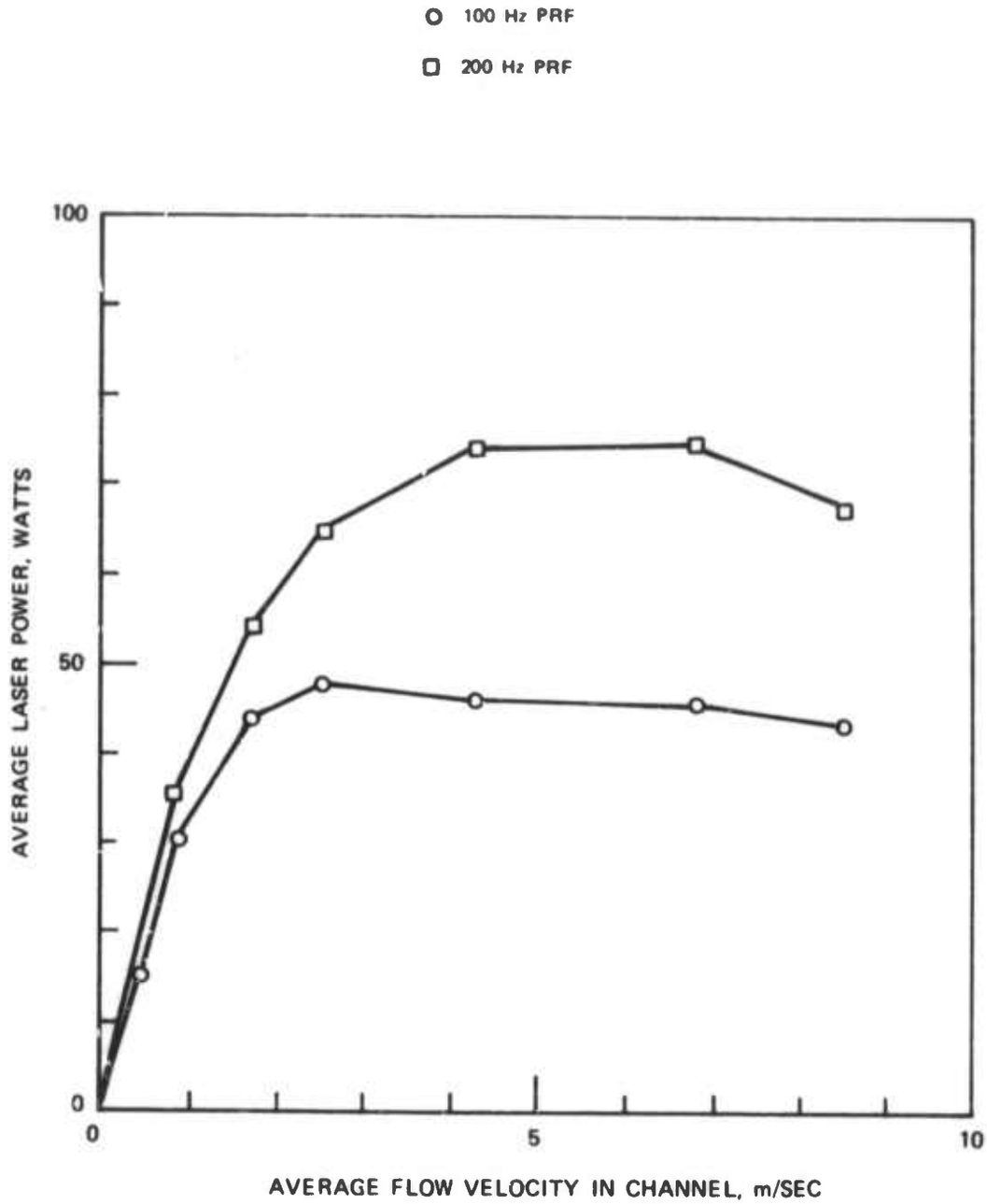

FIG. IV-17

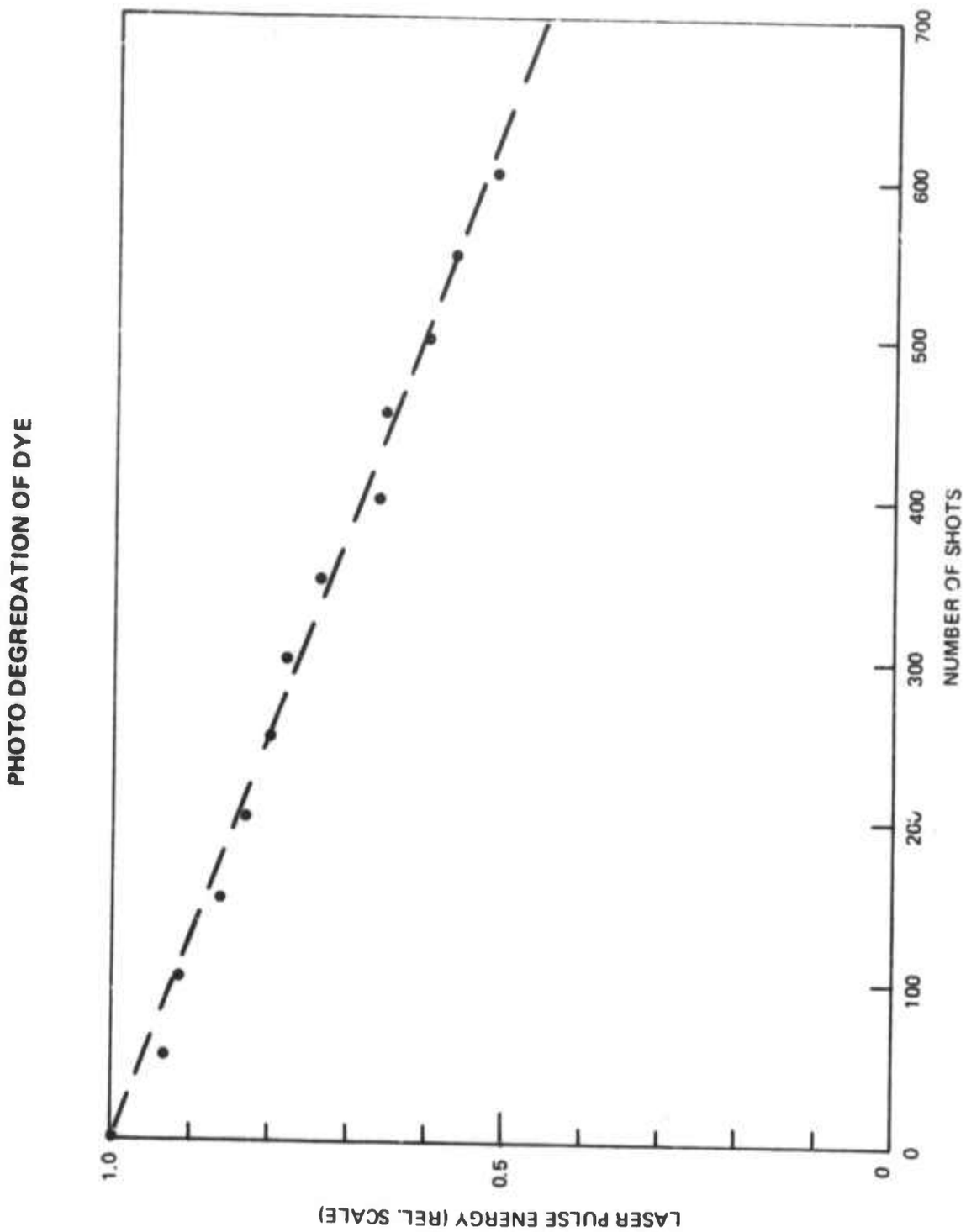
PHOTO DEGREDATION OF DYE
LASER PULSE ENERGY (REL. SCALE)
1.0
0.5
0
0
100
200
300
400
500
600
700
NUMBER OF SHOTS

V. HIGH RESOLUTION DYE LASER RANGING

Modulation Techniques

In many of the applications envisioned for the high power dye laser, it would be desirable to be able to obtain better range or time resolution than that which can be provided by the 1-2 microsecond pulse duration of the dye laser that has been described in previous sections. There are a number of approaches that could be used to obtain better resolution. The most obvious solution of course would be the use of a shorter pulse. This is not attractive since shortening the pulse duration will generally reduce the total pulse energy. One is then led to consider various forms of modulation that could be imposed on the laser to obtain better time resolution while maintaining the overall pulse duration. The situation is similar to the pulse compression problems dealt with in microwave radar. It is different, however, in that in the microwave case we can use coherent processing of the carrier while in the case of the dye laser, this cannot be done. In this section, we consider three possible modulation formats that could be used to obtain better range resolution. These are pulse amplitude modulation, pulse position modulation and optical wavelength modulation. It appears that the last technique offers the most promise and this is discussed in greater detail in the following sections.

The most straightforward type of amplitude modulation would involve mode-locking of the dye laser. This would allow extremely good range resolution (as short as one millimeter), but suffers from large ambiguities at the mode-locked pulse repetition rate. One could consider taking the output of a mode-locked laser and impressing an additional amplitude modulation on the train in order to suppress the range ambiguities. This situation is illustrated in Fig. V-1. The laser output is assumed to consist of a uniform train of pulses separated by a time T_s and having an overall duration T. The modulator is assumed to have no gain so that it multiplies the intensity of each pulse by some number between 0 and 1. This modulated pulse train is transmitted to the target. The received signal, after square law (incoherent) detection, is passed through a filter matched to the envelope of the transmitted waveform. The output of this filter is the autocorrelation of the envelope of the transmitted waveform. Ideally, it should consist of a large central maximum and a small sidelobe level as shown schematically in Fig. V-1c. It will, of course, have a pulsed structure with separation T_s. The ratio of the peak value to the mean sidelobe level provides a measure of the ability of the receiver to distinguish between targets out of the desired range. It may be seen from the discussion below that it is not possible to achieve a high peak-to-sidelobe ratio using this scheme except for trivial and uninteresting cases

First we consider the trivial case. If the modulator acts to pass only one of the N pulses, the sidelobe level vanishes and only the central peak remains. Target discrimination is excellent but the total energy of the signal has been reduced by a factor of N. Clearly, this is an uninteresting case. We consider the general case where the modulator imposes a modulation f(t) on the pulses where $0 < f(t) < 1$. The matched filter output will be

$$a(r) = \int_{-\infty}^{\infty} f(t)\, f(t-r)\, dt$$

The average value of the output is

$$\bar{a} = \frac{1}{2T} \int_{-\infty}^{\infty} a(r)\, dr = \frac{1}{2T} \int_{-\infty}^{\infty} f(t) \int_{-\infty}^{\infty} f(t-r)\, dr\, dt$$

$$= \frac{1}{2}\, T\, (\bar{f})^2$$

While the peak value is

$$a(0) = \int_{-\infty}^{\infty} f(t)^2\, dt = T\, (\overline{f^2})$$

The ratio of the peak to the mean level is thus

$$\frac{a(0)}{\bar{a}} = 2\, \frac{\overline{f^2}}{\bar{f}^2}$$

With the restriction that $0 < f < 1$, it is clear that with the exception of the trivial case discussed above, this ratio cannot be made large. Thus, this type of modulation format does not appear attractive.

Another possible scheme involving pulse position modulation is illustrated in Fig. V-2. Here the laser is made to emit a train of N pulses of duration T_p and having a total time duration T. We assume that each one of the pulses can be placed in any one of $M = T/T_p$ possible positions in the time interval T. It is possible to arrange these pulses in such a way that the maximum sidelobe level never exceeds unity. The peak value of the autocorrelation function will be N, so that the ratio will be N. The number of pulses that can be arranged in such a sequence is $N \sim (M)^{1/2}$. Here M is a measure of the time bandwidth product of the pulse envelope since $\Delta\omega \sim 1/T_p$ and $\Delta\omega T = T/T_p = M$.

To construct a pulse sequence such that the sidelobe level near exceeds unity, it is necessary that all the $N(N-1)/2$ spacings between pairs of pulses in the train differ from each other by at least the pulse width. A simple sequence of this type is a train of N pulses having separations of $N\ T_p$, $N+1\ T_p$, $N+2\ T_p$ . . . . $[N + (N-1)]\ T_p$. The total duration of such a sequence is $N^2 + N(N-1)/2 \sim 1.5\ N^2$ so that $N = (M/1.5)^{1/2}$. This is not an optimum sequence as it does not make full use of the available time bandwidth product. It is possible to construct other sequences that make better use of the time-bandwidth product. One such sequence is series of pulses having the spacings 2, 3, 4, 6, 8, 11, 16, 12, 24 in units of the pulse width T_p. This series of 10 pulses has a total duration of 97 T_p.

Experimental realization of such a modulation format could be very difficult. One possible technique would be to use a cavity dumping scheme as shown in Fig. V-3. In this scheme, the laser is operated with totally reflecting mirrors. The internal energy is dumped out by the electro-optic modulator in accordance with the desired sequence of delays. The output pulse duration would be determined by the cavity transit time, of the order of one nanosecond. Since the overall pulse duration of the unmodulated laser is about 1 microsecond, this would imply that $M = 1000$ and $n \approx 30$. Use of a stagger sequence of the first type described above would allow a sufficient time (~30 passes) between pulses for the radiation field to buildup in the cavity. The requirements on the modulator in this system are rather severe.

A third modulation format that can be considered is optical wavelength modulation. This is shown schematically in Fig. V-4. In this scheme the laser output is a long pulse but the center wavelength of the laser is caused to sweep over the entire available laser line with (100-200 Å) during the time of the pulse. This is termed wavelength modulation rather than frequency modulation since we do not envision a coherent frequency sweep. To perform a coherent frequency sweep over 100 Å in one microsecond is beyond the capability of any present or projected modulator. In the proposed scheme we simply require that the laser be made to oscillate at different parts of its available line width at different times during the pulse. Dye lasers can be made to operate in this way, as will be discussed in the next section. In fact, they tend to operate in this way spontaneously, although not with a sufficiently narrow instantaneous line width to be useful for this application.

Two types of receivers could be used with this transmitted waveform. The first uses a frequency swept filter that is swept in synchronism with the transmitted waveform (with an appropriate delay corresponding to the range of interest). This is analogous to a correlation receiver that correlates the received waveform with a stored replica of the transmitted waveform. It is not a very convenient receiver since it is good for only one range. To detect signals from several ranges simultaneously would require a bank of filters, one for each range resolution element. A better receiver is one that consists of an array of narrow band

of optical filters, each with its own detector. This type of detector is shown in detail in Fig.V-5. For a linearly swept transmitted pulse, each of the detectors is sequentially excited by the received signal and emits a pulse of duration determined by the dwell time of the swept signal in the pass band of the filter. The pulses from the separate detectors can be summed in an appropriate delay network as shown to produce an output pulse containing all of the received energy and having a duration equal to the duration of the individual pulses. The scheme shown in Fig. V-5 is inefficient in that the signal is divided into N channels and only the energy corresponding to the wavelength for which a given channel is tuned is used. This difficulty is easily overcome by using a dispersive device such as a grating or prism for wavelength discrimination, with an array of detectors placed in the focal plane, as shown in Fig. V-6. The range resolution of this system is determined simply by the pulse duration of each tuned channel. This in turn is determined by the sweep rate. Let us consider sweeping the laser line area 100 A in one microsecond with an instantaneous line width of 1A. We could then employ 100 channels with a width of 1A each and obtain 10 nanosecond time resolution. The discrimination against targets at other than the desired range can be made exceptionally good. The response at a time t to a signal received at a time $t-t_o$ is given by the response of the optical filter at a wavelength βt_o removed from its center frequency, β here being the sweep rate in Angstroms/second. If a diffraction grating is used for the wavelength selection, the rejection can easily be made 10^4 to 1. This system is vastly superior to the other modulation formats discussed. The reason for this is that the other systems operated on the detected envelope of the transmitted signal and thus were limited by the limited time-bandwidth product of the signal. Use of modulation of the optical wavelength adds a whole new dimension of flexibility. The available time-optical bandwidth product is of the order of 6×10^8, which allows resolution far in excess of the present requirement. In the following sections implementation of such a system will be discussed.

Frequency Sweeping the Dye Laser

A dye laser normally emits over a wavelength interval of 100-200 A. By placing a narrow band filter in the cavity, the output line width can be narrowed to as little as 10^{-3} A with little energy loss. If the center frequency of such a filter is caused to sweep across the line, the laser output will also sweep. In this section we consider the question of the rate at which the laser can be swept and the loss of power that is entailed by the sweeping. In the next section we shall discuss experimental means for realizing a swept filter.

The treatment of the sweeping can be carried out conveniently in terms of the rate equation for the energy density (per unit wavelength). This equation is:

$$\frac{d\mathcal{E}(\lambda)}{dt} = (g + \gamma + \alpha(\lambda, t)) \frac{c}{\ell} \mathcal{E} + \frac{nh\nu\Delta\Omega}{4\pi\tau_f\Delta f}$$

where g = single pass gain coefficient
$\mathcal{E}$ = energy density
γ = linear loss = $1/2\ \ell n\ R_1R_2$
α = $\ell n\ T(\lambda,t)$ where T is the transmission of the sweeping filter
n = inversion density
τ_f = fluorescence lifetime
Δ_Ω = solid angle subtended by the laser in the cavity
$\Delta\lambda$ = fluorescent line width

The last term is the spontaneous emission term and is simply the total fluorescence per unit wavelength that is emitted in a solid angle equal to the subtended by the laser medium. We shall assume that the dye laser is completely homogeneously broadened, a good assumption. The quantity g is the saturated gain. We will assume that this is related to the small signal gain by a generalization of the Rigrod formula

$$g = \frac{g_o}{1 + (1/I_s)\int I(\lambda)\ d\lambda}$$

where I_s is the saturation intensity and I is the intensity per unit wavelength. We will also assume a very broad lens so that g is independent of λ. We use the relations

$$g = n\sigma\ell \qquad \sigma = \text{gain cross section}$$

and

$$I_s = \frac{h\nu}{\sigma\tau_f} \qquad \mathcal{E}_s = I_s/c$$

and

$$\tau = \ell/c$$
$$k\tau = t \qquad k = \text{number of single passes}$$

to rewrite the equation

$$\frac{d\mathcal{E}}{dk} = (g - \gamma - \alpha)\ \mathcal{E} + \frac{\Delta\Omega}{4\pi\Delta\lambda}\ g\ \mathcal{E}_s$$

$$g = \frac{g_o}{1 + 1/\mathcal{E}_s\int \mathcal{E}(\lambda)\ d\lambda}$$

It is of interest first to consider the predictions of this equation in the absence of a frequency sweep. In the absence of a filter, and in the steady state:

$$\frac{d\mathcal{E}(\lambda,k)}{dk} = 0 = (g - \lambda)\ \mathcal{E}(\lambda, k) + K\, g\, \mathcal{E}_s$$

$$K \quad \frac{\Delta\Omega}{4\pi\Delta\lambda} \ll 1$$

The second term on the right is extremely small compared to $\mathcal{E}_s$. The term $\mathcal{E}$ should be comparable to $\mathcal{E}_s$. The only way that the two terms can cancel is for $(g - \gamma)$ to be essentially zero. Thus,

$$g = \frac{g_o}{1 + (1/\mathcal{E}_s)\int \mathcal{E}\, d\lambda} = \gamma$$

$$1/\mathcal{E}_s \int \mathcal{E}\, d\lambda = g_o/\gamma - 1$$

This determines the total intensity output from the laser. In this case the line shape $F(\lambda)$ is undetermined. This is a consequence of the assumption of a constant g and the homogeneous broadening. If we insert a filter function, the equation becomes

$$(g - \gamma) + \alpha(\lambda))\ \mathcal{E}(\lambda) = -K\, g\, \mathcal{E}_s$$

We assume a filter function of the form

$$T = e^{-(\lambda - \lambda_o)^2}$$

We obtain then

$$\mathcal{E}(\lambda) = \frac{-K\, g\, \mathcal{E}_s}{g - \gamma - (\lambda - \lambda_o)^2} = \frac{K\, g\, \mathcal{E}_s}{(\lambda - \lambda_o)^2 + (\gamma - g)}$$

The laser line is Lorentzian with a width $(\gamma - g)^{1/2}$. The value of g must adjust itself so that $(\gamma - g)$ is a positive number. We find

$$\frac{1}{\mathcal{E}_s} = \int \mathcal{E}(\lambda)\, d\lambda - \frac{\pi K g}{(\gamma - g)^{1/2}} = \frac{g_o}{g} - 1$$

This condition determines the saturated gain g, given the unsaturated gain g_o. It is clear that g must be nearly identical to γ. We can write $g = \gamma - \delta$ and obtain

$$\frac{\pi K \gamma}{\delta^{1/2}} = \frac{g_o}{\gamma} - 1$$

$$\delta = \frac{(\pi K)^2 \gamma^4}{(g_o - \gamma)^2}$$

We note that $K = \Delta\Omega/4\pi\Delta\lambda$ is an extremely small number, of the order of 10^{-9}. Thus the line width $\delta^{1/2}$ is extremely small also, of the order of 10^{-9} A for the 1 Å filter that was assumed. This is just the behavior that would be expected if the laser were truly homogeneously broadened. The output should consist of a single, very sharp line. This narrow output line is not observed experimentally. This is a result of many factors such as dimensional instabilities, time varying refractive indices, spatial hole burning and transverse mode competition. In addition, the cross relaxation time between the levels that produce the broad laser line, though very short, is not zero, so that on a sufficiently fast time scale the laser appears inhomogeneously broadened.

In either case discussed above, however, we find that the total output, integrated over λ is the same.

$$\frac{1}{\mathcal{E}_s} \int \mathcal{E} d\lambda = \frac{g_o}{\gamma} - 1$$

We now assume that the sweeping filter is swept linearly in time (or k) so that

$$\alpha(\lambda, k) = \alpha(\lambda + \beta k) = \alpha(x); \; x = \lambda + \beta k$$

We still assume that the laser line is extremely broad so that g is independent of λ. We shall look for a steady state response, with

$$\mathcal{E}(\lambda, k) = \mathcal{E}(\lambda + \beta k) = \mathcal{E}(x)$$

The rate equation thus becomes

$$\beta \frac{d\mathcal{E}}{dx} = [g - \gamma + \alpha(x)] \; \mathcal{E}(x) + K g \mathcal{E}_s$$

This is a simple linear differential equation that determines the resulting line shape $\mathcal{E}(x)$. There is one complication however. The known parameter is g_o, the unsaturated gain and not g. This is not a serious difficulty. The equation can be solved for an assumed value of g and then the value of g_o can be computed. The value of g can then be changed and the equation resolved until the appropriate value of g_o is obtained.

The following effects would be expected intuitively and are born out by actual solution of the equation:

1. the laser line should lag behind the peak of the filter function and the amount of lag should increase with increasing sweep rate,

2. the laser line should become broader as the sweep rate is increased,

3. the power output should decrease with increasing sweep rate. This effect occurs because the intensity at any given wavelength can only build up while the filter is near the wavelength. As the sweep rate increases, the time available for buildup will decrease.

The equation determining the line shape was solved by direct numerical integration on a digital computer. For simplicity, it was assumed that the filter function was Lorentzian,

$$T(\lambda) = \frac{1}{\left(\frac{\lambda - \lambda_o}{\Delta\lambda}\right)^2 + 1}$$

Typical results are shown in Figs. V-7 and V-8. The laser output line is plotted relative to the position of the line center of the sweeping filter. The parameters used were

$$\lambda = -0.6$$
$$K = 10^{-9}$$
$$\mathcal{E}_s = 1 \text{ (normalization)}$$

Figure V-7 shows the case of $\beta = .05$ (filter linewidths per pass) and Fig. V-8 the case of $\beta = .02$. The laser line is seen to lag behind the filter, and the amount of the lag increases with increasing sweep rate (increasing β). The experimental value of g_o is 1.5 - 2.0; the values of g were chosen so that g_o came out in this range. The integrated output was computed for each case and compared with the value that would be obtained in the absence of the sweep. The efficiency

$$\eta = \frac{1/\mathcal{E}_s \int \mathcal{E}(\lambda)\, d\lambda}{g_o/\gamma - 1}$$

is given for each curve. Curve b of Fig. V-7 and curve a of Fig. V-8 correspond to nearly identical values of g. The efficiency at the faster sweep rate is 19% and at the slower rate is 39%. The efficiency drops off rapidly at faster sweep rates. The line width is seen to be considerably reduced over the filter line width, being about .27 at the faster sweep and .17 at the slower sweep. The crucial parameter that determines the time resolution of the wavelength modulation scheme is the sweep rate in terms of laser line widths per pass, not filter line widths per pass. Thus for the slow sweep

$$\beta' = \frac{\beta}{.17} = \frac{.02}{.17} = 0.118$$

and for the fast sweep

$$\beta' = \frac{\beta}{.27} = \frac{.05}{.27} = 0.185$$

For even the slow filter sweep rate, the effective sweep is greater than .1 laser line widths per pass. The line width is then covered in 10 passes. A lasing line width of 1 Å could be swept across 100 Å in 1 microsecond and would provide 100 range resolution elements with an extremely small amount of cross talk between them, and with a relatively modest loss of output power. This scheme thus appears to be a very attractive way to improve the range resolution.

The example discussed here is oversimplified and serves merely to indicate the feasibility of the proposed technique. One would expect that improved operation could be obtained by a careful design of the line shape of the sweeping filter transmission.

It should also be noted at this point that the wavelength modulation scheme is not restricted to the dye laser. It is applicable to any laser with a wide lasing line width. The Nd:glass laser should be a good candidate for use of this system. It should work even better than the dye laser since the line is inhomogeneously broadened. This is an advantage since the filter in moving from one wavelength to another encounters the unsaturated gain at the new wavelength rather than the saturated gain. This will lead to better efficiency at a given sweep rate and will allow faster sweep rates. The swept output could be doubled using a crystal with a wavelength insensitive phase matching angle (KDP has this property for 1.06 → .53 microns) or by electrooptic control of the phase matching angle. The advantages to be gained by such a system are those gained by any pulse compression technique, primarily the ability to use a large amount of energy in a long pulse with the resolution available in a short pulse.

A Fast Scanning Interferometer For Frequency Sweeping

In order to investigate the characteristics of a frequency swept dye laser, a fast scanning interferometer was constructed.

Relatively low finesse (20 to 30) etalons have been used to narrow the linewidth of flashlamp pumped dye lasers. The experimental results show that the laser linewidth can be narrowed to less than 1 Å by using two such etalons. Tuning of the laser output by tilting the etalons has also been demonstrated in previous experiments. Due to obvious physical limitations, rapid tuning of the dye laser by tilting an intracavity etalon is not practical. Etalon tuning can also be done by varying the distance between the parallel reflecting surfaces which make up the etalon. Thermal tuning is much too slow. Another possibility is to make the solid etalon from an electro-optic material. With a proper choice of crystal orientation and placement of electrodes, the distance between the parallel faces of the crystal could be made to increase or decrease by varying an applied electric field. This method of etalon tuning has a limitation which arises from the small thickness (a few mm or less) of the requisite etalon. Whether a transverse or a longitudinal field is applied to the thin etalon there is a problem of voltage breakdown. The use of a solid etalon made from a piezoelectric material suffers from the same problems as an electro-optic material.

The problems of tuning a solid etalon can be circumvented by the use of an air etalon in which one mirror is fixed and a second parallel mirror is mounted to a piezoelectric tube. Commercially available scanning Fabry-Perots are made in this way. Mechanical displacement is achieved by piezoelectric expansion and contraction of the electrically driven tube and the difficulty of having to use very high voltages to obtain sufficiently large displacements is overcome by driving the tube at its mechanical resonant frequency (Ref. V-1). For a given applied voltage, the resonant displacement amplitude is larger than the static amplitude by a Q factor which, in general, is 100 to 400. Such a resonant-driven Fabry-Perot interferometer was constructed and tested as described below.

Construction of the interferometer, shown schematically in Fig. V-9, follows closely that first reported by Cooper and Greig (Ref. V-1) and later improved by Brannon and Bacon (Ref. V-2). The etalon reflecting surfaces consists of two 1 in. diameter fused quartz optical flats. Three pair of flats were available; one pair coated for 85 percent reflectivity at 6,328 Å was used in the initial testing and checkout of the interferometer, a second pair coated for 85 percent reflectivity at 5,900 Å, and a third pair with the front surface coated for 50 percent reflectivity at 5,900 Å, and the rear surface anti-reflection coated. One optical flat is bonded to the end of a Gulton Industries lead zirconate titanate peizoelectric tube. The low loss tangent and the relatively high mechanical Q of the material makes it suited

for the application. Mechanical displacement of the optical flat is achieved by piezoelectric expansion and contraction of the tube which is excited in the lengthwise mode by a sinusoidal voltage applied between the inner and outer metallized cylindrical surfaces.

At resonance, the total tube extension for a given applied voltage is proportional to the tube length and f, the resonant frequency, inversely proportional to the tube length. Thus, the minimum time required to scan one free spectral range is independent of tube length but depends only on the amplitude of the drive voltage and the Q of the PZT tube. To minimize the decrease in Q by the holding structure, the tube mirror assembly is held at the center mass, which is a mode of vibration, by a nylon ring which is clamped securely to the tube. Experimentally, it is found that only for short tubes (on the order of 3 cm length, or less) does the clamping ring significantly decrease the Q of the PZT element. On the other hand, long PZT tubes (on the order of 7.5 cm or longer) are undesirable since it is difficult to hold good alignment and spurious resonant modes tend to be excited. The choice of tube length is essentially a compromise between a decreased Q value with short tubes and difficulty of maintaining alignment with long tubes. We find a tube of approximately 4 cm length and a resonant frequency of 40 to 50 kHz is a good compromise between these two conflicting factors.

The complete tube-mirror assembly is mounted in an angular orientation device which has differential micrometer screws for precise angular control of the assembly relative to the second interferometer mirror held in a specially designed mirror mount. This second mirror is mounted on a precision translation stage which allows control of the mirror spacing (and thus the interferometer free spectral range) to better than 1 micron. A photograph of the complete interferometer is shown in Fig. 10.

Initial testing of the interferometer was done at 6,328 Å wavelength using mirrors coated for 85 percent reflectance. The time to scan one spectral range, or the scan time, was measured using the experimental configuration shown in Fig. V-9. A number of free spectral ranges were scanned during each half cycle of the drive voltage and typical display of the interferometer output is shown in Fig. V-11. Each spike represents a scan of one free spectral range and the spacing between the spikes is the scan time. A plot of the scan time as a function of the peak drive voltage is shown in Fig. V-12 where a 33 V peak drive resulted in a 0.57 μsec scan time and the corresponding resonance frequency of the 3.81 cm long PTZ element is 48.2 kHz.

The free spectral range of the interferometer used to obtain this data was measured to be 58 Å at 6,328 Å wavelength (or 67 Å at 5,900 Å).

The experimental configuration used in the dye laser frequency sweep experiments is shown in Fig. V-13. The dye laser head consists of a Candela CL-100E' coaxial flashlamp excited by a low inductance drive circuit consisting of a 0.3 μf capacitor and a triggered spark gap. A typical current drive pulse is 2 μsec (FWHM) with a

60 J input to the lamp. A 10^{-4} molar solution of Rhodamine 6G in ethanol was circulated through the flashlamp at a flow velocity of approximately 15 cm/sec. The laser cavity consists of a 1 m radius maximum reflecting mirror adjacent to the laser head, and a flat output mirror of either 30 percent or 80 percent reflectivity and a mirror spacing of 60 cm. The dye laser pulse and the PZT scan voltage are synchronized using a dual pulse generator. The dye laser pulse is delayed to occur near the end of the drive pulse to assure a resonant condition of the PZT and is positioned at the peak of the PZT drive voltage to assure maximum finesse and minimum scan time of the interferometer.

The diagnostic instrumentation used to examine the laser output consisted of a high-speed PIN photodiode, a Fabry-Perot interferometer and a Jarrell Ash 1 m spectrometer. The interferometer is used for a quick check of the laser linewidth and to determine frequency sweeping by observing broadening, or complete disappearance of the fringe pattern.

With no intracavity scanning interferometer and a 30 percent output mirror, the laser output energy was approximately 50 mJ with 60 J input to the flashlamp. A wavelength spectrum and a time display of the laser output, also with no intracavity etalon are shown in Figs. V-14 and V-15, respectively. The laser linewidth is approximately 200 Å centered near 5,900 Å, and the pulse width is approximately 0.5 μsec (FWHM) and 1.5 μsec base width.

Initial operation with the interferometer intracavity to the dye laser showed that 85 percent (at 5,900 Å) mirrors resulted in a high laser threshold and a corresponding low output energy. The laser operation was found to be satisfactory using 50 percent interferometer mirror and an 80 percent reflectivity output mirror. With the intracavity interferometer, the laser output pulse width was essentially unchanged from that with no interferometer and the energy output was reduced to 5 to 10 mJ. The corresponding wavelength spectrum of the laser output is shown in Fig. V-16 where the interferometer was adjusted to have a free spectral range of approximately 30 Å and approximately 60 Å in the top and bottom photographs, respectively. The dye laser output occurs at the multiple peaks of the interferometer transmission, as is expected. Increasing the free spectral range further resulted in the spectrum shown in the top photograph of Fig. V-17. This result demonstrates that a single, low finesse intracavity etalon is adequate to substantially narrow the operating linewidth of the dye laser output. Tuning of the laser output by applying a dc voltage to the PZT element of the interferometer, also shown in Fig. V-17, demonstrates the etalon finesse is adequate to control the laser frequency. Experiments were continued to verify frequency sweeping of the dye laser output with a voltage, at the resonant frequency, applied to the PZT element.

Evidence of sweeping the dye laser output is seen by observing the spectrometer

output; an example of which is shown in Fig. V-18. The laser output with and without a drive voltage to the PZT element are shown in the top and bottom photographs, respectively. With a drive voltage, the laser output is scanned over greater than a 100 Å wavelength range. The fact that the scan does not necessarily begin or end at the wavelength of the laser output with no drive voltage is primarily due to a time difference between the taking of the two photographs during which the center bandpass of the interferometer can change.

An unusual type of spectrum, which illustrates that the experimental results are not yet completely understood, is shown in Fig. V-19 where the output consists of an unswept and two swept parts. The laser may have operated simultaneously or in time sequence in these various modes and time resolution using a streak camera could resolve these differences. The spacing between the two swept portions of the spectrum are separated by approximately 250 Å which is well beyond the 150 Å free spectral range of the interferometer.

In conclusion, a promising technique to rapidly frequency sweep the output of a pulsed, flashlamp pumped dye laser was judged to be a resonant driven air spaced Fabry-Perot interferometer. Such an interferometer was constructed and initial tests revealed that it is possible to scan one free spectral range in approximately 0.6 μsec with a peak drive of 30 V at 48 kHz. A free spectral range to 150 Å has been achieved and 200 Å is believed to be a practical limit. Testing of the fast scan interferometer intracavity in a dye laser showed it is possible to scan the output over greater than a 100 Å range during a single pulse (0.5 μsec FWHM and 1.5 μsec base width). The linewidth of the laser output with no scanning is typically 20 Å.

Conclusions and Recommendations

The scanning interferometer discussed in section V-3 was capable of sweeping the frequency of the dye laser during the pulse. The instantaneous bandwidth was rather large, however, and to reduce it would require a much higher finesse etalon with its attendant losses. Alternately, a second etalon of smaller free spectral range could be used and scanned in synchronism. Since the performance of this work, however, other techniques have been developed which show much more promise for accomplishing the desired end. At this time the most promising techniques appear to be electro-optically driven Fabry-Perot filters or acousto-optic tuning techniques.

Electro-optically driven birefringent Fabry-Perot etalons have been used to tune a dye laser over a range of 135 Å with a linewidth of several Angstroms (Refs. V-3 and V-4). The acousto-optic tuner uses a transverse acousto-optic interaction to provide a beam deflection. The deflected beam is scanned across a grating to achieve a wavelength discrimination. It is estimated that tuning rates of 100 nm/μsec should be achievable (Ref. V-5).

Using either of these techniques, wavelength sweeping of the dye laser during a pulse should be feasible and subsequent compression can reduce the effective duration of the pulse by a factor of 100 or more.

REFERENCES FOR SECTION V

V-1. Cooper, J. and J. R. Greig: J. Sci. Instruments, 40, p. 433 (1963).

V-2. Brannon, P. J. and F. M. Racon: Applied Optics, 12, p. 142 (1973).

V-3. Okada, M., S. Shimizu and S. Ieiri: Applied Optics, 14, p. 917 (1975).

V-4. Okada, M. and S. Ieiri: Optics Communication, 14, p. 4 (1975).

V-5. Hutcheson, L. D. and R. S. Hughes: Applied Optics, 13, p. 1395 (1974).

FIG.V-1

PULSE AMPLITUDE MODULATION

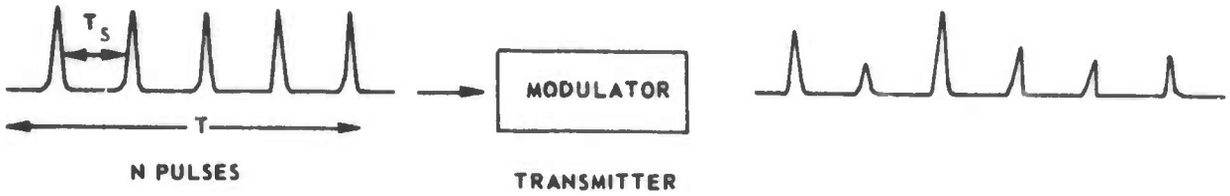

N PULSES

TRANSMITTER

(a)

RECEIVER

(b)

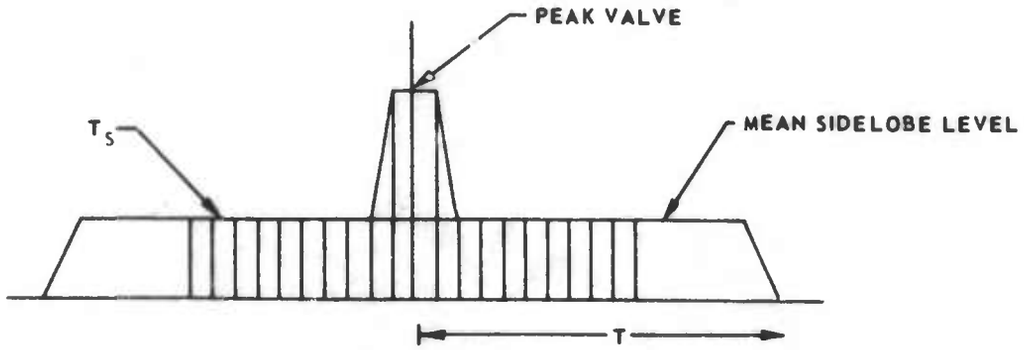

SCHEMATIC CORRELATION FUNCTION

PULSE POSITION MODULATION

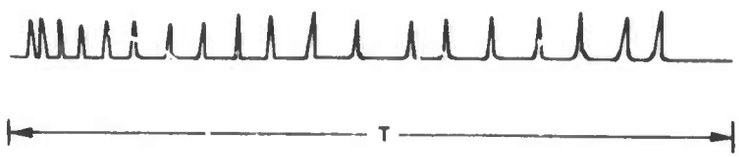

TOTAL DURATION	T
PULSE WIDTH	T_p
NUMBER OF POSSIBLE POSITIONS	$M = T / T_p$
NUMBER OF PULSES	$N = M$

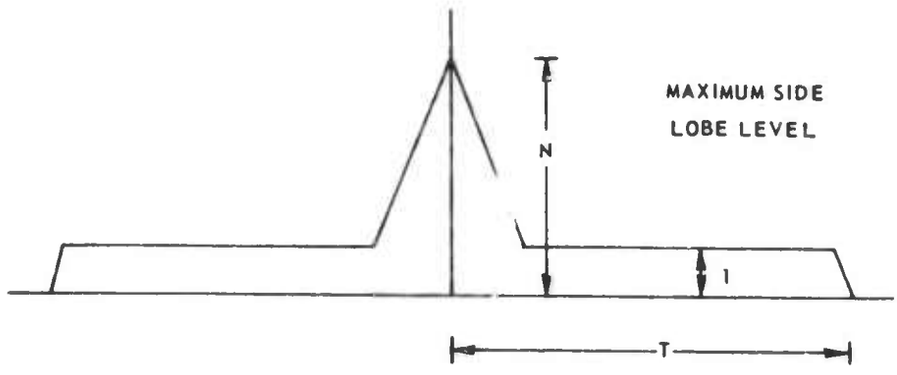

SCHEMATIC CORRELATION FUNCTION

FIG.V-3

CAVITY DUMP MODULATOR

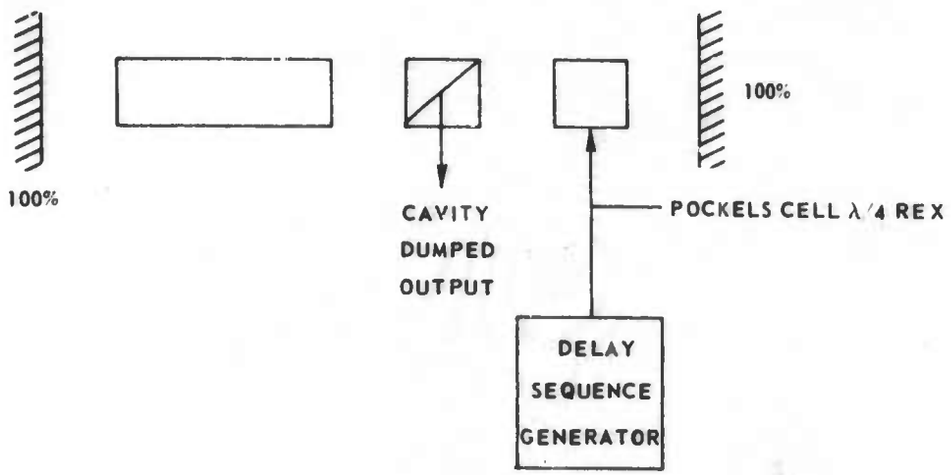

FIG.V–4

OPTICAL WAVELENGTH MODULATION

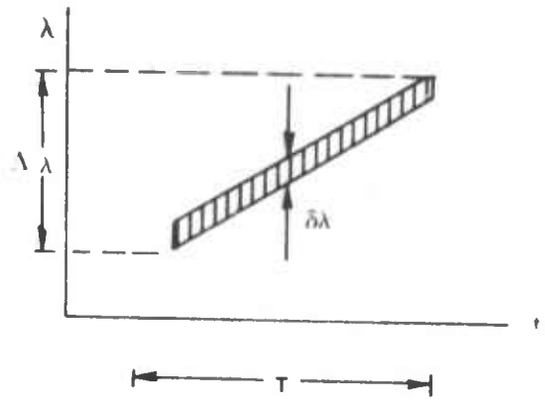

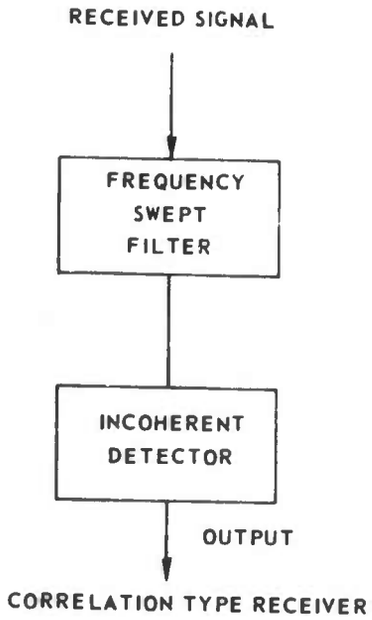

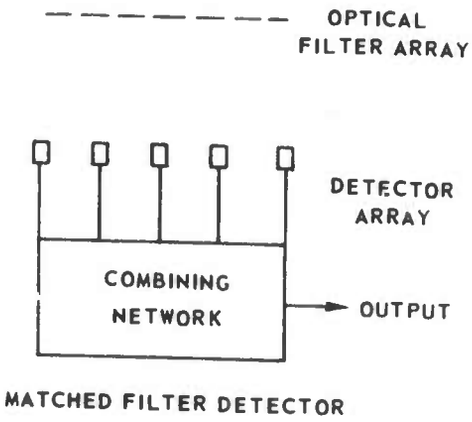

FIG.V-5

SCHEMATIC RECEIVER CONFIGURATION

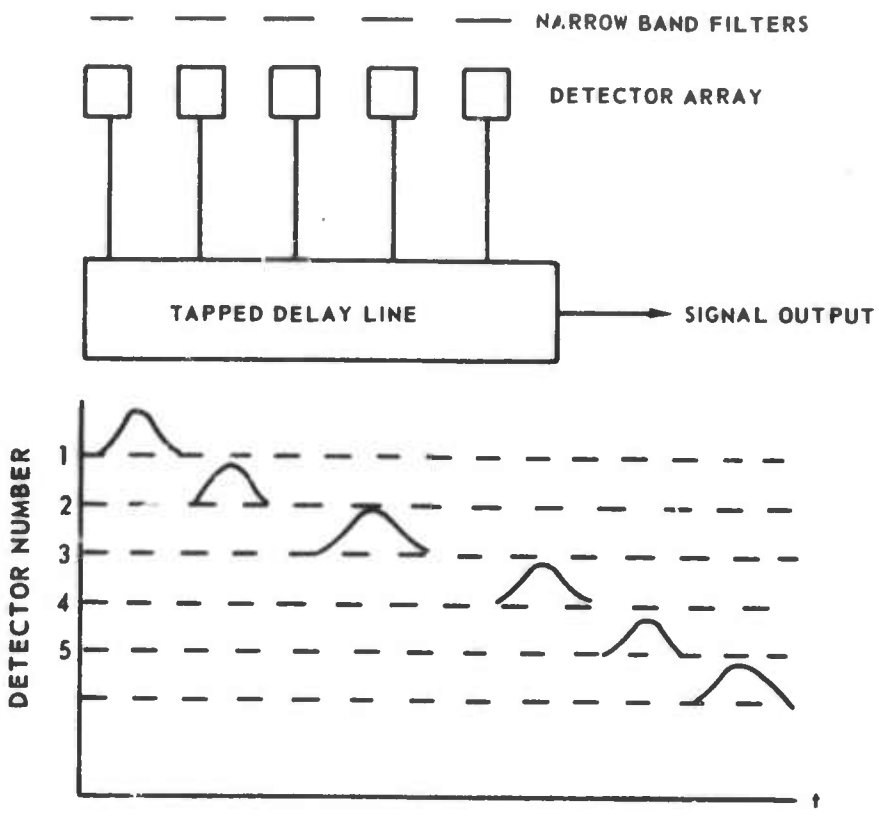

FIG. V-6

EFFICIENT DETECTION SYSTEM

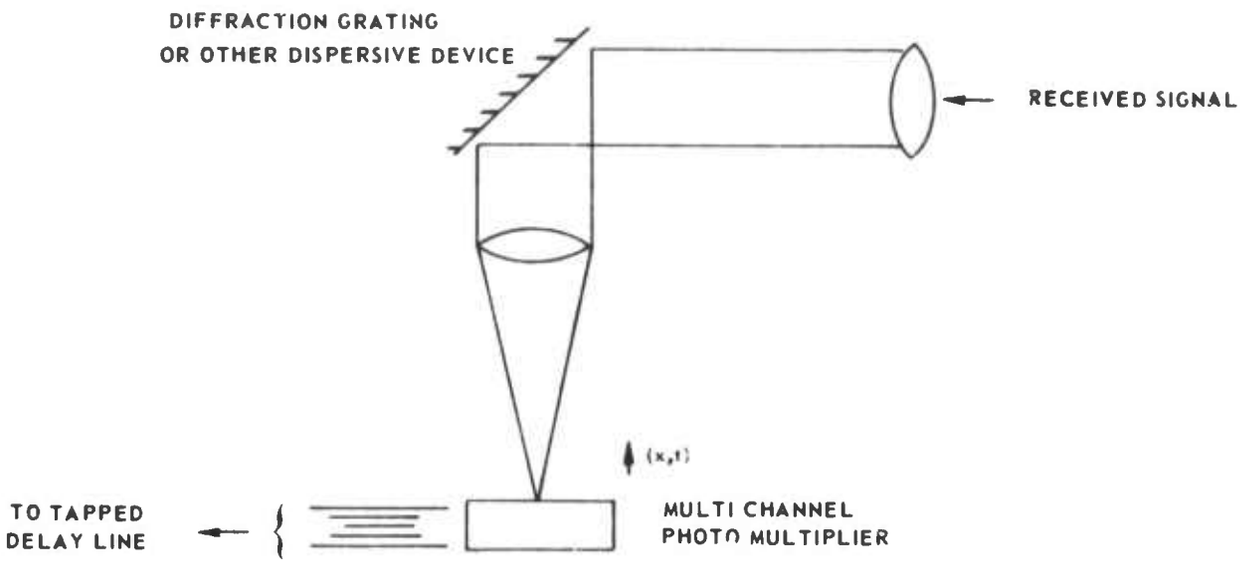

LASER OUTPUT LINE SHAPE

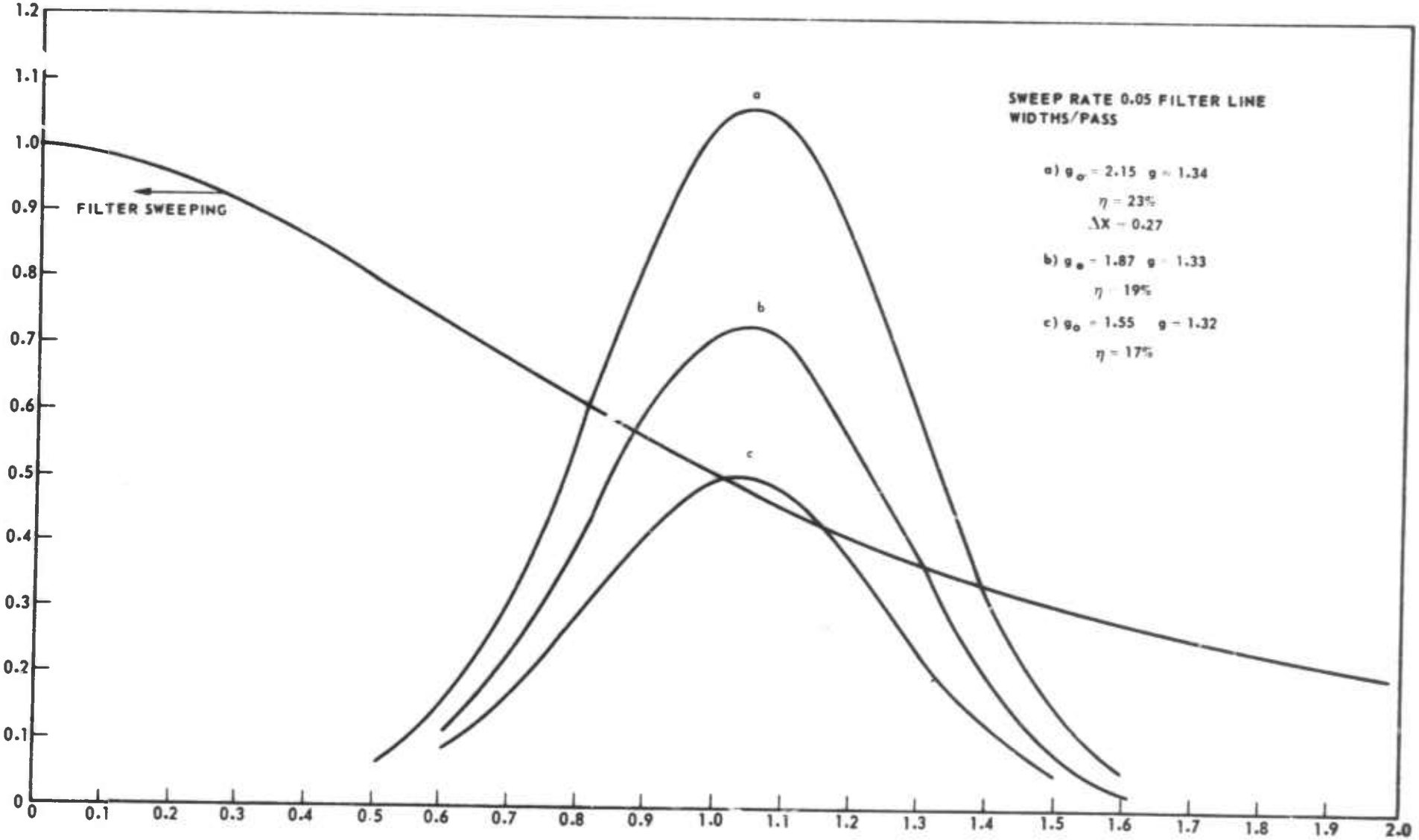

FIG. V-7

LASER OUTPUT LINE SHAPE

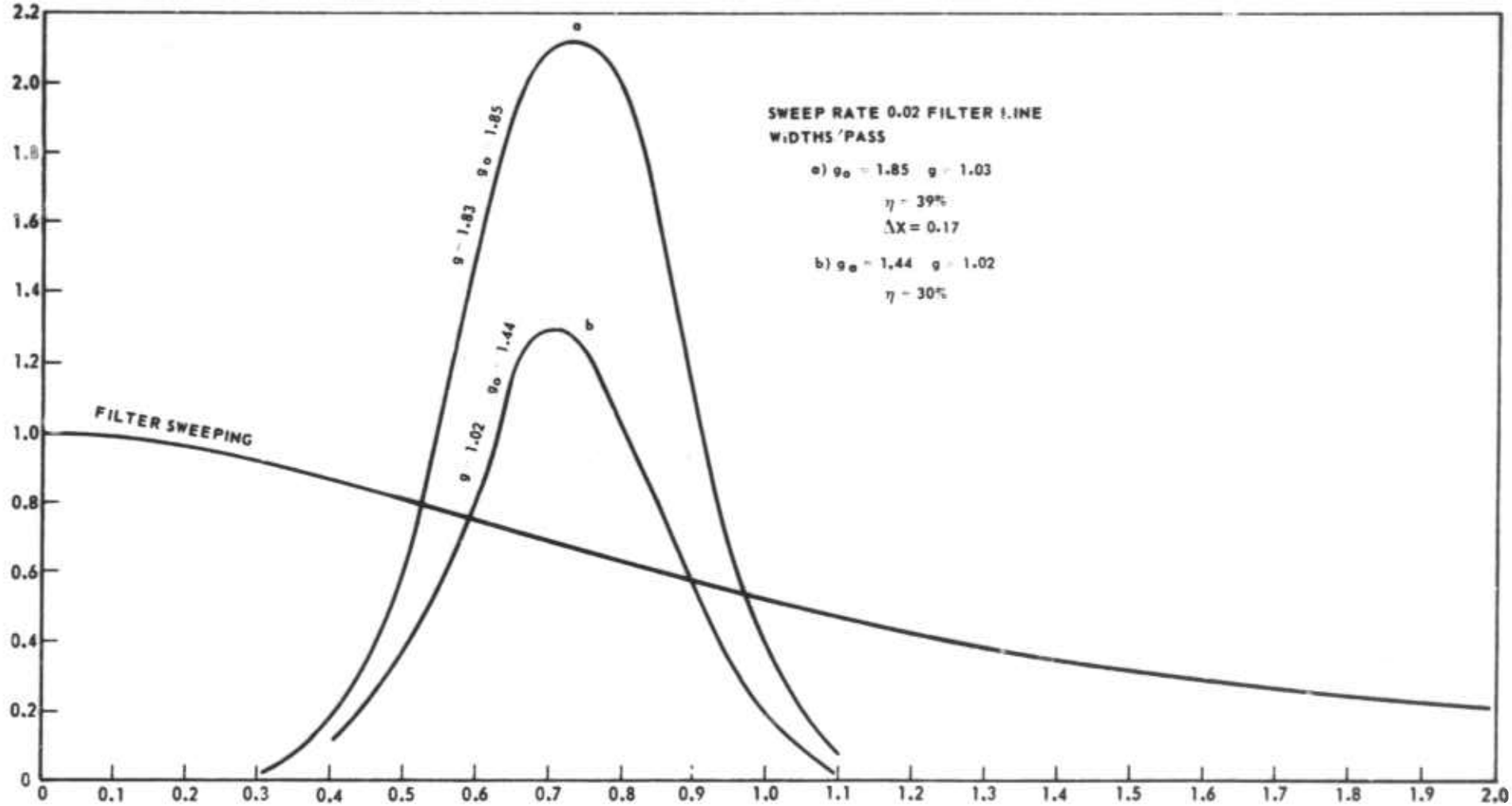

FIG. V-8

FIG.V-9

DIAGRAM OF FAST-SCAN FABRY-PEROT INTERFEROMETER

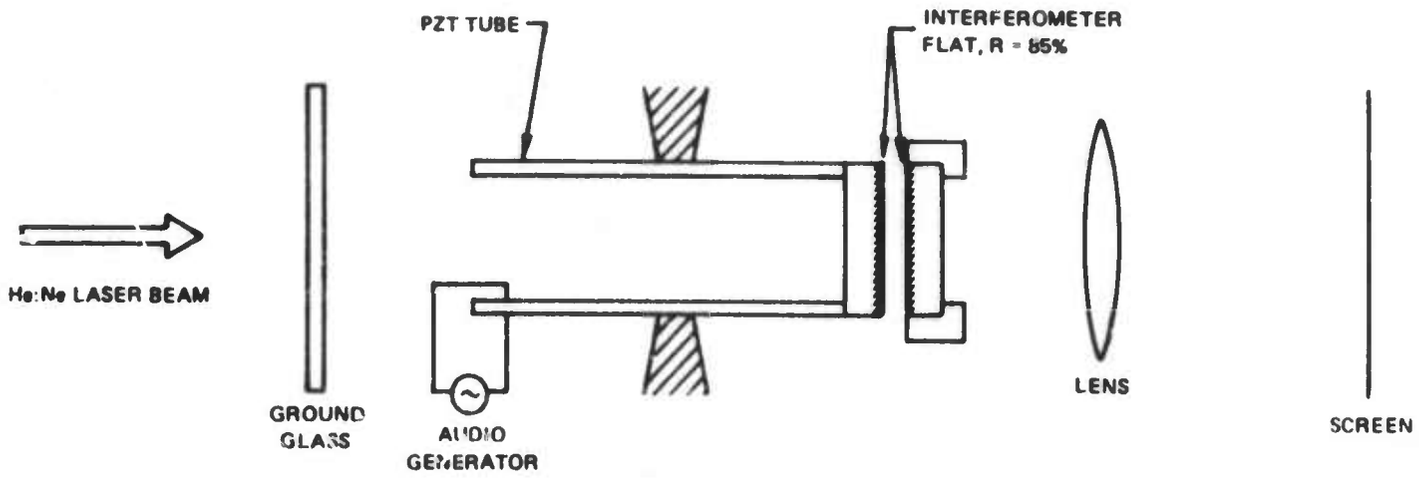

FAST SCAN FABRY-PEROT INTERFEROMETER

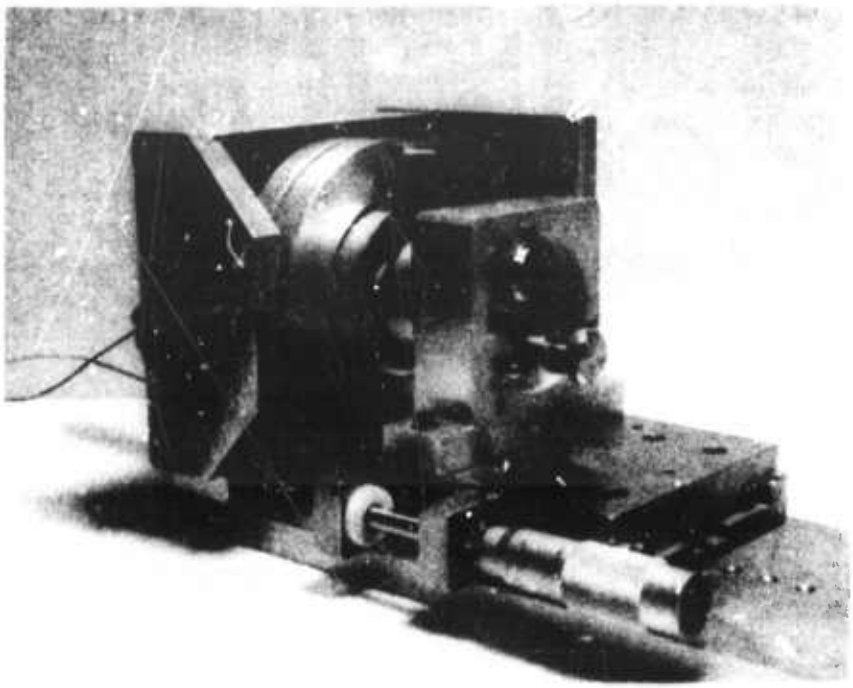

FAST–SCAN FABRY–PEROT INTERFEROMETER

INTERFEROMETER
OUTPUT

PZT DRIVE
20 V/div

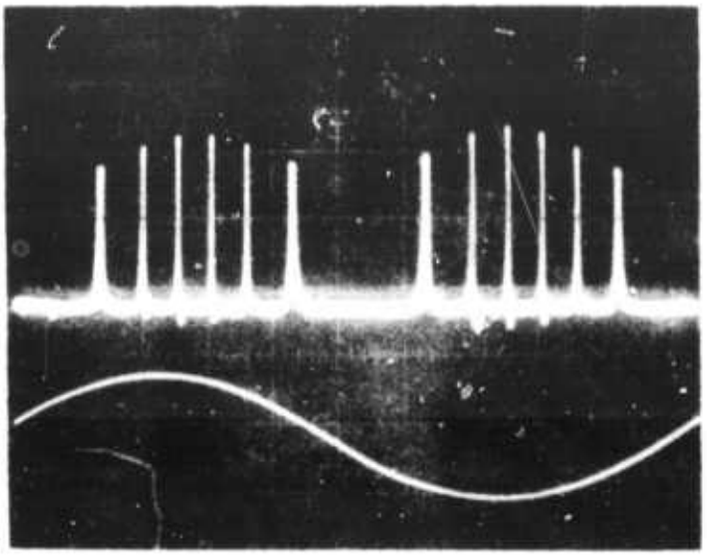

2 μsec/div

FIG.V-12

FAST SCAN INTERFEROMETER CHARACTERISTICS

$f_o \approx 48.2$ kHz

FSR = 58 Å AT 6328 Å

FSR = 67 Å AT 5900 Å

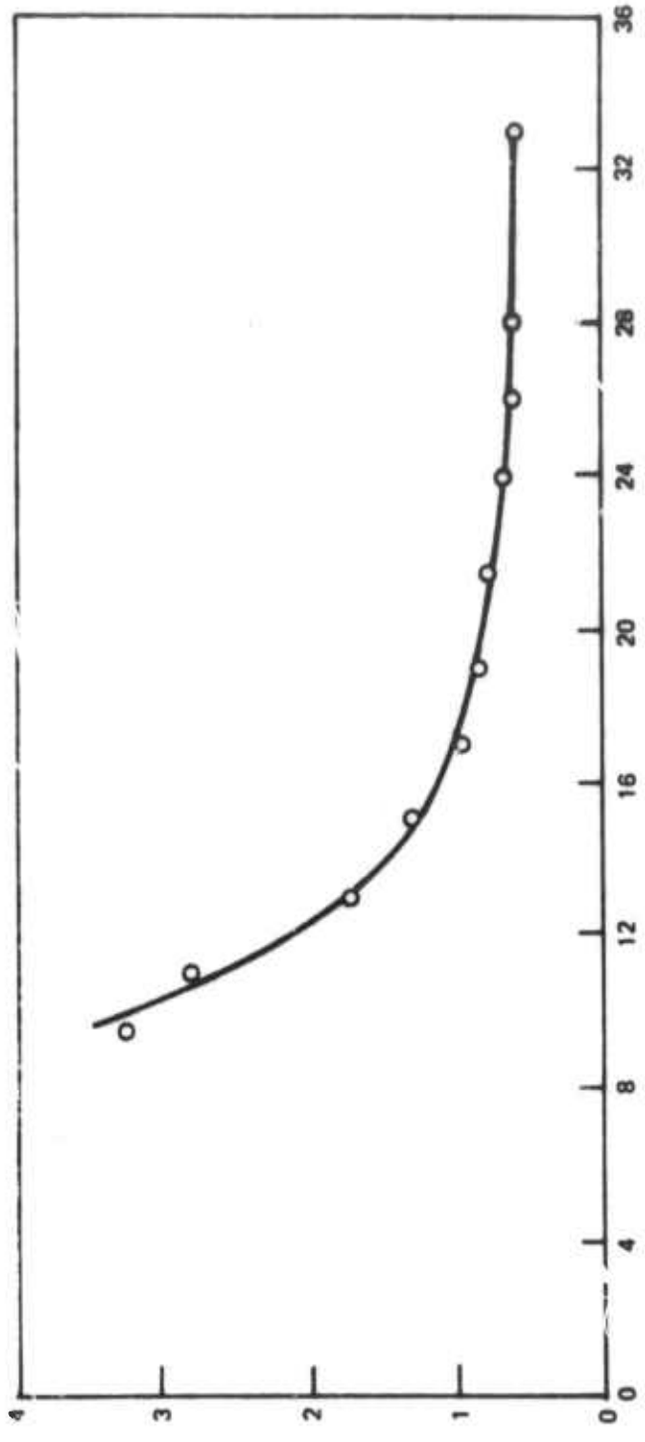

EXPERIMENTAL CONFIGURATION

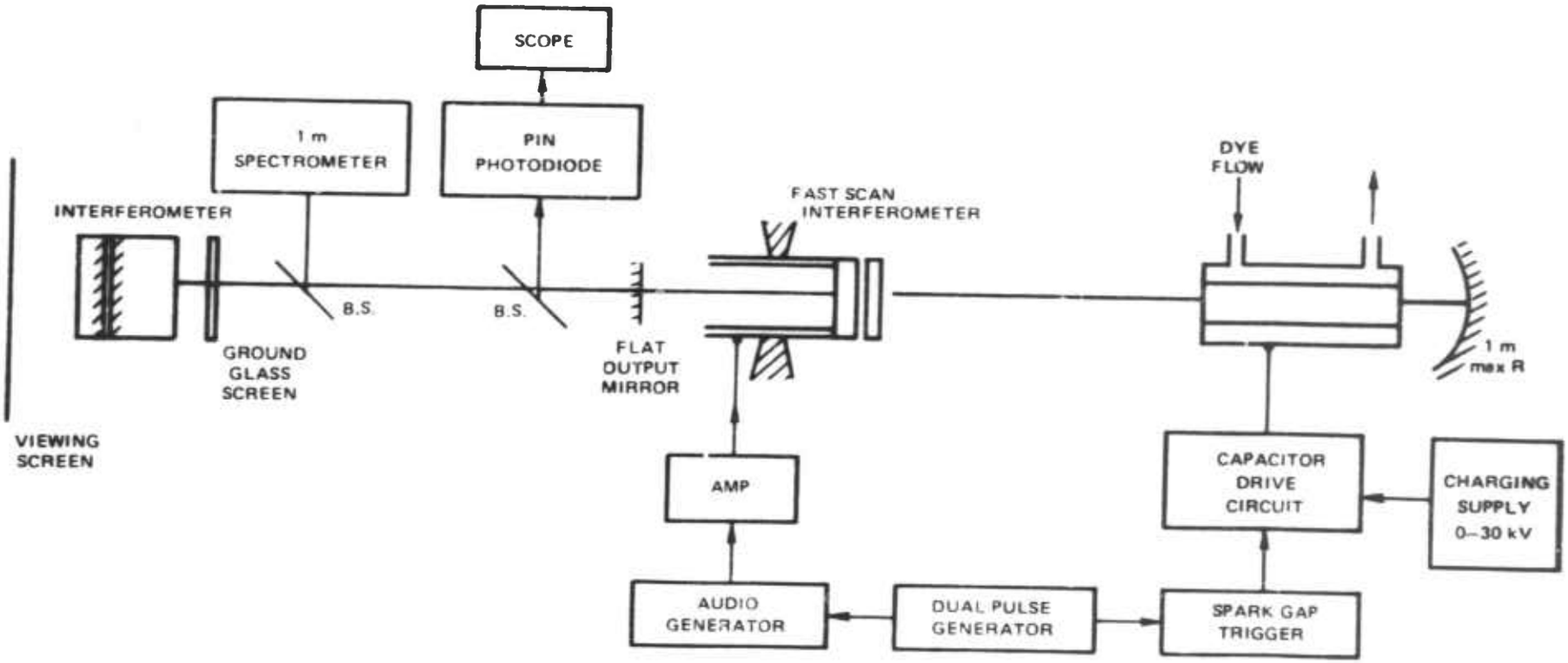

FIG. V-13

DYE LASER OUTPUT SPECTRUM

NO INTRACAVITY ETALON

FIG. V–15

TIME DISPLAY OF DYE LASER OUTPUT

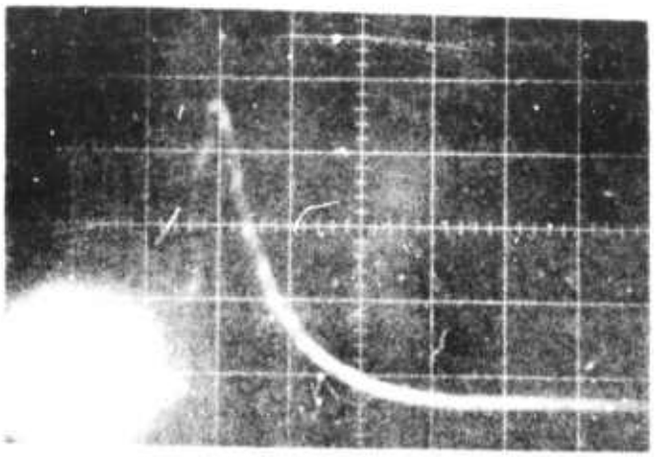

0,5 μsec/div

DYE LASER OUTPUT SPECTRUM

WITH INTRACAVITY ETALON

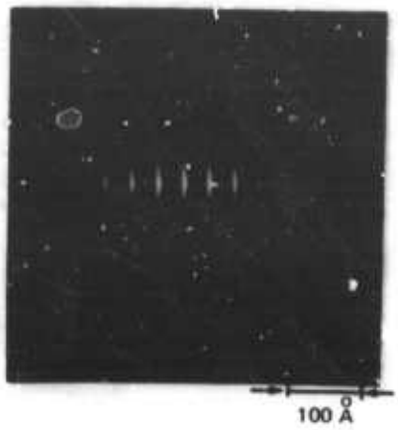

a) INTERFEROMETER FSR = 30 Å

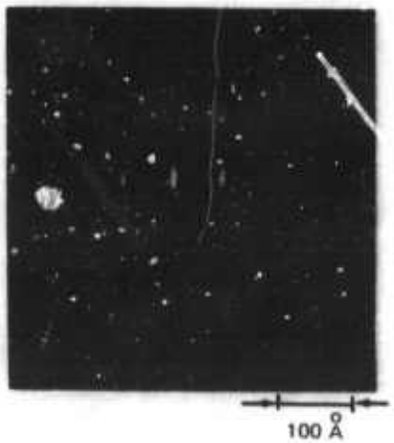

b) INTERFEROMETER FSR = 60 Å

DYE LASER TUNING

a) ZERO VOLTS

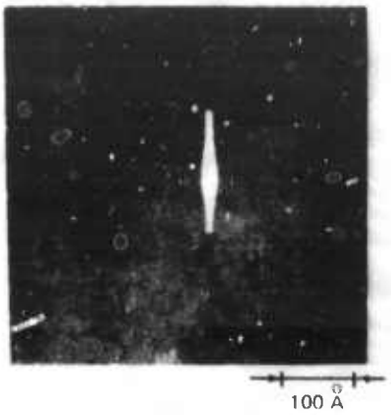

b) 500 VOLTS

c) 1000 VOLTS

DYE LASER OUTPUT SPECTRUM

a) PZT DRIVE VOLTAGE

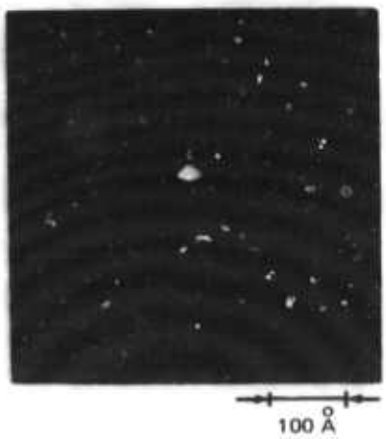

b) NO PZT DRIVE VOLTAGE

DYE LASER SPECTRUM

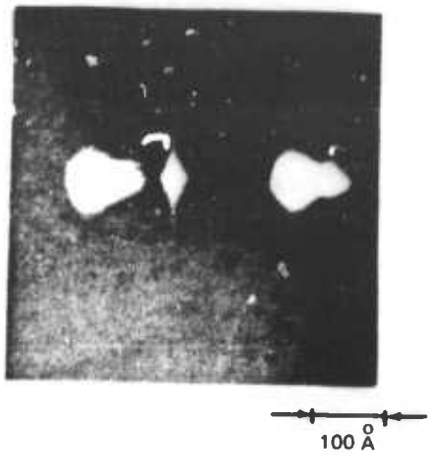

a) PZT DRIVE VOLTAGE

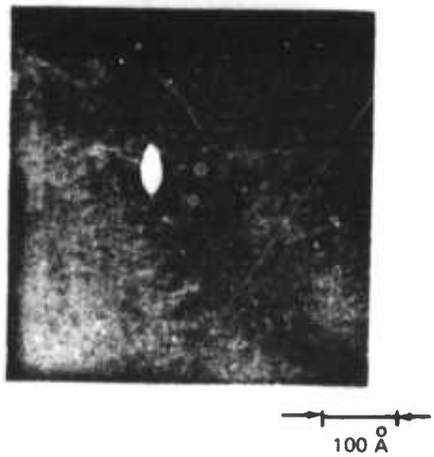

b) NO PZT DRIVE VOLTAGE

VI. CONCLUSIONS

Several flashlamp pumped dye lasers reported in the literature have produced average powers in the 1 to 10 watt range (Ref. IV-1,2). Commercial units are also available that deliver typically 1/4 to 1 1/2 watts average power (Ref. IV-3). The research and development work on this project has extended the average power level of flashlamp pumped dye lasers to over 100 watts, and indications are that considerably more average power could be attained.

A key element in our development of a high average power dye laser has been the vortex stabilized flashlamp. This flashlamp handles higher energy and higher average power loadings per unit length than any other type of short pulse flashlamp, and it holds promise of having an exceptionally long lifetime. We tested a 6 cm long arc version of the flashlamp at 15 kW average input power for periods of several minutes, which is long enough to allow the flashlamp to reach a steady state thermal equilibrium. Power levels over 50 kW have been discharged in the flashlamp intermittently for periods of a few seconds. If the flashlamp envelope were water cooled, we estimate the flashlamp could run for sustained periods at a 100 kw input power level. With the nitrogen gas cooling that is currently used we estimate a 28 to 30 kw limit for sustained operation.

Further development of the vortex flashlamp is required in two areas. First the rotary spark gap could be replaced by a longer lived and possibly higher power switch like a hydrogen thyratron or solid state thyristor unit. In order to operate the thyratron or thyristor switch elements with the flashlamp, the reverse current of the oscillating discharge would have to be eliminated. This could be accomplished either by critically dampening the discharge with a series resistance or by using a clamper circuit to bypass the switch and send the reverse current to the discharge capacitor. The latter method is more attractive, since we can return some of the unused charge to the capacitor and improve the overall laser efficiency. We estimate that if all the charge in the second current swing (which occurs after the laser pulse has terminated) were returned to the capacitor the laser efficiency would be improved 50 percent.

The second area of importance for further flashlamp development would be to build a closed cycle gas handling system to drive the vortex flow in the flashlamp. This would require a compressor, filter, and heat exchanger to circulate between 5 and 10 ℓ/sec (STP) of argon with pressure heads of 10 to 25 psig (depending on input power levels). This is certainly within current technology. A closed cycle gas system would allow us to life test the flashlamp with long running times and measure important parameters like electrode wear which is probably the limiting factor in the lifetime of the flashlamp.

We first used the vortex flashlamp to pump an axial flow dye laser in a spherical reflector. This laser gave an output of 42 watts at a pulse repetition frequency of 100 Hz (Ref. IV-4). The output power was limited by the replacement rate of dye solution in the active region. The dye replacement rate was really only adequate for a 65 Hz repetition rate. When we tried to flow the dye solution faster through the active region, cavitation in the dye cell and pump seal leakage occurred. The axial flow laser gave an efficiency of .4 percent at a repetition rate of 50 Hz. The efficiency dropped to .2% at 100 Hz. We project that reliable, long lived, axial flow dye laser utilizing the vortex stabilized flashlamp could be built that would give an efficiency between 1/2 and 1 percent. This system would use a well polished and coated elliptical reflector and take advantage of the unused energy returned to the capacitor as described above. Since the geometry is an axial flow, the repetition rate would be limited to 60 to 70 Hz. Average powers over 50 watts could be obtained.

The transverse dye laser is inherently less efficient than the axial flow laser. This is because the flashlamp light cannot be collected and focused as efficiently into a sheet of dye flowing transverse to the flashlamp axis. The improvement that the transverse flow gives with repetition rate, however, should outweigh the loss in efficiency. Indeed, we found this to be the case. The transverse flow laser gave 102 watts output at a pulse repetition frequency of 250 Hz. The output was linear up to 150 Hz and fell off from linearity only moderately up to 250 Hz. The principal reason for the small drop in laser pulse intensity at the higher repetition rates was shown to be the drop in flashlamp light intensity. The drop in flashlamp light occurred during the first 4 or 5 shots after which a steady state was reached. Faster gas flows can help eliminate this problem, and we feel that an output significantly greater than 102 watts can be achieved in the near future. The dye solution replacement rate in the transverse system was demonstrated to be large enough to allow operation at pulse repetition frequencies up to about 400 Hz. Repetition rates over 250 Hz, however, are about at the limit of the present power supply and rotary spark gap switch as explained in Section IV.

The laser was run only for a short time at the high power levels because of the spark gap limitations. We feel that there would be no significant drop in laser output if we could run for longer periods. A principal distortion effect that might have a longer time constant would come from heat transfer to and from the dye cell wall and dye solution. A program was set up utilizing the transient heat flow equation to determine the heat transferred between the wall and the dye solution on a shot to shot basis. The analysis showed that this effect reached a steady state after a few seconds, and the heat transferred amounted only to millicalories. Any distortion that would have occurred from this effect would take place mainly in the first half second and cause a continual drop in laser pulse intensity. The pulse intensity, however, reached a steady value after the first few shots.

In addition, an experiment was performed in which the outside surface of the dye cell was heated to 50°C above ambient. When the dye solution was flowing at rates above .32 ℓ/sec no effect on the optical quality of the dye solution was observed.

Burlamacchi and Pratesi have shown (Ref. VI-5, 6) that a waveguide configuration for a dye laser is capable of giving efficiencies of 1.7 percent. This laser geometry takes advantage of the nonuniform distribution of the refractive index set up by the pumping pulse in the active medium. Rays refracted out of the high gain region on the flashlamp side of the waveguide are reflected back into this region from the opposite side of the waveguide. The optimum spacing of the waveguide was found to be 0.4 mm. A transverse flow waveguide dye laser designed for our system could give an enormous increase in average laser power if efficiencies of 1 percent could be attained. If this is the case, then with two vortex flashlamps, one pumping each side of a slab waveguide, we can foresee average dye laser powers over 1 kW.

REFERENCES FOR SECTION VI

VI-1. Jethwa, J. and F. P. Schafer: A Reliable High Average Power Dye Laser. Appl. Phys. 4, 299 (1974).

VI-2. Friedman, H. W., and R. G. Morton: Transverse Flow Flashlamp Pumped Dye Laser. Paper 1.7, 1975 IEEE/OSA Conference on Laser Engineering and Applications, May 1975.

VI-3. Phase-R Company Model DL2100 C, New Durham, N. H., Chromatix Model CMX-4, Mountain View, Calif.

VI-4. Glenn, W. H., W. W. Morey, and C. M. Ferrar: High Power Dye Lasers. Paper 1.10, 1975 IEEE/OSA Conference on Laser Engineering and Applications, May 1975.

VI-5. Burlamacchi, P., and R. Pratesi: High Efficiency Coaxial Waveguide Dye Laser with Internal Excitation. Appl. Phys. Lett. 23, 475 (1973).

VI-6. Burlamacchi, P., R. Pratesi, and U. Vanni: Refractive Index Gradient Effects in a Superradiant Slab Dye Laser. Opt. Comm. 9, 31 (1973).